



Damping in a Timber Column

An Energy-Based Approach
E.R. van der Stap

Damping in a Timber Column

An Energy-Based Approach

by

E.R. van der Stap

to obtain the degree of Master of Science
at the Delft University of Technology,

Student number:	4153537	
Date:	April 2023	
Thesis committee:	Prof.dr. A.V. Metrikine	TU Delft - Civil Engineering and Geosciences
	Dr.ir. S. Sanchez Gomez	TU Delft - Civil Engineering and Geosciences
	Dr.ir. G.J.P. Ravenshorst	TU Delft - Civil Engineering and Geosciences
	Ir. R.W.A. Verhaegh	Adviesbureau Lüning

An electronic version of this thesis is available at <http://repository.tudelft.nl/>.
The cover picture is a photograph of the Yusuvara Wooden Bridge Museum by Takumi Ota.

Preface

Five years later than originally intended, I present to you my Master's thesis.

A rather unfortunate concussion in November 2017 forced me to completely change tack in both my ambition and my approach to daily activities not only with regard to my study but also to my personal life. Years of therapy, improvement and relapses followed during which I learned to play the piano, improved my cooking but also how to deal with my frustrations. Nonetheless, I remained driven to — one day — complete my Master's thesis at Delft University of Technology, not only for the feeling of accomplishment after years of study but also as a way to achieve closure on my predicament.

Therefore, first and foremost, I want to thank my girlfriend, Judit, for her endless support and love, which helped me tremendously during all the difficult times. I would also like to thank my family, especially my father André and brother Florian. Without them, I probably would have never completed this thesis. This journey started five years ago at Arup, and I am very grateful to them for providing me with the opportunity and for their help. I also want to thank them for their continued support during the first years of my concussion. Finally, I really appreciate the encouragement and support I have received from my thesis committee over these years; their patience and their willingness to explore possibilities rather than limitations. Andrei, Sergio, Geert, and Rob, thank you!

*E.R. van der Stap
Utrecht, April 25, 2023*

Abstract

An analytical study of an energy-based approach to damping of a clamped timber column in free vibration under axial, lateral and torsional loading conditions was conducted. Backed by experiments it was confirmed that an energy-based approach, as proposed by Sánchez Gómez [45], could describe the energy dissipation in a laterally vibrating timber column. With the help of an energy balance equation, the energy flow in a timber column was formulated including any energy dissipated during vibration. It was found that the energy in the system could be approximated by an exponential function for which a new dissipation constant E_D (s^{-1}) was introduced. For lateral vibrating columns of Norway spruce, typical values of E_D were 0.4 - 0.6 s^{-1} . Furthermore, a case study on a timber high-rise building demonstrated that damping has a significant influence on reducing peak accelerations which, in turn, could potentially lead to lowered costs. This largely untapped design lever warrants significant research and design improvement for these timber high-rise structures and, hence, several recommendations for follow-up research are offered.

Summary

In recent years, the environmental and cost benefits of timber as main building material has been re-discovered, even for high-rise buildings: it has low weight, relatively high strength and stiffness and is the only carbon-negative construction material. At the same time, compared to steel and reinforced concrete high-rise buildings, complying with the acceleration criteria introduces new challenges for a relatively low-weight timber building. Whilst energy dissipation, also known as damping, is an important factor in any dynamic behaviour, it is relatively little understood. Currently, it is not possible to determine and actively take into account the damping ratio of a building during the design phase, which particularly for a timber high-rise is a missed opportunity.

This research has confirmed with analytical models that an energy-based approach, as proposed by Sánchez Gómez [45], can describe the energy dissipation in a clamped timber column under axial, lateral and torsional loading conditions during free vibration. For lateral vibration the analytic model was further evaluated by conducting experiments. With the help of an energy balance equation, the energy flow in a timber column was formulated including any energy dissipated during vibration. In a timber column, the energy predominantly dissipates as thermal energy because of micro-structural defects or impurities in the material which initiate friction at grain boundaries. The energy balance equations for lateral, axial and torsional vibration cases have been derived. The total energy in the system during vibration consists of kinetic energy and potential energy, while the change of energy over time is equal to the dissipated energy. A set of basic experiments involving lateral vibrations were conducted using Norway spruce, a commonly utilized material, to test the validity of the analytical equations. It was found that the energy in the system can be approximated by an exponential function which introduces an energy dissipation constant E_D (s^{-1}) and the initial energy E_0 (J) as can be seen in equation 1. For lateral vibrating columns of Norwegian spruce, typical values of E_D were 0.4 - 0.6 s^{-1} .

$$E(t) = E_0 \exp(-E_D t) \quad (1)$$

The newly introduced energy dissipation constant E_D proved able to assess damping also in vibrating systems with beating, which is challenging using half-power bandwidth or logarithmic decrement method. Compared to these traditional methods, the energy-based approach is a more fundamental approach. Another advantage of E_D is that it will be easier to compare the damping values for different configurations: potential influences from amplitude, modes or frequency can be avoided due to initial energy being similar and the only varying constant being E_D . Finally, it has been established that damping has a significant influence on reducing peak accelerations and a better prediction of damping could potentially lead to lowered cost. A sensitivity analysis of a case study on the high-rise timber building HAUT showed that increasing the damping from 1.5% to 2% or 2.5% could reduce the mass by 17% or 29%, respectively, while maintaining constant peak accelerations. This largely untapped design lever warrants significant research and design improvement for these timber high-rise structures.

The thesis offers several recommendations for follow-up research, including improving and modifying the experimental set-up and extending it to a timber frame. Not only will this lead to valuable improvement in data quality and deepen the understanding of damping in timber structures but also open the way to a practical application in engineering design. This, in turn, should result in both safer and more economic designs in timber as high-rise buildings of the future.

Contents

Abstract	v
Summary	vii
1 Introduction	1
1.1 Problem Statement	4
1.2 Research Objective	4
1.3 Research Questions	5
1.4 Scope	5
1.5 Reader Guide	5
I Literature Study	7
2 Relevance	9
2.1 Scientific Relevance	9
2.2 Relevance to Engineers	9
2.2.1 Literature	9
2.2.2 Case study HAUT	11
3 Timber	13
3.1 Model Representation Wood	14
3.1.1 Constitutive equations timber	15
3.2 Modulus of Elasticity	16
3.3 Engineered Timber	16
3.3.1 Glued laminated timber	16
3.3.2 Cross-laminated timber	17
3.4 High-Rise Timber Buildings	17
4 Damping	19
4.1 Mathematical Models	19
4.1.1 Viscous damping	19
4.1.2 Quadratic damping	20
4.1.3 Friction damping	20
4.1.4 Hysteretic damping	20
4.2 Physical Models	20
4.2.1 Material damping	21
4.2.2 Structural damping	22
4.2.3 Radiation damping	22
4.2.4 Aerodynamic damping	22
4.2.5 Artificial damping	22
4.2.6 Total damping	23
4.3 Predictive Models	23
4.3.1 Predictive values for timber structures	23
4.4 Eurocode	24
4.5 Damping Identification Methods	25
4.5.1 Logarithmic decrement	25
4.5.2 Envelope fitting	25
4.5.3 Half-power bandwidth method	26

II Theoretical Basis Energy-Approach	27
5 Dynamics	29
5.1 Single Degree of Freedom	29
5.2 Continuous Models	30
5.2.1 Euler-Bernoulli beam	30
5.2.2 Timoshenko beam	31
5.3 Torsional Vibration	32
5.4 Axial Vibration	32
5.5 Selected Beam Models.	32
6 Energy	35
6.1 Energy Flow Analysis	35
6.2 Energy Balance Equation	36
6.2.1 Lateral vibration.	37
6.2.2 Torsional vibration	37
6.2.3 Axial vibration.	37
III Experiment on Timber Column	39
7 Experiment Setup	41
7.1 General Physical Model Setup.	41
7.2 General Numerical Setup	42
7.3 General Analytical Setup.	42
7.4 Conducted Experiment.	43
7.4.1 Physical model setup.	43
7.4.2 Numerical model	46
7.5 Expected Vibration Behaviour	47
8 Results and Analysis	49
8.1 Beating	49
8.1.1 Clamped boundary condition	51
8.1.2 Anistropy	51
8.2 Energy Transfer	52
8.3 Comparing Curvature Determination Methods	53
8.3.1 Displacement shift method.	54
8.3.2 Acceleration fitting method.	54
8.4 Energy Dissipation Trends.	57
8.4.1 Damping ratio trends	57
8.4.2 Energy dissipation constant trends	58
8.5 Validation	59
8.5.1 Comparison damping ratio to the literature	59
8.5.2 Comparison energy dissipation constant and damping ratio	59
8.5.3 Comparison initial energy	59
8.5.4 Validation natural frequency and modulus of elasticity	60
IV Conclusions and Recommendations	63
9 Conclusions	65
10 Recommendations	67
10.1 Follow-up Research	67
10.2 Timber Design	68
Bibliography	69
A Acceleration HAUT - Eurocode Calculation	73
B High-Rise Timber Buildings	75
B.1 Stadthaus.	75
B.2 Forte	76

B.3	Treet.	76
B.4	Tallwood House at Brock Commons.	77
B.5	HAUT	77
B.6	HoHo Wien	78
C	Derivation Equations of Motion	79
C.1	Single Degree of Freedom	79
C.2	Continuous Models	80
	C.2.1 Euler-Bernoulli beam	81
	C.2.2 Timoshenko beam	83
C.3	Torsional Vibration	84
	C.3.1 Warping	84

1

Introduction

As the population grows and housing demand increases, more buildings are being constructed. With the threats and the upcoming awareness of climate change, people are looking to build housing in a more sustainable manner. High-rise buildings have a unique position in this building process as they affect the environment both positively and negatively. The positive impact on the environment is the result of the higher concentration of population in high-rise buildings, resulting in efficient use of both surface area and energy and likely leads to less or more efficient travel and commuting. The negative impact on the environment stems from the relatively high carbon footprint of high-rise buildings: construction of tall buildings requires relatively more material compared to low-rise buildings. As structural systems of high-rise buildings are usually made of steel, concrete or a combination of both and the production and assembly of either material causes a significant amount of CO₂ emissions, its global warming impact is higher. To counter the negative environmental impact of high-rise buildings, engineers are starting to rely once again on the oldest building material available: wood.

Humankind has been building with wood, or rather with its sawn construction form, timber, for a very long time already. The oldest and tallest timber building is the Yingxian Pagoda in China. It was built in 1056 and is 67 meters tall. In its almost thousand years of existence, it endured several earthquakes which demonstrate the durability of wood. The tallest timber structure made to date is the 190 meters high Münhlacker Radio Transmission Tower in Germany. The tower was built in 1930 but destroyed at the end of World War II in order to prevent the Allied forces to use it. The biggest timber structures in the world are seven hangars which were constructed in the USA during World War II. The hangars are 340 meters long by 115 meters wide and 53 meters high and were made in timber due to a shortage of steel during the war [28]. History thus shows the feasibility of timber structures. It is up to contemporary architects and engineers to restart designing and building in timber.

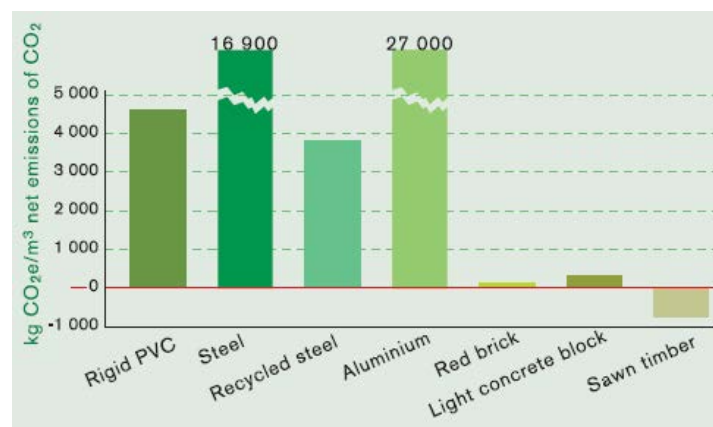


Figure 1.1: Yinxian Pagoda, China.

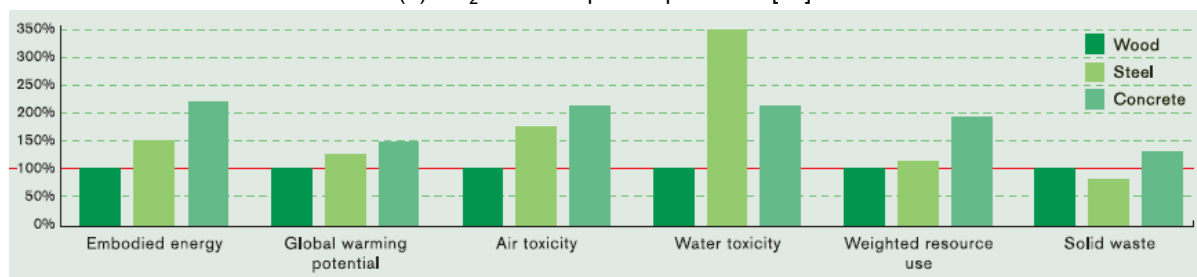


Figure 1.2: Timber hangar, Moffet Field, USA [28]

Tall timber buildings are an ideal opportunity for a sustainable solution as timber is the only construction material which is carbon negative, in other words, the entity in question has a net effect of removing carbon [44]. Due to photosynthesis wood absorbs CO_2 which is stored in the wood for its lifetime, making it a carbon sink. Furthermore, the production of timber is less energy-consuming than concrete or steel, making it by far the most sustainable building resource. In Figure 1.3 the environmental properties of timber are compared to other often-used building materials. Figure 1.3a depicts the carbon emission per cubic meter for production, but as different volumes are needed for different materials, Figure 1.3b gives an overview of the environmental performance of a building being made of either timber, steel or concrete, across its life cycle. It illustrates the potential of timber as sustainable construction material. An extra environmental benefit of using timber is that in the case it is harvested in a sustainable way, it is a renewable resource. Lastly, prefabricated timber could potentially be disassembled and reused after demolition leading to a more circular economy [22]. It is noteworthy that new developments such as 'green steel' and low carbon concrete are as yet not mature enough to be considered at large construction scales and have thus been discarded in this comparison.



(a) CO_2 emission per m^3 produced [44]



(b) Environmental impact of comparative wood, steel, and concrete buildings [53]

Figure 1.3: Comparison environmental effect various building materials.

Besides all the environmental benefits, the use of timber offers more advantages in comparison to traditional high-rise building materials. Table 1.1 provides an overview of the characteristic values of the three most common building materials. The low weight of timber reduces the overall weight of the building thus decreasing the size of the foundation. Despite its low weight, timber is a very strong and stiff material and in fact, compared to steel and concrete has the lowest mass-strength ratio [25]. When building with timber, the lower weight enables easier handling and lower craneage and hence reduced construction time. Due to the possibility to prefabricate many structural components and easily adjust these on-site a shorter site erection time can be achieved. All combined this leads to lower construction costs. This also positively affects the surroundings as less construction noise and hindrance will be experienced.

The completion in 2009 of the 9-storey Stadthaus in London marked the start of the exploration of high-rise timber structures. Nowadays, more high-rise timber buildings have been constructed; the

Table 1.1: Characteristic design values of the three most common building materials.

	E (MPa)	ρ (kg/m ³)	f_{tk} (MPa)	f_{ck} (MPa)
Steel - S235 [14]	210,000	7,850	235	235
Concrete - C40 [13]	35,000	25,000	3.5	40
Timber - C24 [16]	11,000	350	14	21

tallest already being almost three times as tall as Stadthaus. Mjøstårnet is currently the tallest timber building at a height of 85 meters. An overview of different timber high-rises can be found in Figure 1.4. In 2016, engineering firm Arup, architect firm Team V and developer Lingotto started to investigate the possibilities of constructing in timber and proposed a design for a 21-storey tall building in Amsterdam named HAUT, which phonetically means wood in Dutch. The construction of their award-winning design started end of 2018 and was eventually completed in 2022, making it the tallest timber building in The Netherlands.

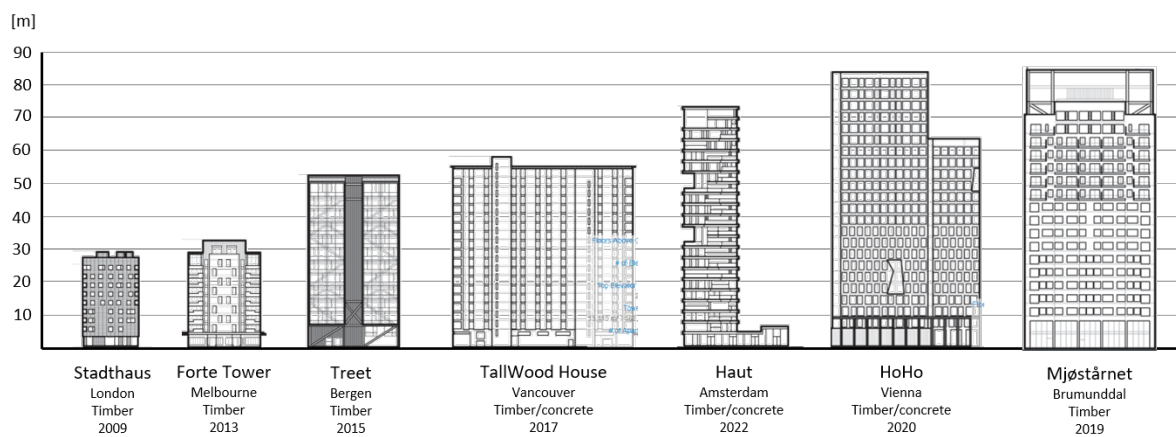


Figure 1.4: Height tallest residential timber buildings [8]

During the design process of HAUT, several challenges had to be overcome, including the dynamic behaviour of the building. While the relatively low weight of the building is a clear benefit for the piled foundation design in the very soft Amsterdam soils, it also poses a disadvantage. The dynamic response due to wind is adversely affected by the low mass, which leads to higher accelerations along the height of the building and notably its top floor, possibly causing residents to feel uncomfortable or even nauseated. Therefore, the lateral acceleration response is a key aspect of timber high-rise designs.

The structural design properties influencing the acceleration due to wind-induced vibrations are the stiffness, mass and damping [55]. Whereas the mass and stiffness of a building can quite accurately be determined, currently no method exists to precisely calculate the damping. Damping of buildings in general is a phenomenon that is not very well understood and the calculation, therefore, is unknown. Smith and Willford [47] states that the difference of measured damping ratio versus assumed can be as high as a factor ten. Fortunately, at least for steel and concrete structures, there are ample references to estimate the damping to avoid gross under- or overprediction. However, for timber structures, this is not the case as only a few buildings have been constructed which differ in their structural configuration as well. To get a better understanding of the damping properties of tall timber buildings more research is needed.

1.1. Problem Statement

Due to the continuing desire to build higher and more slender, the limiting requirements regarding floor acceleration due to wind will become more and more governing for its design, even if design stresses remain well within elastic limits. Especially in buildings constructed out of timber, this will be important, because of the relatively low weight of timber compared to steel and concrete. If the accelerations of the top floor of a building are too high, this can cause discomfort for the residents and can even lead to nausea. Therefore, building codes prescribe a limit to the allowable acceleration at the top floors of buildings. To reduce the acceleration and comply with the code requirements, the damping ratio is key. This makes it valuable to have a better understanding of the damping in order to avoid under or over-designing.

Usually, the designer performs the dynamic design calculations with the standard damping ratio as provided by the Eurocode. These have been simplified to a single material value for either steel or concrete. It is noteworthy that for timber no value for damping ratio is provided [15]. Besides the Eurocode, multiple different equations are developed to estimate the damping ratio of buildings. Using these equations, the damping ratios calculated for the exact same building are hardly ever in agreement with each other or the Eurocode. It would be preferable to be more certain of the lower bound of the damping ratio. This would assure engineers of their choice for damping ratios and hence lead to a more accurate design.

Fundamentally, the energy flow and dissipation in a vibrating system form the basis of damping. However, to date methods to estimate damping have been mostly empirical or phenomenological; merely describing what is observed rather than its fundamental physics. Given that damping is essentially energy dissipation during vibration it would appear logical to try to approach the determination of the damping ratio from a fundamental energy-based perspective.

Damping is currently not actively being taken into account during the design process. Engineers do not consider the different damping performances of joints, materials and structural systems in their design choices. If the damping properties of joint types and bracing configurations could be determined, this could be included in the design process of the building. In summary, an important factor in the dynamic behaviour of a building is left untapped during design, which is odd considering the effort spent in modelling mass and stiffness in high-rise buildings.

High-rise timber buildings are extremely complex systems, consisting of many different structural elements with different shapes and dimensions, as well as many secondary and non-structural components, all connected with different joint details and friction surfaces. It is essential to dissect the problem into basic elements and boundary conditions for each of which a dynamic model can be construed, and basic conclusions can be drawn. Subsequently, the complexity of the models can be increased. In this thesis, the choice has been made to assess the basic system of a one-sided clamped, timber column.

Problem Statement

Compared to steel and reinforced concrete high-rise buildings, the design with relatively low-weight material such as timber, the acceleration criteria will be even more important. Damping is an important factor in any dynamic behaviour but is a little-understood energy dissipation mechanism. It is currently not possible to accurately determine the damping ratio of a building during design. Therefore, damping is not actively taken into account during the design phase, which particularly for a timber high-rise is a missed opportunity.

1.2. Research Objective

To avoid both under and overestimating damping it is desirable to be able to predict the damping of a building with higher precision. This research aims to give a better fundamental understanding of how and where the energy dissipates in a clamped timber column during vibration. The damping of a timber column under axial, lateral and torsional loading is researched. The focus is to derive a method

which shows how the energy dissipates and accurately determines the damping in a simple timber structure. To improve the understanding of damping in a complex system such as a high-rise timber building, firstly the dynamic behaviour of basic structural, timber systems must be understood and combine basic systems to increase complexity thereafter. A simple column is taken as starting point to investigate the possibilities of determining damping using an energy-based approach. If the results are satisfactory, the complexity of the researched structure can be increased.

1.3. Research Questions

The research question to be answered in this master's thesis is:

- *How is the energy dissipated in a clamped timber column under axial, lateral and torsional loading conditions during free vibration and can its damping be predicted using an energy-based approach?*

In order to answer the main research question four sub-questions are formulated.

- *What energy-based approaches exist in order to determine the damping properties of a timber column?*
- *How can the damping of the first mode of a timber column during free axial vibration be determined using an energy-based approach?*
- *How can the damping of the first mode of a timber column under free lateral vibration be determined by using an energy-based approach?*
- *How can the damping of the first mode of a timber column under free torsional vibration be determined by using an energy-based approach?*

1.4. Scope

The energy dissipation of a clamped timber column will be investigated during free lateral, torsional and axial vibration. By an imposed displacement or hammer impact test, energy will be added to the system. Subsequently, the dissipated energy during free vibration will be measured. As the premise of high-rise design codes is linear-elastic it suffices to limit this study to the linear and elastic range.

1.5. Reader Guide

This thesis can be divided into four parts: I Literature Study, II Theoretical Basis Energy, III Experiment Approach and IV Conclusions and Recommendations. The literature study is described in Chapter 2 to 4. It starts with an overview of the relevance of this research. Next, the theoretical background of the thesis relating to timber and damping is discussed. In Part II the theoretical basis of the energy approach is derived and presented. This is done in Chapter 5 and 6, which covers dynamics and energy. Part III contains all the chapters concerning the experiment. It starts with the setup of the experiment in Chapter 7, followed by the results in Chapter 8. In Part IV of this thesis, the conclusion and recommendations are discussed.

The reader is reminded that the symbol E can represent both energy and modulus of elasticity (MOE) in this thesis. Both conventions have been used; in those rare cases where the intended meaning of E was not immediately obvious from the context it has been made explicit.



Literature Study

2

Relevance

It is useful to assess what is already known and researched on this topic, both from a scientific perspective as well as from an engineering perspective. As the exact behaviour and determination of damping is still a mystery to both scientists and engineers, it is very relevant to investigate the nature of damping.

2.1. Scientific Relevance

Investigating damping is an ongoing activity within the field of structural dynamics. This holds for high-rise buildings of all materials, however, as designing tall timber buildings is a recent development, research on the damping of timber buildings is less extensive. It can be noted that understanding the dynamic behaviour of tall timber buildings is key to its successful deployment. While it is possible to determine the stiffness and mass of a building quite accurately, this is not the case for damping. No simple method exists to derive the damping of a building.

In 2019, Sánchez Gómez proposed a promising method to identify damping by using the energy-flux method. The in and outflow of energy in a segment is observed to create the energy balance. The dissipated energy in this energy balance can thus be attributed to the damping. This method gives researchers the opportunity to investigate the damping properties of different sections in a structure. In this thesis, the energy dissipation in a lateral vibrating steel clamped beam and a five-story frame was studied. It will be interesting to continue on this energy-based approach to investigate its applicability to timber structures.

2.2. Relevance to Engineers

To give a better insight into the relevance of a more accurate estimation of damping from the engineer's point of view, the influence of the damping on the peak acceleration of a building is determined. As stated earlier, the peak acceleration of tall timber buildings can be governing during the design. Therefore, knowing the impact of damping on peak accelerations offers an increased understanding of the relevance of estimating damping.

Fundamentally understanding the energy dissipation in a structure during vibration could contribute to actively including damping in the design process. This is relevant to engineers as currently no method is used — unless an artificial damping system is deployed — to add damping to a structure during the design phase. By choosing specific configurations with known higher damping, an increased damping ratio could be achieved in high-rise buildings possibly without extra cost.

2.2.1. Literature

The effect of mass, damping and stiffness on dynamic accelerations has been researched by M. Johansson and Reynolds [30], Van den Berg [54] and Van Oosterhout [55]. While Van den Berg's and Van Oosterhout's research focused on concrete and steel buildings, M. Johansson and Reynolds analysed the effect specifically for timber buildings. Their conclusions were similar despite the difference in the

studied material.

The researchers concluded that increasing the mass has the biggest influence on lowering the acceleration of a building. Mass can be added to a timber building by, for instance, choosing a concrete core. Due to various design requirements, this might be undesirable for the design depending on the circumstance. Nonetheless, an extra positive effect of added mass on the peak acceleration is the decrease in natural frequency. For most codes, the allowed peak acceleration is higher with lower frequencies. Added mass thus allows higher peak accelerations as the natural frequency decreases.

Stiffness does influence acceleration, but the effect depends on the slenderness of a building. For a non-slender building increasing the stiffness positively influences the acceleration. However, for a slender building, this is not so much the case. For buildings with a natural frequency below 1 Hz, increasing the stiffness does not have a significant effect. This is even more enhanced if the allowed peak acceleration of codes is taken into account. Higher natural frequencies, which allow for lower peak accelerations, follow from increased stiffness. Therefore, the decrease of acceleration gained by the increase of stiffness could still lead to unacceptable accelerations as the allowed acceleration will be lower. Increasing the stiffness has the least effect of the three parameters on the peak acceleration.

Damping is an effective measure to reduce the peak acceleration of a building [55]. Whilst mass and stiffness change the natural frequency, damping has no impact to a structure's natural frequency. It only impacts the magnitude of the dynamic response.

In summary, the effect of increasing the stiffness is limited, whereas increasing the mass and damping do have a positive effect on the maximum allowed acceleration. It depends on the circumstances and building requirements if adding mass or damping is the preferred method of lowering the acceleration. In certain situations, it could be unfavourable to add mass, but it might be necessary in some cases. For example, the acoustics could require a higher mass of the floors. It is up to an engineer to decide for each situation which parameter is adjusted in order to comply with the allowed accelerations in the Eurocode. A summary of the influence of the parameters on the acceleration can be found in Figure 2.1 and 2.2. Figure 2.1 depicts the effect on the peak acceleration to changes in mass (m), damping (ζ) and stiffness (k) for either a slender building or a squat building. The influence of doubling or tripling the mass, damping and stiffness in a timber building on the acceleration can be found in Figure 2.2.

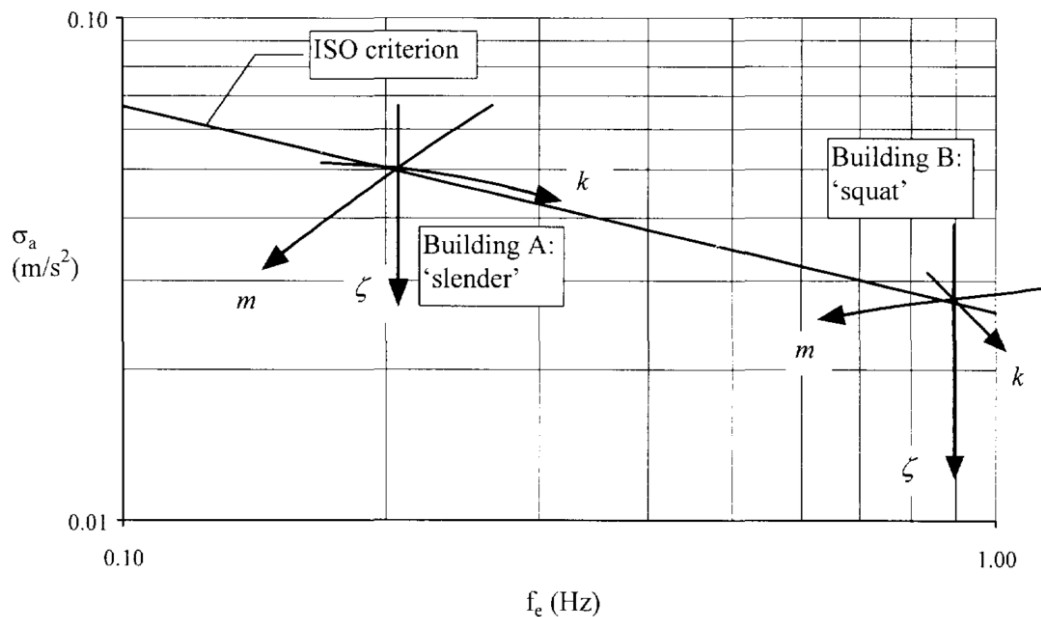


Figure 2.1: Effect on acceleration to changes in mass (m), damping (ζ) and stiffness (k) [55].

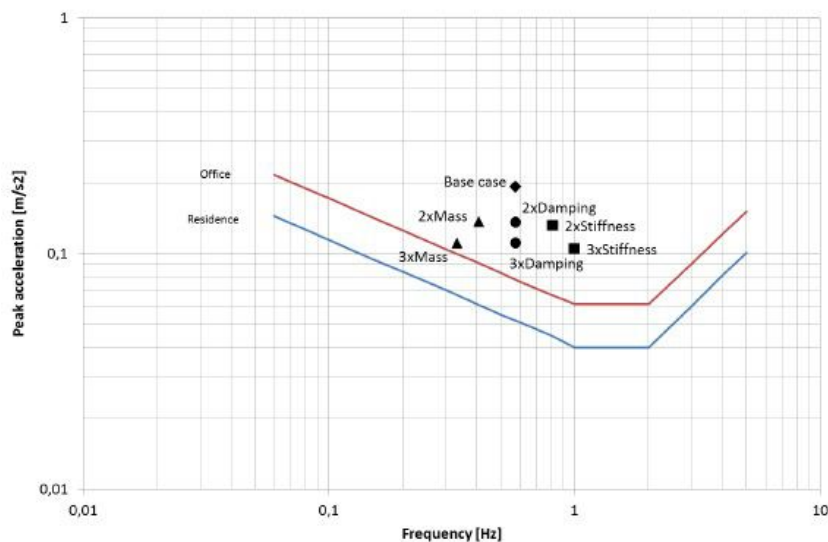


Figure 2.2: Effect on acceleration to changes in mass (m), damping (ζ) and stiffness (k) for a timber building [30].

Smith and Willford [47] state that the difference of measured damping ratio in buildings can be as low as 0.3% and assumed as high as 3%. Assuming that the aerodynamic loading on the building is effectively a broadband random process (in the frequency range in which the natural period of the building lies) the dynamic response is inversely proportional to the square root of the damping coefficient of the building. In other words, the overestimation of damping in design could result in an underestimation of dynamic response loads of more than threefold ($\sqrt{10}$). In the case of timber design, where even less is known of damping values the potential error is likely to be even higher.

2.2.2. Case study HAUT

As part of the literature study, a sensitivity analysis was performed to further assess the relevance of damping in the design of tall timber buildings. The high-rise timber building HAUT was used as a case study. Using the finite element model provided by Arup, the effect of the damping ratio on the acceleration due to wind-induced vibrations were investigated. The analysis was aimed at determining the possible mass reduction if the damping ratio is increased. The acceleration was evaluated using the formula of Eurocode 0. Full calculations can be found in Appendix A.

The sensitivity analysis demonstrated clearly that changing the value of the damping ratio for HAUT has a profound impact on the building's dynamic response. The results showed that by increasing the damping ratio by half a percentage point, the mass can be reduced by 17% while the same acceleration is guaranteed. By increasing the damping ratio up to 2.5%, the mass can even be reduced by 29%. This shows that the damping ratio has a significant influence on the design of a building. By calculating the damping ratio more accurately, it would be possible to drastically reduce the required mass in order to fulfil the requirements of the peak acceleration. This might lower the cost of a building. It remains noteworthy that it highly depends on the circumstances and the building requirements if lowering the mass is preferable. Eventually, it is up to the engineer to identify which solution best suits the design requirements.

Table 2.1: Influence increasing damping ratios on the mass.

Damping ratio [%]	Mass reduction [t]	Mass reduction [%]
1.5	-	-
2	2544	17
2.5	3411	29

3

Timber

Wood is a natural material which serves three main functions in a tree: transport of water, structural support and storage of biochemicals. Understanding both the function and biological structure of wood provides insight into its properties. The following section is based on Wiedenhoef [58].

Two distinct groups of trees can be identified: hardwoods and softwoods. Softwoods are generally evergreen trees with needle-like leaves, whereas hardwoods are deciduous and broad-leaved. Besides their physical dissimilarities, softwoods and hardwoods also differ at the cellular level. Hardwoods contain vessel cells, but softwoods lack these so-called pores. Hence, the wood of softwood is more uniform in structure.

For both soft- and hardwoods, wood can be divided into two sections: sapwood and heartwood. The sapwood is the lighter, active, outer area of the trunk. This part is responsible for the conduction of saps and the storage of biochemicals. The inner, oldest part of the tree is called the heartwood and is darker in colour. The region between the bark and the sapwood is called the vascular cambium. In the cambium, new cells are formed in order for the tree to grow. The cells produced in the early stage of the growth increment are called earlywood and latewood if formed in the later stage. In seasonal climates, these growth increments occur yearly, resulting in growth rings. Depending on the species these growth rings can be clearly visible or difficult to distinguish.

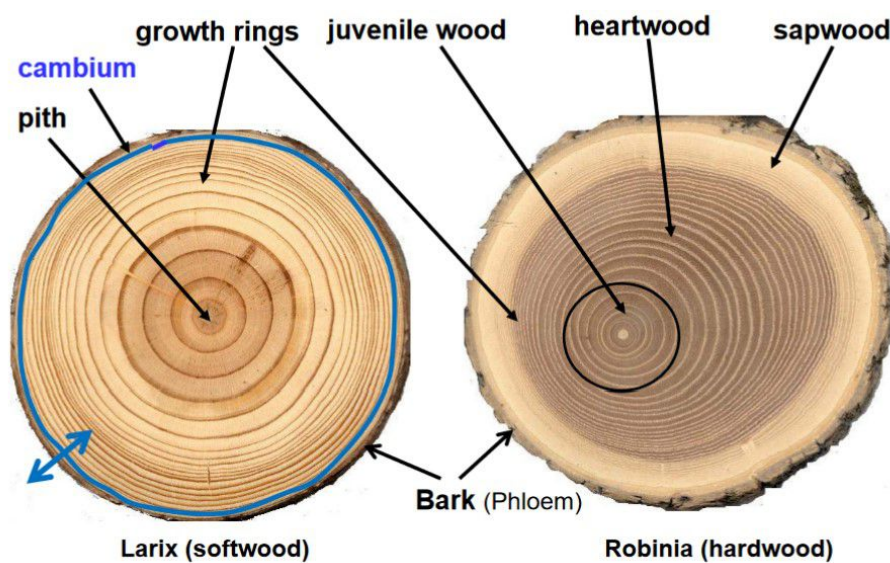


Figure 3.1: Different regions of wood [18].

The cells in wood are different than in other plants. In most plants, the cell is made out of two parts: a living inner part, called the protoplast, and the non-living cell wall. However, for many cells in wood, only the cell wall has a function, resulting in the fact that most mature wood cells remove their protoplast to become functional. The open space left is called the lumen. As a result, wood consists of two domains: air space (mostly lumen) and cell walls. As the lumen is an empty space, the properties of wood are mostly derived from the structure of the cell walls. The cell wall consists of three different components: cellulose, hemicellulose and lignin. Cellulose is an organic polymer with a high tensile strength, which is embedded in a matrix of lignin resisting compressive forces. Hemicellulose binds the cellulose and lignin together.

Most cells in wood are elongated in one direction. These cells generally are oriented either in the axial direction or the radial direction; forming two structural systems. The axial system transports water up and down the tree and provides most of the structural strength. The lateral biochemical transport and storage are mainly a function of the radial system. The structure of the cells in softwood is relatively simple and is characterized by two types of cells. The tracheids compose the axial system and the radial system consists of ray parenchyma cells. Tracheids are long, thin cells, which can be a hundred times longer than wide. They make up ninety per cent of the wood volume in softwood. Ray parenchyma cells are not as long as tracheids and are shaped like rectangular prisms.

Hardwood on the other hand has a cell structure which is more complicated. The size, proportion and structure of the types of cells can vary over different hardwood species. The axial system is defined by three types of cells: vessels, fibres and axial parenchyma. Vessels are not as long as tracheids but are typically wider. They are also called pores. The conducting of water is done by the vessels. The vessels are supported by fibres. The fibres are two to ten times longer than vessels. Hardwood's density and mechanical properties are mainly governed by the thickness of the fibre cell wall. The last group of cells is the axial parenchyma. These are similar to the ray parenchyma but orientated axially. Just as in softwood, the ray parenchyma cells make up the radial system. The configuration of the ray cells however can be different.

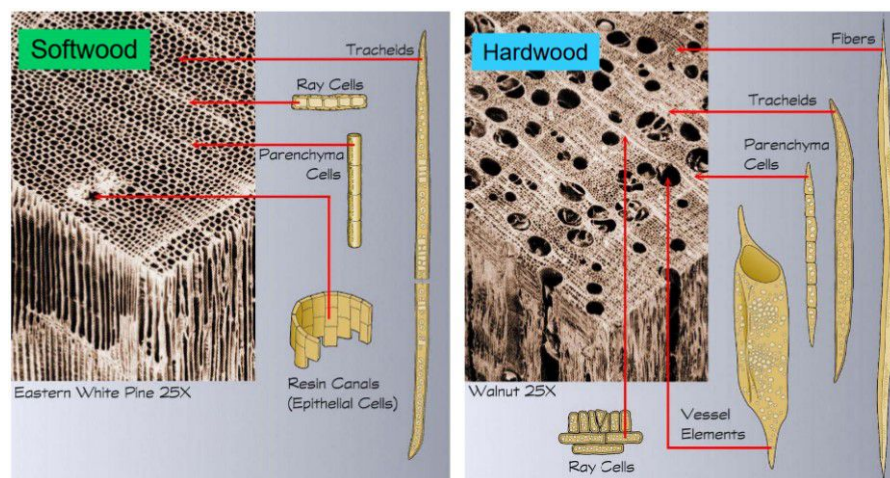


Figure 3.2: Different type of cells in softwood and hardwood [18].

3.1. Model Representation Wood

Due to the fact that wood forms in natural conditions and is made out of fibres, challenges rise if a model representation of wood must be derived. To model all the irregularities formed during the growth of wood is impossible. Therefore, a simplification in the model always has to be assumed. The current most accurate model with the least simplification is a non-homogeneous, cylindrical orthotropic model. In this way, the difference between the earlywood and latewood in each growth ring is accounted for. Nairn [36] found that the pattern of the growth rings can lead to a reduction of the transverse modulus. Normally, however, the distinction between early- and latewood is disregarded.

This leads to a homogeneous cylindrical orthotropic model. By using this model the curvature of the growth rings is taken into account. N. Labonnote and Malo [35] states that the curvature reduces the mechanical properties of wood. By considering either smaller cross-sections or cross-sections further away from the pit, the curvature of the rings could be decreased. Thus the reducing effect on mechanical properties becomes negligible. For simplicity's sake, the cylindrical model is therefore generally replaced by a rectangular orthotropic model. Different studies discovered an effect on the mechanical properties by the grain angle θ [35]. In the Eurocode, nevertheless, a further simplification is made. Only two different directions in the wood are acknowledged: parallel (0° direction) and transverse (90°) plane to the fibres. This transversal isotropic model is currently being used in timber engineering.

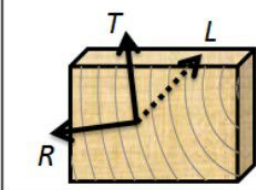
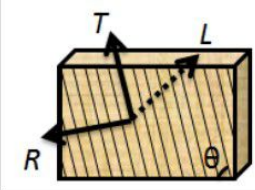
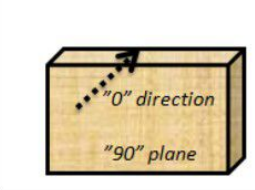
		
E_R, E_T, E_L $\nu_{RT}, \nu_{RL}, \nu_{LT}$ G_{RT}, G_{RL}, G_{LT}	E_R, E_T, E_L $\nu_{RT}, \nu_{RL}, \nu_{LT}$ G_{RT}, G_{RL}, G_{LT}	E_0, E_{90} ν G_0, G_{90}

Figure 3.3: Different models for wood and its corresponding material properties: a) cylindrical orthotropy, b) rectangular orthotropy, c) transversal isotropy [25].

3.1.1. Constitutive equations timber

The relationship between strains (ϵ) and stresses (σ) are given by the constitutive equations. In general, a linear relationship between strain and stress can be written as:

$$\epsilon_{ij} = S_{ijkl}\sigma_{kl} \quad (3.1)$$

where S_{ijkl} is called the compliance tensor. A full compliance tensor would consist of 81 components. However, due to the symmetry of both ϵ_{ij} and σ_{kl} , the tensor reduces to 36 elements. As S_{ijkl} is also symmetric, only 21 independent components remain [43]. For an orthotropic material, this reduces further to:

$$\begin{Bmatrix} \epsilon_1 \\ \epsilon_2 \\ \epsilon_3 \\ \gamma_4 \\ \gamma_5 \\ \gamma_6 \end{Bmatrix} = \begin{bmatrix} \frac{1}{E_1} & -\frac{\nu_{21}}{E_2} & -\frac{\nu_{31}}{E_3} & 0 & 0 & 0 \\ -\frac{\nu_{12}}{E_1} & \frac{1}{E_2} & -\frac{\nu_{32}}{E_3} & 0 & 0 & 0 \\ -\frac{\nu_{13}}{E_1} & -\frac{\nu_{23}}{E_2} & \frac{1}{E_3} & 0 & 0 & 0 \\ 0 & 0 & 0 & \frac{1}{G_{23}} & 0 & 0 \\ 0 & 0 & 0 & 0 & \frac{1}{G_{13}} & 0 \\ 0 & 0 & 0 & 0 & 0 & \frac{1}{G_{12}} \end{bmatrix} \begin{Bmatrix} \sigma_1 \\ \sigma_2 \\ \sigma_3 \\ \tau_4 \\ \tau_5 \\ \tau_6 \end{Bmatrix} \quad (3.2)$$

The compliance tensor for a transversely isotropic material simplifies slightly as $E_2 = E_3$, $\nu_{12} = \nu_{13}$ and $G_{12} = G_{13}$.

$$\begin{Bmatrix} \epsilon_1 \\ \epsilon_2 \\ \epsilon_3 \\ \gamma_4 \\ \gamma_5 \\ \gamma_6 \end{Bmatrix} = \begin{bmatrix} \frac{1}{E_1} & -\frac{\nu_{21}}{E_2} & -\frac{\nu_{21}}{E_2} & 0 & 0 & 0 \\ -\frac{\nu_{12}}{E_1} & \frac{1}{E_2} & -\frac{\nu_{32}}{E_2} & 0 & 0 & 0 \\ -\frac{\nu_{12}}{E_1} & -\frac{\nu_{23}}{E_2} & \frac{1}{E_2} & 0 & 0 & 0 \\ 0 & 0 & 0 & \frac{1}{G_{23}} & 0 & 0 \\ 0 & 0 & 0 & 0 & \frac{1}{G_{12}} & 0 \\ 0 & 0 & 0 & 0 & 0 & \frac{1}{G_{12}} \end{bmatrix} \begin{Bmatrix} \sigma_1 \\ \sigma_2 \\ \sigma_3 \\ \tau_4 \\ \tau_5 \\ \tau_6 \end{Bmatrix} \quad (3.3)$$

The simplest compliance tensor only has two independent components, which holds for isotropic material.

$$\begin{Bmatrix} \epsilon_1 \\ \epsilon_2 \\ \epsilon_3 \\ \gamma_4 \\ \gamma_5 \\ \gamma_6 \end{Bmatrix} = \begin{bmatrix} \frac{1}{E} & -\frac{\nu}{E} & -\frac{\nu}{E} & 0 & 0 & 0 \\ -\frac{\nu}{E} & \frac{1}{E} & -\frac{\nu}{E} & 0 & 0 & 0 \\ -\frac{\nu}{E} & -\frac{\nu}{E} & \frac{1}{E} & 0 & 0 & 0 \\ 0 & 0 & 0 & \frac{1}{G} & 0 & 0 \\ 0 & 0 & 0 & 0 & \frac{1}{G} & 0 \\ 0 & 0 & 0 & 0 & 0 & \frac{1}{G} \end{bmatrix} \begin{Bmatrix} \sigma_1 \\ \sigma_2 \\ \sigma_3 \\ \tau_4 \\ \tau_5 \\ \tau_6 \end{Bmatrix} \quad (3.4)$$

$$\text{with } G = \frac{E}{2(1+\nu)}$$

An overview of the necessary material constants for orthotropic or transversely isotropic material can be found in Figure 3.3. These constants vary for each wood specie but can be found in the literature (for example in Kretschmann [24]).

3.2. Modulus of Elasticity

Although values for the modulus of elasticity (MOE) can be found in the literature, they also can be easily derived experimentally. A quick way of determining the MOE is using the dynamic method. For this method, a longitudinal stress wave is initiated by a hammer impact into a beam supported on wooden sticks. The acceleration is measured on the other side of the beam. The first natural frequency (f) can hence be obtained. Combined with the length (L) and density (ρ) of the beam, the modulus of elasticity can be determined [41].

$$MOE_{\text{dyn}} = 4\rho f^2 L^2 \quad (3.5)$$

This modulus of elasticity is calculated for the longitudinal direction. The MOE obtained is called the MOE_{dyn} as the wood is vibrating during the test. To determine the bending modulus, the calculated modulus is reduced by 5% and is called the MOE_{loc} [41].

3.3. Engineered Timber

As discussed previously, the properties of wood are anisotropic due to wood's cellular structure and natural forming. Because of differences in environment and circumstances, not only do species differ in their properties, but also within species differentiation in properties can be found. To safely design timber structures it is necessary to take these uncertainties into account. To provide reliable wood characteristics which can be designed, two methods have been developed: grading and engineered timber. The wood can be graded by various aspects, such as knots and the age of the wood, in order to determine its quality. Subsequently, it is possible to create engineered timber by glueing smaller parts of graded timber into structural timber elements [6].

For high-rise timber buildings mainly engineered timber is used. During the production process of engineered timber, the wood is first graded. After grading smaller pieces of wood are glued together in order to create engineered timber. Knots and other properties influencing growth characteristics are hence distributed over the timber, leading to a more homogeneous material. The variability of wood is decreased by reconstituting the wood. Engineered timber does not have a higher average capacity, but the variation of the strength properties is decreased and thus the characteristic strength is increased [6]. Two of the most used engineered timbers in tall timber buildings are glued laminated timber (glulam) and cross-laminated timber (CLT). Therefore, these timber products are discussed in more detail in the next sections.

3.3.1. Glued laminated timber

Glulam consists of laminated solid timber bonded together by adhesives. The timber layers' orientation is all in the same direction, with the grains parallel to the axis. The lamination of the glulam beam leads to a more homogeneous material. The mean strength and stiffness properties of a glulam beam are thus, as stated before, increased. The strength can be further improved by manufacturing beams with higher-graded timber at higher-loaded positions. A beam in bending, for instance, could have laminations of higher strength at the outer layers. This also results in more economic use of the available wood.

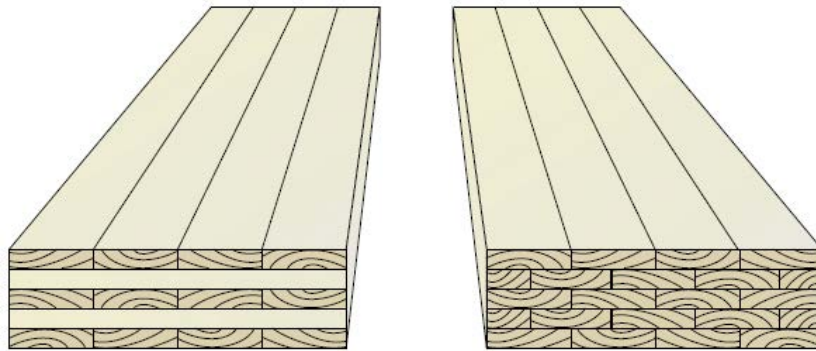


Figure 3.4: Orientation Cross-laminated timber (left) and Glued laminated timber.

Glulam is generally used as beams and columns. An advantage of glulam is that beams and columns of almost all sizes can be produced. Dimensions can theoretically be unlimited, but production halls and transportation in reality limit the dimensions. It is also possible to create a curved or tapered glulam beam, but in general straight beams are manufactured. Additionally, an advantage of glulam being prefabricated is the high dimensional accuracy. Since correct dimensions are important for rapid construction, accurate dimensions avoid delays during construction time [6].

3.3.2. Cross-laminated timber

In the 90s, universities and companies in Austria started researching and developing an innovative engineered timber product for larger panels: cross-laminated timber (CLT). Over the years, building with CLT has started to become common practice. Not only the sustainable performance but also the fast construction time due to its easy handling and its high level of prefabrication contributed to the rise of CLT.

CLT is also made from laminated solid timber. Most of the panels are made out of Norway spruce [51]. In contrast to glulam, for which the timber is orientated in the same direction, every layer is rotated 90° compared to the previous one. The layers are glued together on their wide faces and sometimes also on their narrow faces. Between three and nine layers of timber can be stacked to create CLT. Normally, the layers are orientated alternating, but special configurations do exist in which consecutive layers are orientated in the same direction. Due to the cross-laminating, it is possible to construct big panels of timber. The width of a panel can be up to 3 meters and the length up to 18 meters. Some companies do manufacture panels which exceed these dimensions. The limiting factor of the panel dimension may be imposed by transportation regulations. The bigger dimension makes CLT panels very suitable for floors and walls. Furthermore, the cross-laminating process provides high in- and out-of-plane strength and stiffness properties. Due to the alternating orientation of the timber in a CLT floor, it is capable of two-way action similar to a reinforced concrete slab [22].

3.4. High-Rise Timber Buildings

In the last years, an increased number of timber high-rise buildings have been constructed. An overview of a selection of these buildings and their heights is depicted in Figure 1.4 and an overview of the main properties is given in Table 3.1. For completeness, it is noted that high-rise timber buildings are strictly speaking 'hybrid' timber buildings. Some steel and concrete details remain required to meet building norms (floor deck layers or joint connections). However, if the main structural elements are made out of timber, the building is classified as a mass timber building. If concrete and/or steel are used in addition to timber for the structural system, the building is referred to as a hybrid timber building.

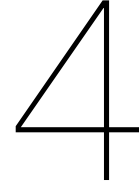
From the various timber structural designs, some conclusions can be drawn. The smaller buildings make extensive use of CLT. For taller buildings it is however necessary, considering stability, to design a concrete core. The taller buildings generally also make more use of glulam columns, instead of only CLT walls. Another trend that can be observed for taller buildings is that a hybrid system is chosen. This not only includes the aforementioned concrete core, but also hybrid concrete CLT floors, concrete

beams, and concrete/steel connections.

Compared to concrete/steel high-rise buildings, timber buildings have some different properties. As mentioned before the weight is reduced. For HAUT the weight was 30-50% lower compared to a similar concrete building [56]. Although the stiffness of timber is lower, the global stiffness of a timber building should be similar to non-timber buildings as the same stiffness is needed to comply to the Eurocode. However, concrete/steel buildings could be stiffer than necessary for the codes due to their material properties. So a stiffness comparison between timber and concrete/steel buildings could vary for each situation. Furthermore, it is assumed that the damping in timber connections is higher due to the lower rigidity. More friction will occur during vibration, which will lead to higher damping properties. This point will be further elaborated on in the next chapter.

Table 3.1: Overview properties discussed high-rise timber buildings.

	Stadthaus	Forte	Treet	Tallwood	HAUT	HoHo
Height [m]	29	32	49	58	73	85
Location	London	Melbourne	Bergen	Vancouver	Amsterdam	Vienna
Completion	2009	2013	201	2017	2022	2020
Material	Timber	Timber	Timber	Timber/concrete	Timber/concrete	Timber/concrete
Structural system	Core	Core	Truss	Core	Core+shear wall	Core+shear wall
Core	Timber	Timber	Timber	Concrete	Concrete	Concrete
Joints	Steel angle brackets	Steel angle brackets	Slotted-in steel	Hollow steel	Various	Glued reinforcement bar



Damping

Damping is the irreversible conversion of mechanical energy into other forms of energy, for instance, thermal energy or energy release to the surrounding medium [26]. In a vibrating system, the energy that is dissipated is connected to damping; it causes the amplitude decay of a vibration. As previously mentioned the exact process behind damping is not fully known. The complexity is increased by the fact that in a structure the damping depends on the amplitude the structure is excited in and the mode in which it vibrates.

There exist various methods for the modelling of damping. In this chapter, the theoretical background of the mathematical models describing the physical mechanisms of damping is described. This is done both mathematically, by presenting the appropriate equations and physically by describing the form of damping. Subsequently, the various forms of physical damping are carefully outlined. Finally, predictive models to assess the damping ratio of buildings are discussed.

4.1. Mathematical Models

Every mathematical term which enforces energy dissipation over time in a system could be a mathematical model for damping. Therefore, various models could be used to model damping in formulas. Each model has different properties which make it suitable for specific damping or calculations. The most common mathematical damping models are considered.

4.1.1. Viscous damping

The most frequently used model for damping is viscous damping, meaning that the damping force is proportional to the velocity and in the opposite direction of the displacement. The damping force F_d is thus:

$$F_d = c\dot{x} \quad (4.1)$$

The energy dissipated in one cycle during harmonic motion $x = \hat{x} \sin(\omega t)$ for viscous damping is described by [49]:

$$E_{diss} = c\pi\omega\hat{x}^2 \quad (4.2)$$

The dissipated energy is thus proportional to the damping coefficient c , frequency ω and the amplitude \hat{x} squared. Viscous damping results in a convenient linear mathematical formula, which is solved relatively easily. Although most damping is non-linear and independent of the frequency, for small oscillations and low damping, viscous damping is fairly accurate [50]. Therefore, viscous damping is the preferred damping if it is applicable.

Another way to model the damping and retain linearity is by using equivalent viscous damping. The energy dissipated from non-linear damping mechanisms is equalled to the energy dissipated from viscous damping. The equivalent viscous damping coefficient c_{eq} can thus be calculated. The equivalent

viscous damping coefficient can be used in a linear calculation which dissipates the same amount of energy during a cycle as the corresponding non-linear damping mechanism. A non-linear damping model can thus be used to derive a linear equation [49].

4.1.2. Quadratic damping

With quadratic damping, the damping is proportional to the velocity squared. This is a better approximation for systems with higher velocities. Quadratic damping is associated with the motion of a solid through a fluid or gas. The quadratic damping force is described by [49]:

$$F_d = \frac{1}{2}c|\dot{x}|\dot{x}, \quad (4.3)$$

The associated dissipated energy is stated as:

$$E_{diss} = \frac{4}{3}c\hat{x}^3\omega^2 \quad (4.4)$$

4.1.3. Friction damping

Friction damping is based on the force that occurs due to two surfaces moving relatively. Various models exist for friction damping. Here only the friction damping by Coulomb is described. The damping is only activated after a certain amount of force, after which the energy is dissipated constantly. The friction damping only depends on the friction coefficient μ and the normal force F_N [12].

$$F_d = -Sgn(\dot{x})\mu F_N \quad \text{with } Sgn(\dot{x}) = \begin{cases} 1, & \dot{x} > 0 \\ 0, & \dot{x} = 0 \\ -1, & \dot{x} < 0 \end{cases} \quad (4.5)$$

The friction damping is therefore independent of the magnitude of the displacement and the velocity. The direction of the damping force is always opposed to the direction of the displacement. The energy dissipated during a harmonic motion $x = \hat{x} \sin(\omega t)$ is equal to:

$$E_{diss} = 4\mu N\hat{x} \quad (4.6)$$

4.1.4. Hysteretic damping

In the case of hysteretic damping, the damping is independent of the frequency. In most research, it is shown that the damping of structures behaves independently of the frequency [32], but is dependent on the squared amplitude [19]. Although further research stated that a certain dependency on frequency does exist, hysteretic damping is still believed to be theoretically more accurate. Hysteretic damping is formulated by a viscous damping coefficient which is inversely proportional to the frequency ω . This results in a frequency-independent damping force

$$F_d = c\dot{x} = \frac{d}{\omega}\dot{x} \quad (4.7)$$

where d is the hysteretic damping coefficient. The energy dissipated in a cycle is given by:

$$E_{diss} = \pi d\hat{x}^2 \quad (4.8)$$

If the equivalent viscous damping coefficient is calculated by equating the dissipated energy, it can indeed be found that $c_{eq} = \frac{d}{\omega}$.

4.2. Physical Models

In reality, different damping mechanisms occur simultaneously in a structure during vibration, which exacerbates the problem. Five damping mechanisms for high-rise buildings can be determined, which all have different characteristics. Each of the mechanisms is based on different laws and therefore the determination of the total damping of a structure is very complicated. This complexity causes a unique damping ratio for each structure. The five damping mechanisms and the corresponding mathematical models are discussed briefly.

Table 4.1: Overview of mathematical damping models.

	$F_{damping}$	E_{diss}	c_{eq}
Viscous	$c\dot{x}$	$c\pi\omega\hat{x}^2$	c
Quadratic	$\frac{1}{2} \dot{x} \dot{x}$	$\frac{4}{3}c\omega^2\hat{x}^3$	$\frac{4}{3\pi}c\omega\hat{x}$
Friction	$Sgn(\dot{x})\mu N$	$4\mu N\hat{x}$	$\frac{4\mu N}{\pi\omega\hat{x}}$
Hysteretic	$\frac{d}{\omega}\dot{x}$	$\pi d\hat{x}^2$	$\frac{d}{\omega}$

4.2.1. Material damping

Material damping is an intrinsic property of each material due to energy dissipation associated with micro-structural defects. It is caused by internal friction within a material. These can, for example, occur in grain boundaries, impurities or between glued surfaces [10]. Material damping is also prominent at the foundation due to the intrinsic damping of the soil [31].

For composite materials, such as wood, four mechanisms play a role in energy dissipation:

1. Visco-elastic behaviour of the fibre materials
2. Thermo-elastic damping due to cyclic heat flow from compressive to tensile stress regions
3. Coulomb friction due to slip in unbounded areas of fibre interface
4. (Poorly understood) damping at cracked or delaminated areas

Of the four mechanisms, visco-elastic damping appears to be the dominant damping mechanism in small amplitude vibrations of composites [20].

Different mathematical models exist to model material damping. The two fundamental models are a) a single spring and b) a single dashpot. A single spring only represents the elastic property of a material and does not represent any damping, while a dashpot generates a damping force proportional to the velocity. Both are not a very accurate representation of actual material behaviour [5]. However, more accuracy — and more complexity — can be achieved through various combinations of these two.

Two-parameter models have commonly used combinations: a spring and dashpot are either placed in parallel (Maxwell) or in series (Kelvin-Voigt) to represent the material behaviour. For visco-elastic fluids, the Maxwell model can be used as a fair approximation [5]. This model, however, cannot account for internal stresses and is less accurate for any slow, time-dependent response of the structure (such as creep). Contrary, the Kelvin-Voigt model accurately describes this behaviour, as it is a good representation of a visco-elastic solid. The setback of the Kelvin-Voigt model is that no elastic response occurs during the application or release of loading and the creep rate approaches zero during long times of loading [5]. The damping force and dissipated energy are equal to that of a viscous damping model as the damping is proportional to the velocity.

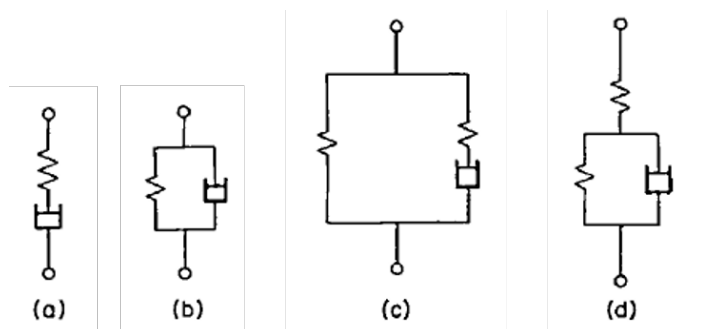


Figure 4.1: Two- and three-parameter visco-elastic models, (a) Maxwell, (b) Kelvin-Voigt, (c) and (d) three-parameter models.

For a continuous system, the damping force of a Kelvin-Voigt model corresponds to strain-rate damping, which is determined as:

$$F_d = cI \frac{\partial^5 w}{\partial x^4 \partial t} \quad (4.9)$$

In contrast to Gibson [20], Labonnote et al. [27] applied hysteretic material damping for timber. However, it has to be noted that Labonnote et al. applied it specifically for timber and Gibson only specified the type of damping for general composite materials. For an SDOF system, the hysteretic damping can be formulated by using the equivalent viscous damping c_{eq} :

$$m\ddot{x} + c_{eq}\dot{x} + kx = F(t) \quad \text{with } c_{eq} = \frac{h}{\omega} \quad (4.10)$$

However, this model was criticized because this formula does not provide a definition for ω and it violates the causality principle [7]. Various models were proposed with different drawbacks, until Ribeiro et al. [42] derived the complex stiffness:

$$m\ddot{x} + k^*x = F(t) \quad \text{with } k^* = k(1 + i\eta_s) \quad (4.11)$$

For an Euler-Bernoulli beam, the modulus of elasticity is replaced in the equation of motion by the complex modulus of elasticity in order to account for the damping.

$$E^* = E(1 + i\eta) \quad (4.12)$$

$$F_d = i\eta EI \frac{\partial^4 w}{\partial x^4} \quad (4.13)$$

In this formula, η is a loss factor which is independent of ω . It has to be noted that the damping force is complex-valued which could complicate calculations.

4.2.2. Structural damping

Energy dissipation caused by the friction between different components of a structure as they move relative to each other is called structural damping. Structural damping is also caused by impacting or intermittent contact between various components of a structure [11]. In contrast to material damping, structural damping is not only dependent on material properties but on the mechanical system as well.

To model structural damping all the mathematical models are theoretically applicable. The use of these is generally the preferred method, as viscous damping produces a linear equation of motion, which allows for relatively simple calculations.

4.2.3. Radiation damping

As buildings vibrate the soil-structure interaction causes radiation of energy waves to the soil. This is called radiation damping. Radiation damping plays an important role during earthquakes. In contrast, during regular operation of any structure, the wind-induced vibrations only cause low-frequency rocking of the foundation, which causes very low radiation damping. Thus, in the soil, the material damping normally has a larger impact than the radiation damping [3].

4.2.4. Aerodynamic damping

The difference between the velocity of the wind and the velocity of the building produces aerodynamic damping. Energy is dissipated through waves from the structure into the surrounding airflow. Generally, the aerodynamic damping — for small to moderate wind speeds — is small compared to the other damping mechanisms. Moreover, for higher wind speeds the aerodynamic damping could even become negative [23].

4.2.5. Artificial damping

Artificial damping is defined as active or passive damping added to the structures. This can, for instance, be applied in the form of a tuned mass damper. A tuned mass damper is a dynamic vibration absorber, which can mitigate the structure's vibrations if the frequency of the mass is carefully tuned [40]. Artificial damping is the only damping that can already easily be determined. The use of artificial damping in high-rise timber buildings is uncommon.

4.2.6. Total damping

Previous research has demonstrated that as energy is an additive quantity, damping is also an additive quantity [49]. For a structure which is subject to many forms of damping, the total damping, ζ_{eq} , can therefore be expressed as the sum of all damping factors:

$$\zeta_{eq} = \zeta_1 + \zeta_2 + \dots \quad (4.14)$$

4.3. Predictive Models

Over the years several models have been developed to predict the damping ratio of a building. Four different models exist: Jeary (1986), Davenport and Hill-Carroll (1986), Lagomarsino (1993), and Tamura et al. (2000). All the predictor formulas are derived from different damping databases and follow the same equation (Equation 4.15 and Equation 4.16). A baseline damping is defined to which an amplitude-dependent damping is added. The difference between the models comes from the various coefficients that are model specific. The values of the parameters for each model can be found in Figure 4.2.

$$\zeta_s(X) = \zeta_b + \zeta_c(X) \leq \zeta_{s,max} \quad (4.15)$$

$$\zeta_c(X) = \alpha X^a \quad (4.16)$$

Reference	Baseline damping ratio	Amplitude coefficient	Amplitude exponent	Maximum damping ratio
Jeary (1986)	$\zeta_b = 0.01f \approx \frac{0.46}{H}$	$\alpha = \frac{10\sqrt{0.72}}{H}$	$a = 1$	$\zeta_{s,max} = 6 \times 10^{-5}H + 0.013^b$
Davenport and Hill-Carroll (1986)	$\zeta_b = 0$	$\alpha = \frac{\alpha_1}{H^2}$	$a = \alpha_2$	(None specified) ^c
Lagomarsino (1993)	$\zeta_b = \beta_1 f + \beta_2 / f$	$\alpha = \frac{\beta_3}{H}$	$a = 1$	(None specified)
Tamura et al. (2000, 2012)	$\zeta_b = \gamma_1 f + \gamma_2 \approx \frac{\gamma_3}{H} + \gamma_2$	$\alpha = \frac{\gamma_4}{H}$	$a = 1$	$\zeta_{s,max} = \gamma_1 f + \gamma_2 + 2 \times 10^{-5} \gamma_3^d$

^a f =natural frequency, H =building height, D =horizontal building dimension, α_1, α_2 =parameters dependent upon the number of storeys and primary construction material, $\beta_1, \beta_2, \beta_3$ = parameters dependent upon primary construction material and $\gamma_1, \gamma_2, \gamma_3, \gamma_4$ =parameters dependent upon primary construction material.

^b As mentioned by Lagomarsino (1990).

^c Model suggests maximum applicability is up to $X/H \approx 10^{-2}$.

^d Evaluated at $X/H = 2 \times 10^{-2}$, which is the upper limit of measurements. The model is also intended only for amplitudes within the linear elastic limit of the structure.

Figure 4.2: Values of the parameters for the different damping predictors [4].

As shown in figure 4.2, the formulas only depend on the natural frequency, height, depth and used material. The chosen structural system of the building, however, does not influence the damping ratio calculated by these models, nor does the soil-structure interaction. Furthermore, no material constants are provided for timber buildings.

The predictor formulas are based on measurements at low amplitudes. The damping increases with higher amplitude, up to a maximum value. Aquino and Tamura [4] found that damping ratios do increase with increasing amplitudes, but up to a certain value. After this value, the damping ratio actually decreases. This only occurs if the drift ratio X/H is higher than 10^{-4} . For wind-induced vibrations the drift ratio, however, is generally below 10^{-4} , meaning that the possible decrease of the damping ratio does not occur if wind loads are applied [4].

4.3.1. Predictive values for timber structures

For timber structures, values for different types of damping are given in Petersen and Werkle [39]. The material damping is stated to be between 0.4 and 0.8%, which is almost equal to reinforced concrete (0.4 - 0.9%) and higher than steel (0.1 - 0.3%). The structural damping attributed to dowel-type connections is given as 0.6 to 0.8%, whereas glued elements contribute 0.2 - 0.4% to the total damping. An extra 0.1 - 0.3% is given by the type of support. It is stated that the secondary structure accounts for 0.1 - 0.4%. However, these are values for concrete or steel buildings. Although no specific values are available for timber structures, it is understood that non-structural components provide additional sources of damping. For example, offices generally have lower damping ratios than a similar residential building, due to the smaller number of walls [47].

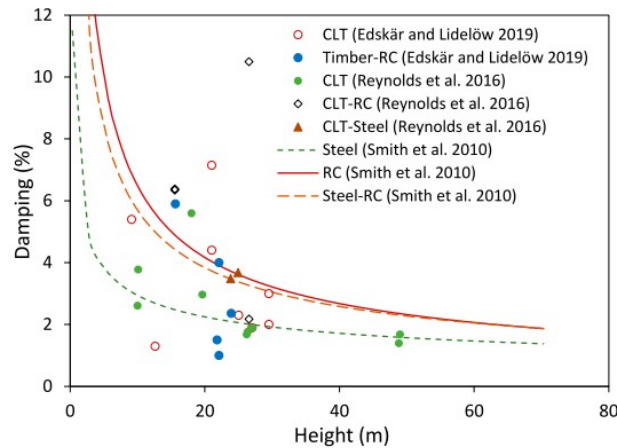


Figure 4.3: Variation of damping with height [52].

Additionally, Feldmann et al. [17] researched the damping properties of timber towers and buildings. It was observed that the damping ratio of timber towers with glued elements was lower than with dowel-type connections. This is probably due to the higher friction experienced between elements. Towers with slotted steel plate connections were found to have the highest damping ratio. The cladding of towers also increased the damping ratio by approximately 0.6%. This could be caused by the additional friction through the secondary structure. For the timber buildings, an increase in damping for buildings with concrete cores was found. The damping for buildings was higher than for towers. Once again this could be due to the non-structural elements.

From Petersen and Werkle [39], a damping ratio of 0.8 to 2.3% can be predicted for timber structures. The values found in Feldmann et al. [17] are between 0.5 and 3%. If only looked at buildings, the values range between 1.5 and 3%. However, it must be noted that only three buildings were examined all of a relatively low height of around 25 meters. It has been established that damping ratios decrease with increasing heights [31]. So for timber high-rise buildings the damping ratio probably will be lower. An overview of different timber buildings and their damping ratio is shown in Figure 4.3. The scatter for the various timber buildings is high. However, it can be concluded that a lower bound of around 1% exists.

4.4. Eurocode

In order to design a building in the Netherlands, the Eurocode is normally followed. The Eurocode provides the necessary formulas to calculate the damping and the acceleration. As mentioned before, only generic damping ratios are provided. The damping ratio is calculated in Eurocode 1 Part 4 by dividing the logarithmic decrement by 2π . The logarithmic decrement consists of three parts: structural damping (δ_s), aerodynamic damping (δ_a) and artificial damping (δ_d).

$$\delta = \delta_s + \delta_a + \delta_d \quad (4.17)$$

The logarithmic decrement is defined as:

$$\delta = \frac{1}{p} \ln \frac{x_{n+p}}{x_n} \quad (4.18)$$

In this equation x_n is the amplitude at a certain point and x_{n+p} is the amplitude at p peaks away. The damping ratio can be calculated by:

$$\zeta = \frac{\delta}{2\pi} \quad (4.19)$$

For different constructions and materials, the structural logarithmic decrement is given. Some values can be found in Table 4.2. It has to be noted that no decrement is given in the Eurocode for a timber building. However, values are given for a timber bridge. Compared to bridges made out of steel and

concrete it can be said that for most cases timber has a higher decrement. It is assumed that structural logarithmic damping is a combination of the material and structural damping from the physical models. The material damping is probably already included, because for different materials different damping values are found.

Table 4.2: Structural logarithmic damping for various constructions [15].

Structure	Structural damping (δ_s)
Reinforced concrete building	0.10
Steel building	0.05
Steel/concrete construction	0.08
Steel bridge with regular bolts	0.05
Concrete bridge without cracks	0.04
Concrete bridge with cracks	0.10
Timber bridge	0.06-0.12

The aerodynamic decrement can be derived by using the following equation:

$$\delta_a = \frac{c_f \cdot \rho \cdot v_m(z_s)}{2 \cdot n_1 \cdot \mu_e} \quad (4.20)$$

where c_f is the force coefficient, μ_e is the equivalent mass, $v_m(z_s)$ is the mean wind speed at height z_s and n_1 is the first natural frequency.

The last decrement only has to be calculated if artificial damping is added to the structure. Due to the nature of this damping — carefully tuned — it is possible to derive this value relatively accurately, either theoretically or experimentally.

The soil-structure interaction is not taken into account in the derivation of total damping in the Eurocode. It is unknown if the soil material damping and the radiation damping are included in the total material damping. If this is not the case, this would be reasonable for the radiation damping as this has minimal impact on the structure. For the soil material damping, this may not be the case.

4.5. Damping Identification Methods

Various methods exist to identify the damping in a structure. Some of these methods are discussed in the following section.

4.5.1. Logarithmic decrement

The logarithmic decrement method can be applied to structures in free vibration. The ratio between different amplitudes is calculated by using equation 4.18. This method is simple to use and thus frequently applied. However, as it is often found that damping is amplitude dependent, the logarithmic decrement will vary for higher amplitude vibrations. If different peaks are inserted in the formula, different damping ratios could be obtained. It is also found that applying this method to timber did not yield consistency and repeatable results [26].

4.5.2. Envelope fitting

Another method which could be applied to free vibrations is envelope fitting. The peaks of the decaying motion are enveloped by a function in the form of:

$$X(t) = A \exp(-\zeta \omega_n t) \quad (4.21)$$

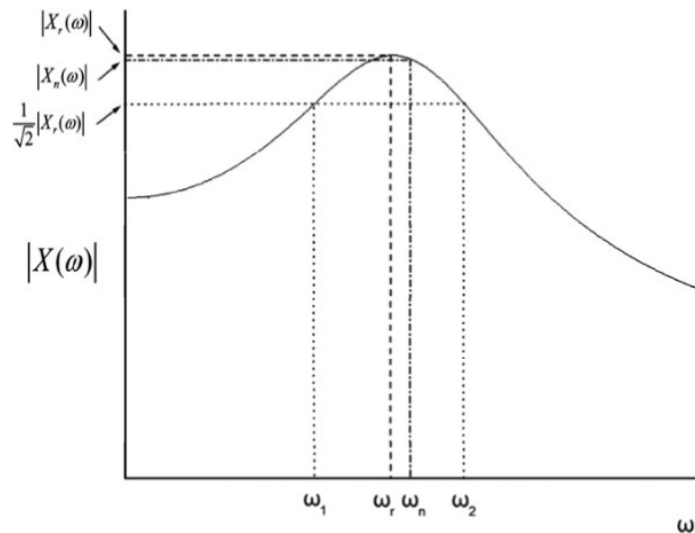


Figure 4.4: The half-power bandwidth method for estimation of the damping ratio [38].

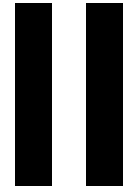
The accuracy is higher than for the logarithmic decrement as all peaks are taken into consideration. Nonetheless, both methods have similar drawbacks. They only base information about damping on a limited amount of data: at the peaks. Furthermore, the accuracy depends highly on the sampling rate. With a low sampling rate, the peaks could become less accurate leading to a misinterpretation of where the actual peaks are [26].

4.5.3. Half-power bandwidth method

The half-power bandwidth method is based on the frequency domain. In the frequency response function, the peak of the resonance frequency serves as starting point. For low-damped systems the damping ratio is determined by [38]:

$$\zeta \approx \frac{\omega_2 - \omega_1}{2\omega_r} \quad (4.22)$$

In this equation, ω_r is equal to the resonance frequency in the frequency response function. The values for ω_1 and ω_2 correspond to the two frequencies at $\frac{1}{\sqrt{2}}$ of the peak resonance value as demonstrated in Figure 4.4. This method is very sensitive to the accuracy of the resonance peak and thus the sampling rate [26]. Furthermore, problems arise if two closely spaced frequencies exist.



Theoretical Basis Energy-Approach

5

Dynamics

Structural dynamics constitutes the analysis of structures subject to time-dependent forces [34]. In this section, the dynamic behaviour of a simple degree of freedom system is described to illustrate how damping affects vibrating motion. Next, the system is expanded to a continuous system and two different beam equations of motion (Euler-Bernoulli and Timoshenko) are used to describe the damping dynamic response of a cantilevered beam system in preparation for the energy-based approach to damping. Only the equations of motion and the solutions are given in this chapter. The full derivations can be found in Appendix C.

5.1. Single Degree of Freedom

Single-degree-of-freedom systems consist of a mass which can vibrate in only one direction. The system is generally represented by a mass, spring and dashpot. If no external force is present and the system is excited by an initial displacement or velocity, the system is in a state of free vibration. The equation of motion is described by [34]:

$$m\ddot{x} + c\dot{x} + kx = 0 \quad (5.1)$$

In the equation, m represents mass, c viscous damping coefficient and k spring stiffness. x denotes the displacement in the direction of the degree of freedom.

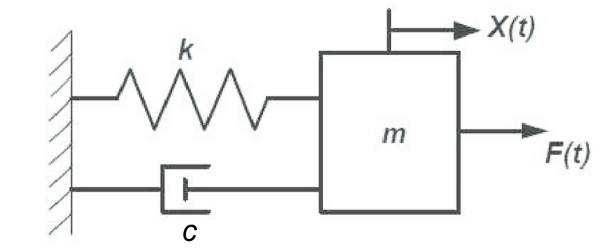


Figure 5.1: Single degree of freedom.

If the damping coefficient is small relative to the spring constant ($n < \omega_n$), the mass is vibrating and represents damped free vibrations. The displacement is described by:

$$x(t) = A_0 \exp(-nt) \cos(\omega_i t - \phi_0)$$
$$\text{with } n = \frac{c}{2m}, \quad \omega_i = \sqrt{\omega_n^2 - n^2}, \quad \omega_n = \sqrt{\frac{k}{m}} \quad (5.2)$$
$$A_0 = \sqrt{x_0^2 + \left(\frac{v_0}{\omega_1} + \frac{nx_0}{\omega_1}\right)^2}, \quad \phi_0 = \arctan\left(\frac{v_0 + nx_0}{x_0\omega_1}\right)$$

From Equation C.8 it is clear that the vibration of the mass is enveloped by $A_0 \exp(-nt)$ as is shown in Figure C.2. The rate of decay depends on the value of n .

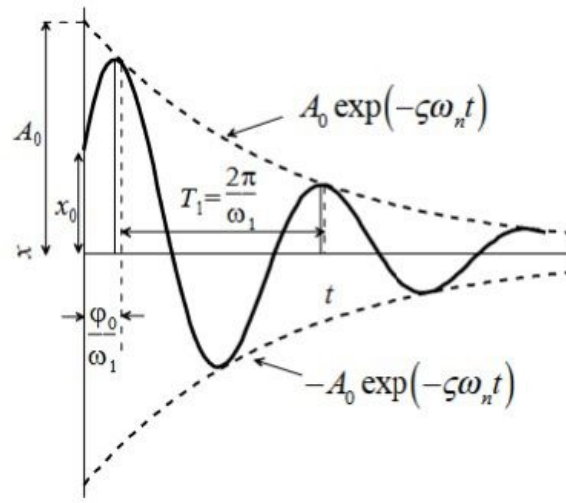


Figure 5.2: Displacement-time curve of damped free vibrations.

5.2. Continuous Models

Two different models for describing the motion of a beam are discussed in this section: Euler-Bernoulli and Rayleigh. Both are differential equations in which the manner of support is not included, because the differential equations make use of an infinitesimal part of the beam. The supports are introduced by means of imposing boundary conditions.

5.2.1. Euler-Bernoulli beam

The bending of an Euler-Bernoulli beam is described by the following fourth-order partial differential equation [34]:

$$EI \frac{\partial^4 w(x, t)}{\partial x^4} + \rho A \frac{\partial^2 w(x, t)}{\partial t^2} = f(x, t) \quad (5.3)$$

It is important to note that a few assumptions were made in order to simplify the model. The first assumption is that the cross-section remains perpendicular to the neutral line. Therefore, no shear deformation is taken into account. It is also assumed that plane cross-sections remain plan, meaning that the strain is linear over the height of the beam. Lastly, the rotational inertia has not been taken into account in the Euler-Bernoulli beam. By making use of these assumptions, the equation is simplified but still accurate for slender beams and low natural frequencies.

The solution for a free vibrating cantilever beam is described by:

$$w(x, t) = \sum_{n=1}^{\infty} W_n(x) \sin(\omega_n t + \phi_n) \quad (5.4)$$

$$\text{with } \omega_n = \beta_n^2 \sqrt{\frac{EI}{\rho A}}$$

$$\text{and } W_n(x) = A_n \left(\frac{\cosh \beta_n x - \cos \beta_n x}{\cosh \beta_n L + \cos \beta_n L} - \frac{\sinh \beta_n x - \sin \beta_n x}{\sinh \beta_n L + \sin \beta_n L} \right) \quad (n = 1, 2, \dots)$$

The values for A_n and ϕ_n are still unknown but can be derived by the initial conditions. For an initial displacement, the boundary conditions are as follows:

$$\begin{aligned} w(L, 0) &= a \\ \frac{\partial w(L, 0)}{\partial t} &= 0 \end{aligned} \quad (5.5)$$

This will lead to

$$\begin{aligned} w(x, t) &= \sum_{n=1}^{\infty} W_n(x) \cos(\omega_n t) \\ \text{with } A_n &= \frac{a}{\psi_n(L)} \end{aligned} \quad (5.6)$$

Damping

In the above equations of motion, no damping was included. The described beams would thus vibrate indefinitely. Therefore, a term must be added in order to account for the damping. As discussed in Chapter 4, different terms may be added to account for energy dissipation. Two models are elaborated on in this section: Kelvin-Voigt damping and viscous damping along the beam. The resulting equation of motion of a clamped beam with Kelvin-Voigt damping is hence formulated as:

$$\left(E + E^* \frac{\partial}{\partial t} \right) I \frac{\partial^4 w(x, t)}{\partial x^4} + \rho A \frac{\partial^2 w(x, t)}{\partial t^2} = f(x, t) \quad (5.7)$$

The solution for this equation of motion can be found as:

$$\begin{aligned} w(x, t) &= \sum_{n=1}^{\infty} W_n(x) \exp^{-B\zeta\omega t} \cos(\omega_1 t - \phi) \\ \text{with } \omega_1 &= \omega \sqrt{B - B^2\zeta^2} \quad \text{and} \quad B = \frac{\int_0^L W_n''(x)^2 dx}{\int_0^L W_n(x)^2 dx} \end{aligned} \quad (5.8)$$

For a beam modelled with viscous dampers along its length, the equation of motion slightly differs.

$$\begin{aligned} \omega_n^2 \frac{\partial^4 w(x, t)}{\partial x^4} + \frac{\partial^2 w(x, t)}{\partial t^2} + 2\zeta\omega_n \frac{\partial w(x, t)}{\partial t} &= 0 \\ \text{with } \zeta &= \frac{c}{2\beta^2 \sqrt{\rho A E I}} \quad \text{and} \quad \omega_n^2 = \beta^4 \frac{E I}{\rho A} \end{aligned} \quad (5.9)$$

The displacement is then described by:

$$\begin{aligned} w(x, t) &= \sum_{n=1}^{\infty} W_n(x) \exp^{-\zeta\omega t} \cos(\omega_1 t - \phi) \\ \text{with } \omega_1 &= \omega \sqrt{B - \zeta^2} \end{aligned} \quad (5.10)$$

To determine A_n and ϕ_n the boundary conditions as given in equation 5.5 can be imposed.

5.2.2. Timoshenko beam

Lord Rayleigh introduced the effect of rotary inertia to the beam theory by Euler-Bernoulli. Subsequently, the influence of shear deformation was added by Timoshenko. The result is a coupled linear partial differential equation with the dependent variables w , the lateral displacement, and ϕ , the angle of the cross-section to the neutral plane.

$$\begin{aligned} \rho A \frac{\partial^2 w}{\partial t^2} - q(x, t) &= kGA \left(\frac{\partial^2 w}{\partial x^2} - \frac{\partial \phi}{\partial x} \right) \\ \rho I \frac{\partial^2 w}{\partial t^2} &= \frac{\partial}{\partial x} \left(EI \frac{\partial \phi}{\partial x} \right) + kGA \left(\frac{\partial w}{\partial x} - \phi \right) \end{aligned} \quad (5.11)$$

In this equation k is the shear coefficient, which takes into account the variation of shear stresses across the cross-section and depends on its geometry. For a rectangular cross-section, this is generally taken as $5/6$. G is the shear modulus and I the second moment of inertia. For a linear, isotropic, homogeneous beam of constant cross-section, the two coupled differential equations can be combined:

$$EI \frac{\partial^4 w}{\partial x^4} + m \frac{\partial^2 w}{\partial t^2} - \left(\rho I + \frac{EI m}{kGA} \right) \frac{\partial^4 w}{\partial x^2 \partial t^2} + \frac{m \rho I}{kGA} \frac{\partial^4 w}{\partial t^4} = q(x, t) + \frac{\rho A}{kGA} \frac{\partial^2 q}{\partial t^2} - \frac{EI}{kGA} \frac{\partial^2 q}{\partial x^2} \quad (5.12)$$

For free vibrations, this simplifies to:

$$EI \frac{\partial^4 w}{\partial x^4} + m \frac{\partial^2 w}{\partial t^2} - \left(\rho I + \frac{EI m}{kGA} \right) \frac{\partial^4 w}{\partial x^2 \partial t^2} + \frac{m \rho I}{kGA} \frac{\partial^4 w}{\partial t^4} = 0 \quad (5.13)$$

5.3. Torsional Vibration

If a torque is applied to a column, torsion will occur. For a circular cross-section, the cross-section will remain plane during the torsion. However, for a non-circular cross-section warping will occur. Warping is the phenomenon where the cross-section distorts during torsion; the cross-section does not remain plane. If warping is neglected and the column is homogeneous the equation of motion is [34]:

$$\rho J \frac{\partial^2 \psi}{\partial t^2} - GJ_t \frac{\partial^2 \psi}{\partial x^2} = m_i \quad (5.14)$$

The solution to the equation of motion can be represented by the multiplication of a time-dependent part and a space-dependent part.

$$u(x, t) = U(x)\Psi(t) \quad (5.15)$$

This solution is substituted into the equation of motion. Two solutions follow one for the function dependent on time and the function dependent on spatial coordinates. They are given by:

$$\begin{aligned} \Psi(t) &= A \sin(\omega t) + B \cos(\omega t) \\ U(x) &= C \sin(\beta x) + D \cos(\beta x) \end{aligned} \quad (5.16)$$

A boundary condition at $x = 0$ is determined and at $x = L$,

$$\phi(0) = 0 \quad \text{and} \quad GJ_t \frac{\partial \psi(L)}{\partial x} = 0 \quad (5.17)$$

With the use of the boundary and initial conditions, the unknown constants A, B, C and D can be determined.

5.4. Axial Vibration

The equation of motion for axial vibration is very similar to that of torsional vibration. By substituting the rotational parameters with parameters associated with axial motion, the equation of motion is derived.

$$\rho \frac{\partial^2 u}{\partial t^2} - E \frac{\partial^2 u}{\partial x^2} = 0 \quad (5.18)$$

The same holds for the boundary conditions.

$$u(0) = 0 \quad \text{and} \quad EA \frac{\partial u(L)}{\partial x} = 0 \quad (5.19)$$

5.5. Selected Beam Models

In the remainder of this thesis, the Euler-Bernoulli beam model is used for simplicity, while the analysis of the Timoshenko beam is beyond the scope of this research. As the experiment will be conducted on a slender beam and at low frequencies, it is assumed that the Euler-Bernoulli beam will be accurate. Although the EB theory assumes isotropic behaviour, it is still decided to apply this theory to timber, which is an anisotropic material. It is expected to yield satisfactory results, but further research should

confirm this assumption.

For the torsional vibration, warping will be neglected. As a square cross-section is used, the occurred warping will not be so big. Besides, warping will make the calculations unnecessarily complex at this stage.

6

Energy

This chapter introduces the energy-based method used for identifying damping. The energy balance equations for lateral, torsional, and axial vibrations of an Euler-Bernoulli beam have been derived.

Energy (E) is defined as the capacity to do work. Work is defined as the force applied to a mass times the displacement due to that force. A clear distinction between energy and work exists: energy is 'possessed' by the system and forces in the system 'perform' work. Energy cannot be generated or lost, but can only change form. Work is done when energy changes form. The mechanical energy of a column consists of kinetic (K) and potential (P) energy. In a vibrating system, energy is dissipated by irreversibly converting mechanical energy into other forms. All energy that is dissipated during vibration is ascribed to damping.

Kinetic energy is the energy of an object due to its motion. For a mass m with a velocity v the kinetic energy can be determined as:

$$K = \frac{1}{2}mv^2 \quad (6.1)$$

The capacity to perform work because of its configuration or position is called potential energy. The potential energy can consist of different sorts of energy. A mass with a certain height to a reference position possesses energy due to gravity. For this research, elastic energy is of interest. Elastic energy refers to the energy that an elastic object stores when a force is applied to deform it. This energy remains stored until the force is released, causing the object to return to its initial shape, doing work in the process. For a spring this leads to:

$$P = \frac{1}{2}kx^2 \quad (6.2)$$

The elastic potential energy is always related to an elastic stiffness constant and an associated deformation.

6.1. Energy Flow Analysis

The energy flow analysis is a tool to determine the flow of energy in a structure. For a segment of a structure, the balance of energy is formulated. The variation in energy over time in such a segment is equal to the energy entering or exiting the boundaries (energy flux S) plus the dissipated energy (W_{diss}) [46].

$$\frac{dE(t)}{dt} = S(x, t)|_{x-\Delta L}^{x+\Delta L} + W_{\text{diss}}(t) \quad (6.3)$$

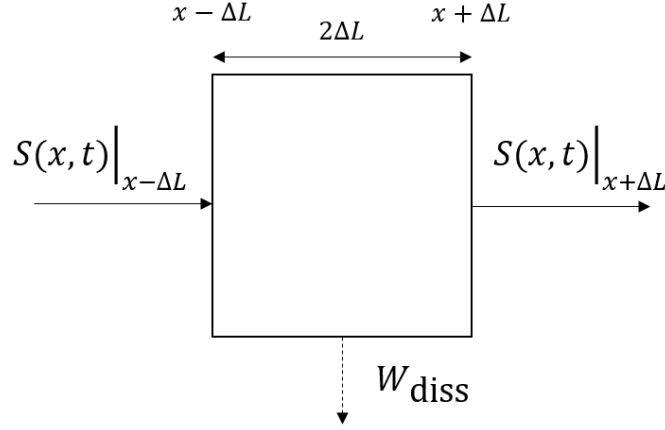


Figure 6.1: Energy balance of segment with width $2\Delta L$ and boundaries $x - \Delta L$ and $x + \Delta L$.

The energy flux crossing the boundaries of the segment is equal to the power that is transmitted in the structure. For a transversely vibrating beam, this is done by two internal mechanisms: the shear force and the moment. The power transmitted by the shear force is equal to the shear force times the velocity. The moment times the angular velocity is the power associated with the moment [59]. So for an EB beam, the following relation for the energy flux exists:

$$S(x, t)|_{x-\Delta L}^{x+\Delta L} = q_s + q_m \quad (6.4)$$

$$q_s = EI \frac{\partial^3 w}{\partial x^3} \frac{\partial w}{\partial t} \quad (6.5)$$

$$q_m = EI \frac{\partial^2 w}{\partial x^2} \frac{\partial^2 w}{\partial x \partial t} \quad (6.6)$$

The dissipated energy consists of all the terms associated with the damping and loss factors. These depend on the chosen mathematical models for the structure. If the total energy and the energy flux can be derived, it is possible to calculate the dissipated energy and therefore the damping and loss factors.

6.2. Energy Balance Equation

For a system where no energy crosses the boundaries and no external energy is introduced by external loads, the energy balance is given by:

$$\frac{dE(t)}{dt} = W_{\text{diss}}(t) \quad (6.7)$$

So, the change in energy over time at t is equal to the dissipated energy at t . Because no energy is added or lost at the boundaries, the rate of energy must be equal to the dissipation. Subsequently, it follows that the difference in energy in a certain period is equal to the total dissipated energy:

$$E(t) \Big|_{t_0}^{t_0+t} = \int_{t_0}^{t_0+t} W_{\text{diss}}(t) dt \quad (6.8)$$

This equation demonstrates that the energy present in the system at time t is equivalent to the initial energy of the system at t_0 minus the energy that has been dissipated over time.

$$E(t_0 + t) = E(t_0) - \int_{t_0}^{t_0+t} W_{\text{diss}}(t) dt \quad (6.9)$$

The energy balance equation is provided for the three vibration cases in the following subsections. If the displacement and its corresponding derivatives are known, the energy can be calculated at a given time.

6.2.1. Lateral vibration

The energy of an Euler-Bernoulli bending beam can be described by:

$$E(t) = \int_0^L \left[\frac{1}{2} \rho A \left(\frac{\partial w(x,t)}{\partial t} \right)^2 + \frac{1}{2} EI \left(\frac{\partial^2 w(x,t)}{\partial x^2} \right)^2 \right] dx \quad (6.10)$$

From the energy balance equations follows that:

$$W_{\text{diss}}(t) = \frac{d}{dt} \int_0^L \left[\frac{1}{2} \rho A \left(\frac{\partial w(x,t)}{\partial t} \right)^2 + \frac{1}{2} EI \left(\frac{\partial^2 w(x,t)}{\partial x^2} \right)^2 \right] dx \quad (6.11)$$

This equation describes the energy dissipation per unit of time in the system. To determine the total dissipated energy for a given time period, the following equation is used:

$$\int_{t_0}^{t_0+t} W_{\text{diss}}(t) dt = \int_0^L \frac{1}{2} \rho A \left(\frac{\partial w(x,t)}{\partial t} \right)^2 dx \Big|_{t_0}^{t_0+t} + \int_0^L \frac{1}{2} EI \left(\frac{\partial^2 w(x,t)}{\partial x^2} \right)^2 dx \Big|_{t_0}^{t_0+t} \quad (6.12)$$

6.2.2. Torsional vibration

The energy of a torsional beam is given by:

$$E(t) = \int_0^L \left[\frac{1}{2} \rho J \left(\frac{\partial \psi(x,t)}{\partial t} \right)^2 + \frac{1}{2} G J_t \left(\frac{\partial \psi(x,t)}{\partial x} \right)^2 \right] dx \quad (6.13)$$

Subsequently, the energy rate can be determined.

$$W_{\text{diss}}(t) = \frac{d}{dt} \int_0^L \left[\frac{1}{2} \rho J \left(\frac{\partial \psi(x,t)}{\partial t} \right)^2 + \frac{1}{2} G J_t \left(\frac{\partial \psi(x,t)}{\partial x} \right)^2 \right] dx \quad (6.14)$$

The dissipated energy for a specific time period is described by:

$$\int_{t_0}^{t_0+t} W_{\text{diss}}(t) dt = \int_0^L \frac{1}{2} \rho J \left(\frac{\partial \psi(x,t)}{\partial t} \right)^2 dx \Big|_{t_0}^{t_0+t} + \int_0^L \frac{1}{2} G J_t \left(\frac{\partial \psi(x,t)}{\partial x} \right)^2 dx \Big|_{t_0}^{t_0+t} \quad (6.15)$$

6.2.3. Axial vibration

The energy of a rod can be described as:

$$E(t) = \int_0^L \left[\frac{1}{2} \rho A \left(\frac{\partial u(t)}{\partial t} \right)^2 + \frac{1}{2} EA \left(\frac{\partial u(t)}{\partial x} \right)^2 \right] dx \quad (6.16)$$

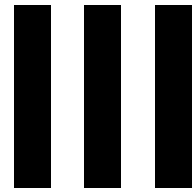
The energy dissipation per unit of time is thus given by:

$$W_{\text{diss}}(t) = \frac{d}{dt} \int_0^L \left[\frac{1}{2} \rho A \left(\frac{\partial u(t)}{\partial t} \right)^2 + \frac{1}{2} EA \left(\frac{\partial u(t)}{\partial x} \right)^2 \right] dx \quad (6.17)$$

To determine the total dissipated energy during a time period, the following equation can be used.

$$\int_{t_0}^{t_0+t} W_{\text{diss}}(t) dt = \int_0^L \frac{1}{2} \rho A \left(\frac{\partial u(t)}{\partial t} \right)^2 dx \Big|_{t_0}^{t_0+t} + \int_0^L \frac{1}{2} EA \left(\frac{\partial u(t)}{\partial x} \right)^2 dx \Big|_{t_0}^{t_0+t} \quad (6.18)$$

Having derived the three fundamental energy balance equations, everything is now set up for answering the research question through experiments.



Experiment on Timber Column

7

Experiment Setup

To determine the energy dissipation of a cantilever beam, the setup for the experiment is introduced in this chapter. Firstly, the setup of the physical model has to be established in line with the research questions. Next, an analytical representation has to be made to calculate the energy flow in the model. An overview of the steps necessary to derive the energy dissipation is given in Figure 7.1. The left part (green) of the flowchart describes the actions in the physical model. The numeral steps executed by a script, in this case MATLAB, can be found in the middle column (blue). Lastly, the right column (orange) consists of the mathematical steps of the process, which are mainly discussed in Chapter 6.

Due to circumstances, the experiments could not be conducted in a professional lab environment. Therefore, an alternative experiment setup was carried out in a home setting. The first sections (Section 7.1 to 7.3) discuss the experiments as if they would be performed at the lab. In Section 7.4 a description is given about the alternative setup at home.

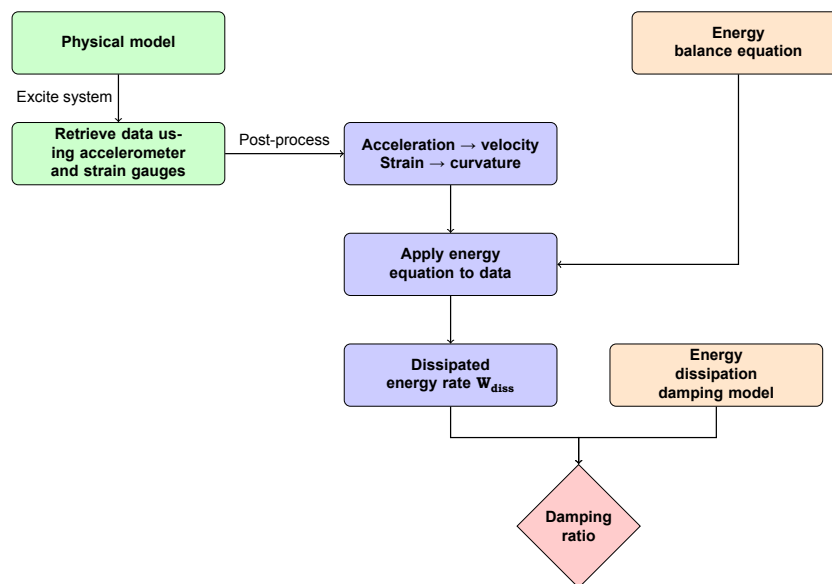


Figure 7.1: Flowchart assessing damping with energy-based approach.

7.1. General Physical Model Setup

As stated in Chapter 1, the aim of the study is to investigate the energy dissipation in a clamped timber column in the first mode. The type of wood used in this experiment is spruce and the column's cross-section is rectangular. The damping will be observed under axial, lateral and torsional loading. For the lateral and torsional directions, an initial displacement or rotation is imposed at the top of the column

and after release, free vibration occurs in the column. The system will predominantly vibrate in the first mode. A hammer impact is used to excite the system during the axial vibration tests. During the experiments, the vibrations are measured by two sensors: an accelerometer and a strain gauge. The acceleration will vary from zero at the clamp to the maximum value at the top and vice versa for the curvature. Therefore, the accelerometer is mounted at the top, while the strain gauge is attached to the bottom. An overview of the experimental setup is presented in Figure 7.2.

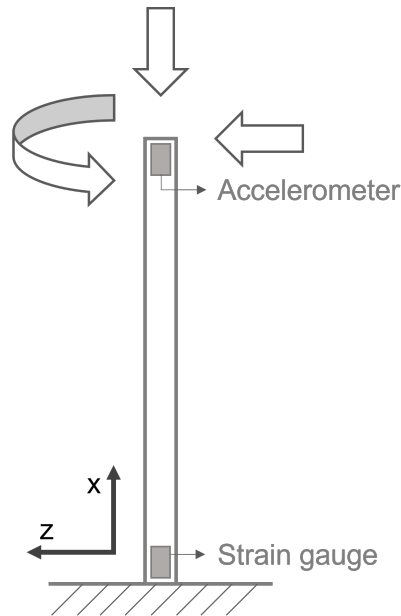


Figure 7.2: Setup of the model.

7.2. General Numerical Setup

After the experiments are conducted, the data from the accelerometer and strain gauge can be retrieved. To complete the energy equation and only have the dissipated energy as unknown, the velocity and the curvature must be derived (see Section 6.2). Depending on the data, some post-processing may be necessary to clean up the data. To obtain the velocity, the acceleration is integrated. For the curvature, the derivative with respect to x is taken. With the velocity and curvature established, the energy balance equation can be applied and the energy dissipation rate for the system can be calculated.

7.3. General Analytical Setup

The aforementioned energy balance equations (Section 6.2) are applied to obtain the dissipated energy. The last step is to determine the corresponding damping values. All the dissipated energy is associated with the damping of the system. As for different types of modelled damping the energy loss can be determined, and the damping values thus can be calculated. For viscous damping, it holds that:

$$W_{\text{diss}}(t) = c \int_0^L \left(\frac{\partial w(x,t)}{\partial t} \right)^2 dx \quad (7.1)$$

so that

$$c = \frac{\int_t W_{\text{diss}}(t) dt}{\int_t \int_0^L \left(\frac{\partial w(x,t)}{\partial t} \right)^2 dx dt} \quad (7.2)$$

By combining this with the following equation, the damping ratio can be found.

$$\zeta = \frac{c}{2\beta^2 \sqrt{\rho A E I}} \quad (7.3)$$

In the same manner, the damping constant for Kelvin-Voigt damping can be determined.

$$E^* = \frac{\int_t W_{\text{diss}}(t) dt}{\int_t \int_0^L \frac{\partial^5 w(x,t)}{\partial x^4 \partial t} \frac{\partial w(x,t)}{\partial t} dx dt} \quad (7.4)$$

$$\zeta = \frac{E^* I}{2\beta^2 \sqrt{\rho A E I}} \quad (7.5)$$

7.4. Conducted Experiment

As mentioned earlier, a modified experiment setup was executed in a home setting. Not surprisingly, the setup had its limitations and was therefore prone to more inaccuracies.

The energy dissipation due to two different loading directions was examined: axial and lateral. All displacements or loads were only applied initially, resulting in a free vibrating column. The axial load was performed by a hammer impact on the top of the timber column. The lateral load was applied in the form of a forced displacement. The biggest difference in the setup compared to the original setup was the absence of a strain gauge. Hence, the curvature could not directly be determined using the obtained data, which altered the process. The adjusted flowchart can be found in Figure 7.3.

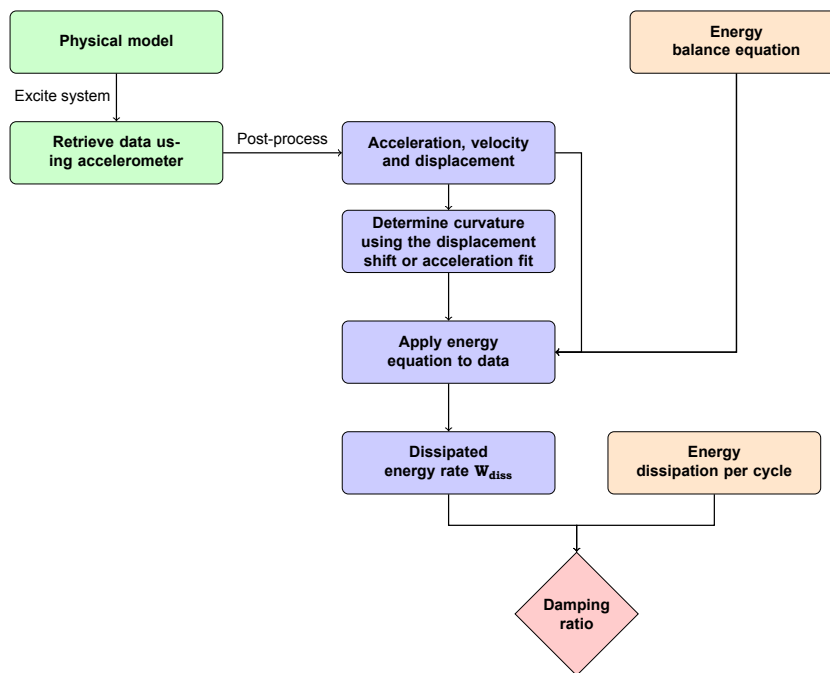


Figure 7.3: Flowchart assessing damping from conducted experiments.

7.4.1. Physical model setup

A physical “Do It Yourself” model was built in the form of a clamped column. Rectangular timber sections were cast in a twenty-centimetre-thick, concrete foundation. Three long, square pieces of FSC-certified, untreated pine wood were purchased at a local DIY shop in The Netherlands. Table 7.1 presents the properties and design values of all timber beams used during the experiment.

Table 7.2: Overview of four different experimental setups.

Setup	Beam	Free standing length [m]	Position accelerometer [m]
1	1	0.405	0.375
2	1	1.908	1.878
3	2	1.915	1.885
4	3	1.915	1.885

Table 7.1: Properties of timber samples used in the experiments.

Beam	Mass [kg]	Length [kg]	Cross section [mm]	ρ [kg/m ³]	m [kg/m]	I [mm ⁴]	A [m ²]
1	2.42	2.7	44x44	463	0.90	312341	1940
2	1.19	2.1	34x34	490	0.57	111361	1156
3	0.64	2.1	27x27	419	0.31	44287	729

Setup configurations

Four different configurations, referred to as setups, were built. To easily investigate the impact of natural frequency and varying amplitude three different clamped columns with decreasing cross-sections but identical lengths were selected. In addition, a short stubby test piece with only 40cm free-standing length was added to mimic a very stiff column. Once all four test columns were prepared, the 20cm concrete foundation was poured. The resulting, four, parallel, experimental set-ups are presented in Table 7.2 and Figure 7.4.

For each of the four set-ups, three different tests were conducted. To assess consistency and allow limited statistical analysis, each of the twelve tests was repeated five times, resulting in a total of sixty simulations. As setup 1 was shown too stiff to be manually displaced it was decided to use this setup for the axial test. The axial vibration was induced by striking with a rubber hammer weighing approximately 360 grams. For setups 2, 3 and 4, which could be bent manually to a defined amplitude, initial offsets of 0.5 cm, 1 cm and 2 cm were chosen. Initial offsets were measured as shown in Figure 7.5. Due to the limitations of the at-home lab, the imposed initial displacement is not very precise and could be off by a few millimetres.



Figure 7.5: Setting initial displacement.

Table 7.3 summarizes the final test programme executed for this research. With an average test duration of approximately one minute, all sixty tests were carried out over a period of two days: 4th and 5th of January 2023. The average room temperature recorded during the tests was 18°C and the humidity

50%.

Table 7.3: Test programme for 60 experiments of the study.

Setup	Test	Version	Loading	Direction	Vibration magnitude
1	1	1-5	Bending	z-axis	small
1	2	1-5	Bending	z-axis	medium
1	3	1-5	Axial	x-axis	medium
2	1	1-5	Bending	z-axis	± 0.5 cm
2	2	1-5	Bending	z-axis	± 1.0 cm
2	3	1-5	Bending	z-axis	± 2.0 cm
3	1	1-5	Bending	z-axis	± 0.5 cm
3	2	1-5	Bending	z-axis	± 1.0 cm
3	3	1-5	Bending	z-axis	± 2.0 cm
4	1	1-5	Bending	z-axis	± 0.5 cm
4	2	1-5	Bending	z-axis	± 1.0 cm
4	3	1-5	Bending	z-axis	± 2.0 cm

Accelerometer

The accelerometer mounted on the test columns was the commercially available, Witmotion Shenzhen Corporation, BWT901CL sensor. This AHRS IMU sensor measures 3-axis angle, angular velocity,



Figure 7.4: The physical models: four clamped columns. Note that the adopted set-up numbering 1 - 4 is in the picture from right to left; the column on the right is the stiffest (setup 1), ending with the most flexible (setup 4) on the left.

acceleration and magnetic field. Set at an output ratio of 200Hz it measured and recorded all data in time steps of 5ms. As it is a relatively small and light sensor — approximately 4cm width by 6cm height — it could be easily fixed to the top of the column without concerns that it would (materially) impact results, as shown in Figure 7.6. Similarly, its Bluetooth 2.0 connection, avoids the risk of cable motions or weight as all measurements are wireless transmitted to the PC.



Figure 7.6: The accelerometer used in the experiments.

Technical details and selected settings of the BWT901CL accelerometer are provided in Table 7.4. The accelerometer was outfitted with an automatic detection and calibration feature to create zero bias. The orientation of the axis system was confirmed before conducting the experiments.

Table 7.4: Technical specification BWT901CL.

Witmotion BWT 901CL Mini IMU v.6.2.69	
Witmotion Firmware	version V18426
Calibration bias	0
Working Temperature	-40~85 °C
Data output frequency	200 Hz
Range Acceleration	±16 g
Resolution Acceleration	0.005 g
Angle Accuracy	0.05° (Static) – 0.1° (Dynamic)
Baud Rate	115200
Weight	15 gram

7.4.2. Numerical model

Because of the absence of a strain gauge, the curvature had to be derived numerically. Two methods were proposed: displacement based and acceleration based. For the first method, the displacement

was calculated by integrating the acceleration twice. With the use of the Euler-Bernoulli beam theory, the associated curvature for each displacement could be found.

The second method was based on the acceleration data. The acceleration of the theoretical Euler-Bernoulli beam was fitted to the retrieved acceleration. Hence, the theoretical curvature of the Euler-Bernoulli beam could be determined at each time step and used as input data for the energy balance equations.

7.5. Expected Vibration Behaviour

After the release of the column, it is expected to vibrate freely with decaying amplitude. With the help of the EB beam theory, the vibrations and corresponding energy flow can be predicted. The column's oscillation is depicted in Figure 7.7 and in Figure 7.8 the associated energy is shown. Figure 7.8a clearly illustrates the decrease of energy in the system over time. The kinetic energy depends on the velocity whereas the curvature determines the potential energy. The column's position with respect to its equilibrium state determines the values of curvature and velocity. During the free vibration of a column, the maximum value of the velocity is at its equilibrium state, whilst being zero at maximum excitation. For the curvature, the inverse applies. Consequently, the kinetic and potential energy fluctuates between a maximum value and zero out of phase, which can be observed more closely in Figure 7.8b. This figure also illustrates that no energy dissipates if the potential energy is at its highest. An explanation for this behaviour can be given by the fact that the velocity is zero at this point. Therefore, the column is stationary at this moment in time, so no energy is dissipated. Figure 7.9 demonstrates this behaviour very clearly.

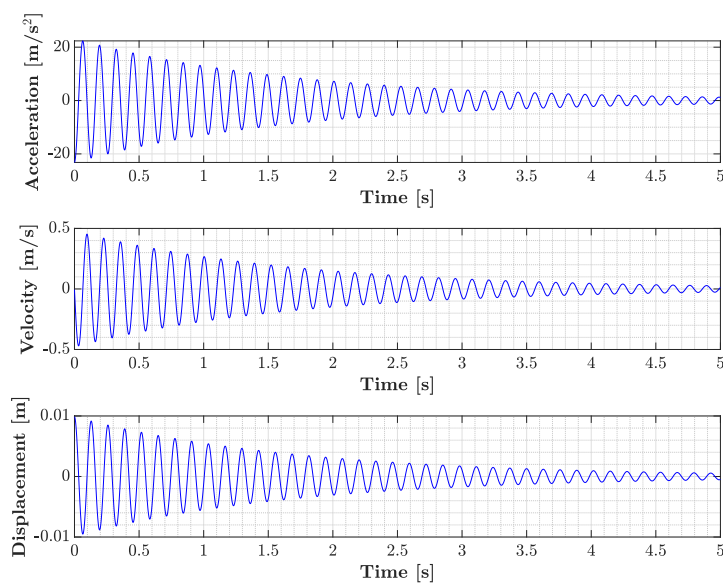


Figure 7.7: Acceleration, velocity and displacement for damped free vibrating clamped EB beam with an initial displacement

Furthermore, the initial energy in the system at $t = 0$ could be predicted. The initial energy consists only of potential energy as the velocity is equal to zero. The curvature was determined theoretically using the matlab script for the three initial displacements and setups. Therefore, the potential energy at $t = 0$ could be calculated. This resulting initial for the planned experiments on setups 2, 3 and 4 is presented in Table 7.5.

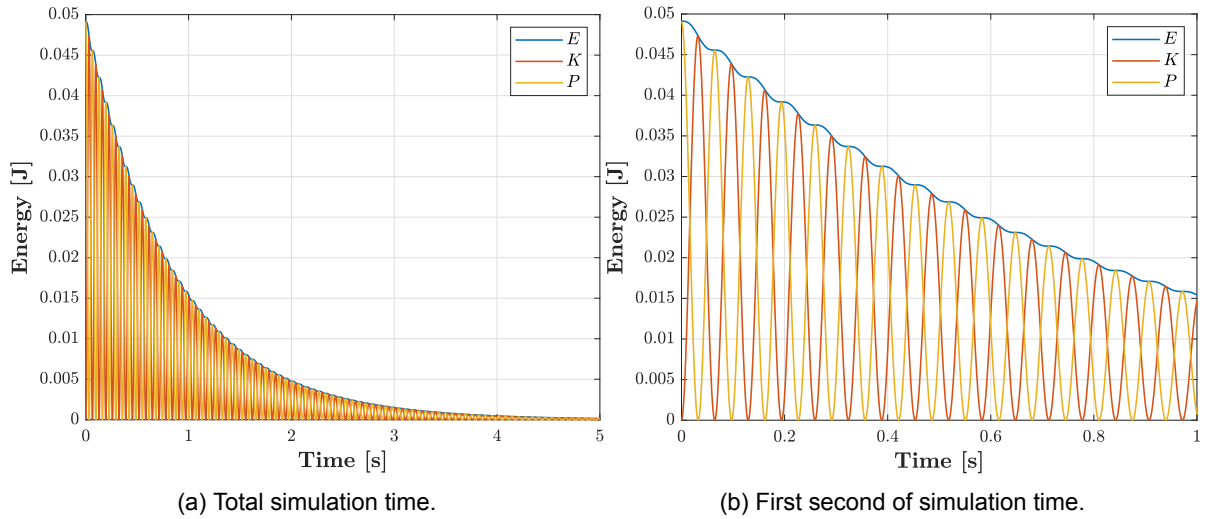


Figure 7.8: Energy in a damped freely vibrating EB column.

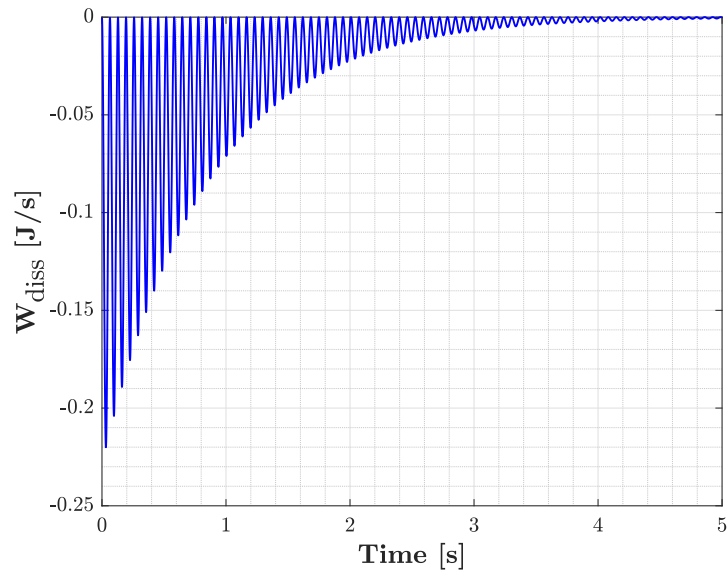
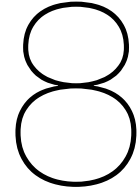


Figure 7.9: Energy dissipation in EB column.

Table 7.5: Initial energy for every setup and initial displacement in Joule.

Setup	5 mm	10 mm	20 mm
2	0.013	0.052	0.21
3	0.007	0.027	0.11
4	0.002	0.008	0.033



Results and Analysis

This chapter presents the results of the conducted experiments. While the axial test for setup 1 did not yield data which could be used, tests for setups 2, 3, and 4 were able to be further analyzed. The results were evaluated to compare the curvature determination methods and to validate the experiments.

The results of the experiment were not as initially expected: instead of a decaying vibration in the main direction, the timber vibrated alternatively in both the excited direction and the perpendicular direction. This phenomenon is known as beating. As a result, it was more challenging to determine the damping in the column, as damping occurred in two directions. However, the dissipated energy of the entire, coupled system could be determined.

As a result of the lack of a strain gauge, the curvature data could not be measured. Instead, a numerical process was applied to obtain the curvature of the beam. As the kinetic and potential energy depends on the velocity and the curvature, these inputs must be accurate and correspond, to depict the energy precisely. It was challenging to retrieve this data in a manner which correctly showed the energy in the column. The data needed to be extensively fitted to obtain satisfactory outcomes. In the end, an overview of energy dissipation could be given. However, it must be noted that due to all the necessary numerical processes, the result is less accurate than initially expected. Additionally, the experiments were conducted at home, resulting in a less robust setup, which is more prone to errors.

Nonetheless, despite its limitations, the method proposed seems to be adequate to determine the energy dissipation during vibration in a timber column. If these experiments are conducted in a professional lab setting, it is expected that the energy dissipation can be determined with sufficient accuracy.

8.1. Beating

During all executed tests of setups 2, 3 and 4, beating was observed. Beating is a well-known phenomenon in dynamics whereby two different vibration systems interact with each other, resulting in combined responses which differ from the two original systems. Beating occurs in case there is soft coupling between two different systems which have natural frequencies close to each other.

Figure 8.1 illustrates two undamped vibrations with close natural frequencies resulting in a beating response. The impact of beating to the vibration of the coupled system is threefold:

- The resulting vibration occurs in a frequency which equals the average of the two different system frequencies: $f_n = \frac{(f_{n,1} + f_{n,2})}{2}$
- A coupled response occurs displaying increasing and decreasing amplitudes over time, whereby the maximum amplitude is the sum of the initial amplitudes.
- The amplitudes of the coupled responses follow a secondary, low, 'beating' frequency f_b , which equals the delta between the frequencies of the two different systems: $f_b = f_{n,1} - f_{n,2}$.

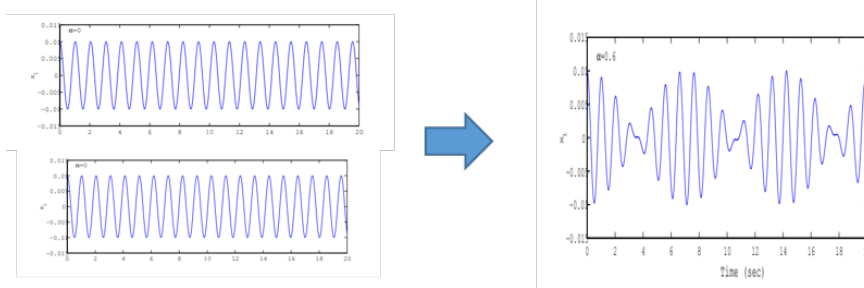


Figure 8.1: Development of beating from two, almost identical, undamped vibrations

In the experiments, the two different vibrating systems were the lateral bending vibration in the z - and y -direction. In the experiments, the z -direction was the direction in which the column was initially displaced. It was clearly visible that the free vibration rapidly moved back and forth between the z - and y -direction. This is demonstrated in the data found in Figure 8.2. The accelerometer measurements confirmed that the natural frequencies of the first modes in either axis were close to each other for each of these three set-ups. This is shown in the frequency spectrum response presented in Figure 8.3. The difference between the frequencies varied between 0.1 to 0.8 Hz, which is in accordance with the secondary frequency observed in the data.

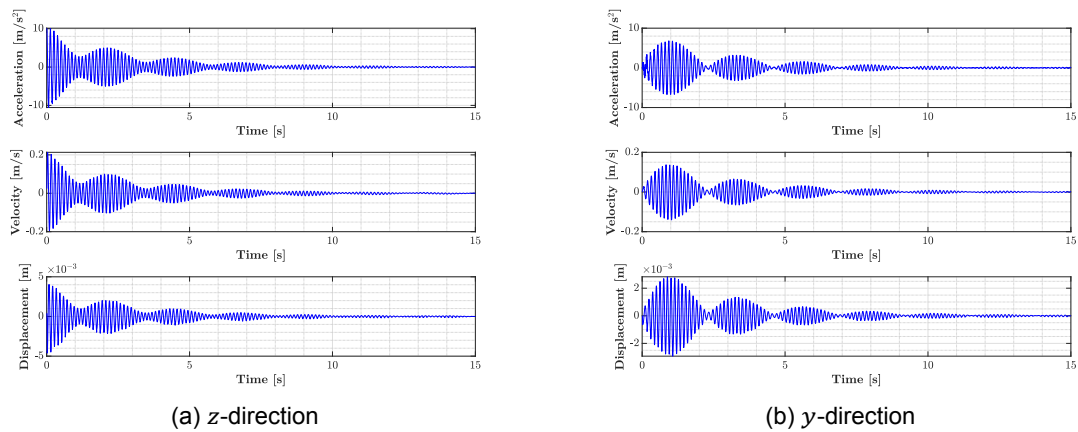


Figure 8.2: Acceleration, velocity and displacement in z - and y -direction of lateral vibrating column demonstrating beating.

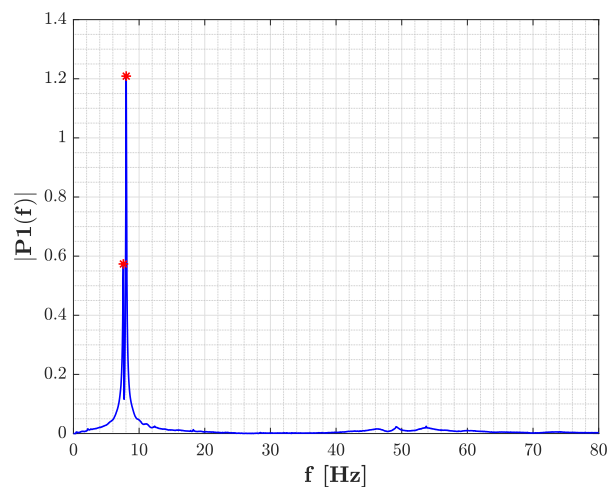


Figure 8.3: Frequency spectrum of setup 2. The two peaks of the spectra correspond to the first natural frequency in the z - and y -direction.

It should be noted, that, in theory, in a clamped column no beating occurs. The two lateral vibrating systems should not have been coupled if the column was excited in only one direction due to clamped boundary condition. It is expected that the beating occurred due to the imperfect boundary condition and that the anisotropy of timber could also have an effect. Furthermore, if a rectangular cross-section rather than a square cross-section had been selected, it is improbable beating had been observed as the difference in natural frequency in z - and y -direction would likely be too large.

8.1.1. Clamped boundary condition

The clamped boundary condition was imposed by pouring concrete around the timber columns. The concrete showed cracks during the experiments and in combination with shrinkage, it could be expected that an imperfect clamped boundary condition was created. It is probable that the displacement at $x = 0$ in both z - and y -direction was not equal to zero. The same could be expected for the angle. As some movement was possible at the interaction between the timber and the concrete, the two lateral vibrating systems probably became coupled, which lead to the observed beating.

Consequently, in practice, some friction would have occurred between the immersed part of the timber column and the concrete. This would have led to damping at the connection, which is classified as structural damping. Theoretically, the only damping expected was the material damping in the column, but in this setup, it appeared that some energy dissipation was also found at the boundary condition. In this research, it was not possible to determine how big the effect of the structural damping in the clamped column was on the total damping. Further research could give insight into the ratio between structural and material damping.

8.1.2. Anisotropy

The z and y natural frequencies being close indicated that there was a slight difference in geometry and/or stiffness across these two axes over the length of the column. With respect to geometry, it was possible that the square section is not perfectly symmetrical along its length or that there was a small out of straightness or curvature along its length due to the quality of sawing. However, more likely, the primary cause for the difference in natural frequency was caused by a difference in MOE as a result of anisotropy with fibres and a-symmetric knots in the timber cross-section along its length. This was shown in Figure 8.4. The a-symmetrically spread knots both across z and y direction, length and cross section for the three set-ups observed.



Figure 8.4: A-symmetric fibres and knots causing anisotropy in the timber columns.

8.2. Energy Transfer

The observed beating phenomenon has complicated the interpretation and analyses of the test results as the energy is now dissipated across both lateral vibrating systems. Furthermore, the energy is transferred from one direction to the other and back during vibration. A schematic of this observed energy flow in the experiments is presented in Figure 8.5.

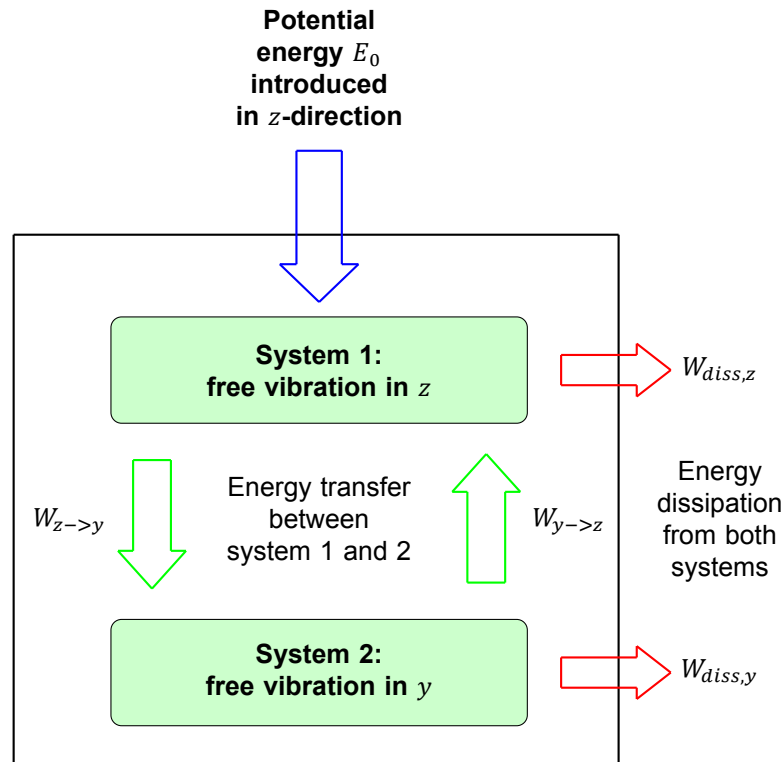


Figure 8.5: Energy flow observed in experiments.

Energy is a scalar without direction. So therefore it cannot be said that energy is transferred from one direction to the other as energy is always possessed by the total system. However, to discern the two vibrating systems, in this section the energy associated to the velocity and curvature in a direction is being described as energy in that specific direction. The dissipated energy in the energy balance equation consists of two parts: damping and transfer.

$$W_{\text{diss}} = W_{\text{transfer}} + W_{\text{damp}} \quad (8.1)$$

The energy balance equation for each direction thus looks as follows:

$$\begin{aligned} \frac{dE_z}{dt} &= W_{\text{transfer},z \rightarrow y} + W_{\text{transfer},y \rightarrow z} + W_{\text{damp},z} \\ \frac{dE_y}{dt} &= W_{\text{transfer},y \rightarrow z} + W_{\text{transfer},z \rightarrow y} + W_{\text{damp},y} \end{aligned} \quad (8.2)$$

As the energy transfers within the system from one direction to another, no energy is dissipated out of the system. Therefore, it can be stated that the dissipated energy for the total system consists of the dissipated energy associated with damping in both directions.

$$\frac{dE}{dt} = W_{\text{damp},z} + W_{\text{damp},y} \quad (8.3)$$

This complicates matters, as two unknown terms appear. It is thus not possible to determine the dissipated energy for each direction. Only the total energy dissipation can be calculated.

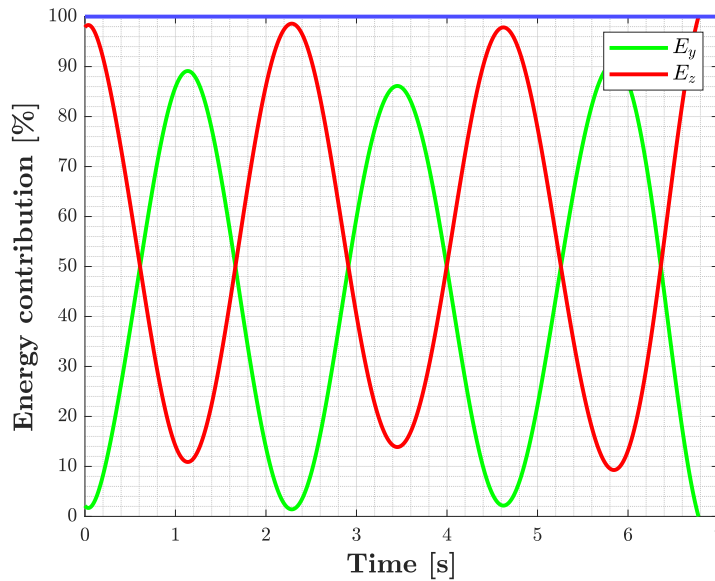


Figure 8.6: Contribution of the energy in z -, y -direction to the energy at t (blue line).

In Figure 8.6, the ratio between the energy in the z - and y -direction compared to the total energy in the system at time t is depicted. It clearly shows how the energy in the system is transferred from one direction to the other and back. For most tests, the pattern is similar. At the peaks, around 90% of the total energy is due to the work in one direction. In Figure 8.7, the dissipated energy is also added to the graph. So now the ratios are between the energy in the z -, y -direction and the dissipated energy compared to the initial energy. The energy dissipation contribution seems to follow a negative exponent curve, which seems to be constant for most tests and in accordance with the expectation of the theoretical EB column. It also corresponds to theory as more energy is dissipating while the velocity is higher.

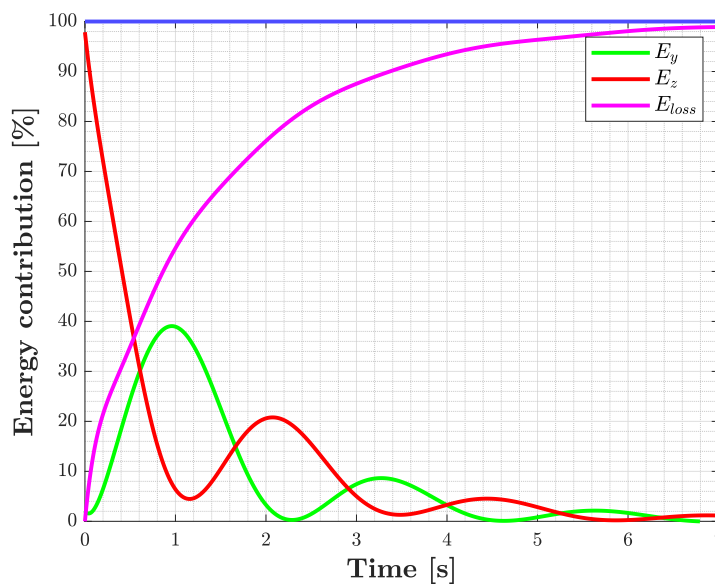


Figure 8.7: Contribution of the energy in z -, y -direction and the dissipated energy compared to the initial energy (blue line).

8.3. Comparing Curvature Determination Methods

As discussed in the previous chapter, two methods were proposed for determining the curvature: acceleration fit and displacement shift. The results of both methods are discussed in this section.

8.3.1. Displacement shift method

The first method was based on the displacements derived from the experiment. By using a MATLAB script, the acceleration data is filtered and integrated twice to obtain the displacement. The Euler-Bernoulli beam theory is then used to determine the shape of the column in the first mode as it is observed that the column only vibrates in its first mode. For each time step, the displacement is known. So by imposing this displacement in the EB column, the corresponding curvature can be determined.

However, a problem was encountered. The derived displacement data was physically incorrect, which was probably due to the double integration and filtering of the data. In contrast to what it should be, the mean of the displacement was non-zero. This resulted in values for the curvature which were incorrect. To counteract this issue, the displacement data was shifted such that the mean of the displacement became zero. For each cycle, a written MATLAB script ensured the mean was zero by subtracting the cycle's mean value. This resulted in usable displacement data. The shifted displacement compared to the original data is shown in Figure 8.8.

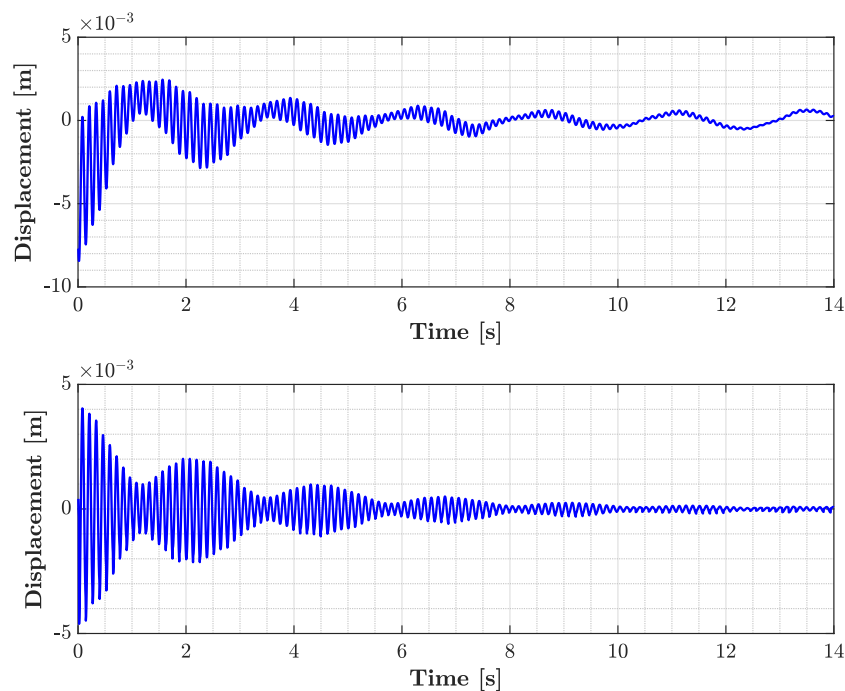


Figure 8.8: Displacement data from Setup 2, Test 1, Version 1 before (top) and after (bottom) displacement shift is applied.

Since the adjustment is made for each individual period, the resulting curve is not smooth at the transition point between cycles as depicted in Figure 8.9. As a result, the energy calculated from the experiments was not continuously decreasing as expected but showed non-physical peaks in the potential and total energy. The energy time histories were hence fitted, giving feasible results and allowing for a better interpretation of the results.

8.3.2. Acceleration fitting method

For this method, a MATLAB script was written to fit the acceleration of a beam using the EB beam theory to the measured data. All the properties gained from the experiment are implemented for the EB beam. The beating phenomenon was replicated by simulating two modes with the two measured closely spaced natural frequencies. For both modes, the same β (see Section C.2.1) was applied that corresponds to the first mode as the beam vibrates in the first mode for both directions. The only unknown quantity in the EB equation is ζ . The script optimized the zeta value by finding the fit with the lowest Root Mean Squared Error. At this point, the theoretical acceleration was fitted to closely match the experimental data. Subsequently, the fitted acceleration is used to theoretically determine the displacement and finally the curvature. A comparison between the fitted and experimental data

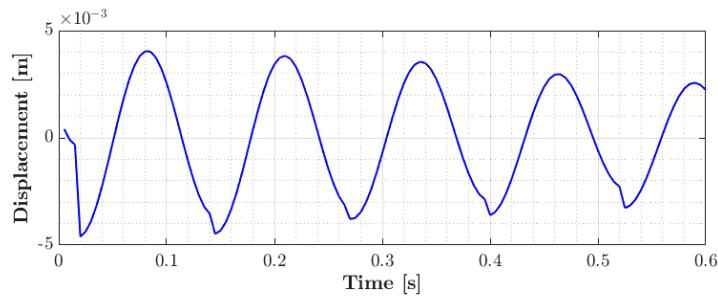


Figure 8.9: Jumps in displacement data at transition points.

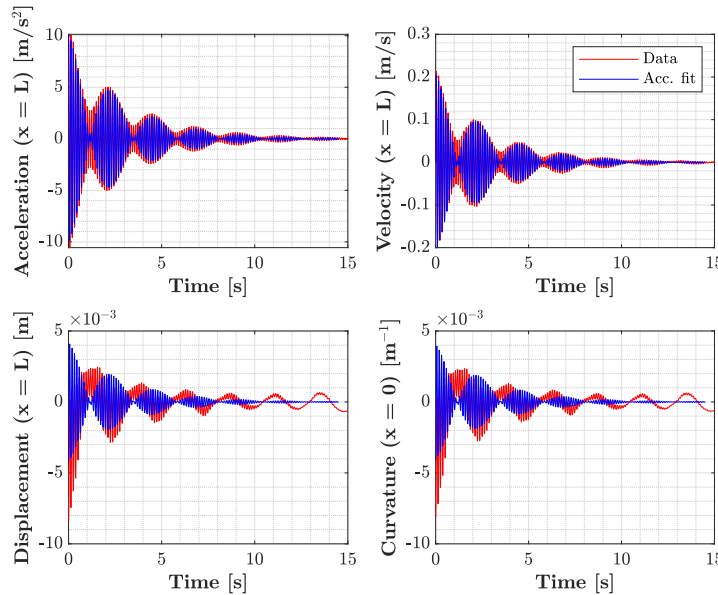


Figure 8.10: Comparison of the Acceleration, velocity, displacement and curvature between the experimental data and the acceleration fitting method.

can be found in Figure 8.10. This figure also depicts a comparison between the experimentally and theoretically acquired velocity, displacement and curvature.

Despite applying the natural frequencies obtained from the experiments to the two fitted vibrations, the fitted and the experimental data were occasionally observed to be slightly out of phase, indicating that the derived frequency was not entirely correct. For simplicity, the ζ and the β values were assumed equal for the two fitted vibrations, as they are assumed to be the first modes. Yet it is unsure whether this is entirely correct. The aforementioned limitations and assumptions highly influence the results as the final energy calculations strongly depended on these values, hence a small change could lead to oscillations in the total calculated energy. For more consistent results, the kinetic, potential and total energy was thus fitted to interpret the results better.

For both methods, the energy decays for the experiment from setup 1 with an initial displacement of 5 millimetres are presented in Figures 8.11 and 8.12. The energy for the acceleration-fitted method was less smooth than for the method with the shifted displacement. This was the case for almost all the experiments. The fitted data being slightly out of phase with the experimental data could have led to this less smooth curve. Especially for the first second, it was observed that the energy with the acceleration fit encountered unexpected behaviour. For some experiments, the energy even increased, which was physically impossible. The necessary estimation of the velocity and curvature for the first second explained this behaviour. Compared to the expected behaviour of Figure 7.8, the shifted displacement returned more satisfactory results. Although this expected behaviour did not experience

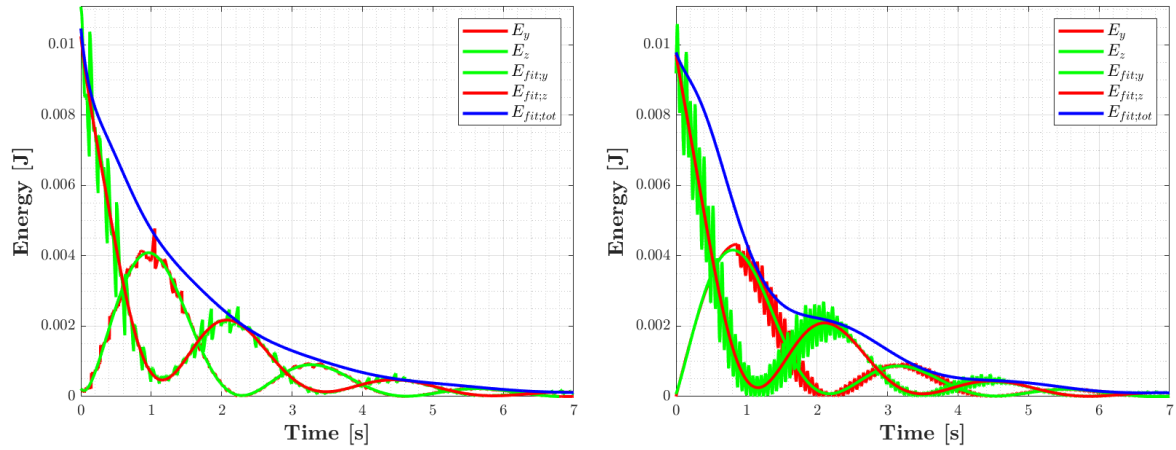


Figure 8.11: Energy decay using shifted displacement method. Figure 8.12: Energy decay using acceleration fitting method.

beating, a more smooth decay was to be anticipated. The plateaus at the peaks of the potential energy however were not discovered in the experiments. The absence of a strain gauge and therefore reduced accuracy of the data explained the lack of these plateaus in the obtained energy graphs. As the displacement shift method's results were more in line with the expected outcomes, this method was applied for the remainder of this analysis.

The decay of energy in the system was found to follow a decaying exponential function. Hence a constant regarding the energy dissipation could be presented: E_D . This value was obtained by matching a decreasing exponential function to the total energy in the system. E_0 is the initial value of the energy at $t = 0$. Subsequently, the E_D was derived by finding the value for which the lowest Root Mean Squared Error was found compared to the original energy curve.

$$E(t) = E_0 \exp(-E_D t) \quad (8.4)$$

Figure 8.13 compares the energy plotted with the obtained E_0 to the energy calculated with the shifted displacement. A high level of agreement exists between the two lines. For most of the experiments the retrieved E_0 showed a good fit. As comparison the dotted blue line represents the fitted energy for the acceleration fitting method.

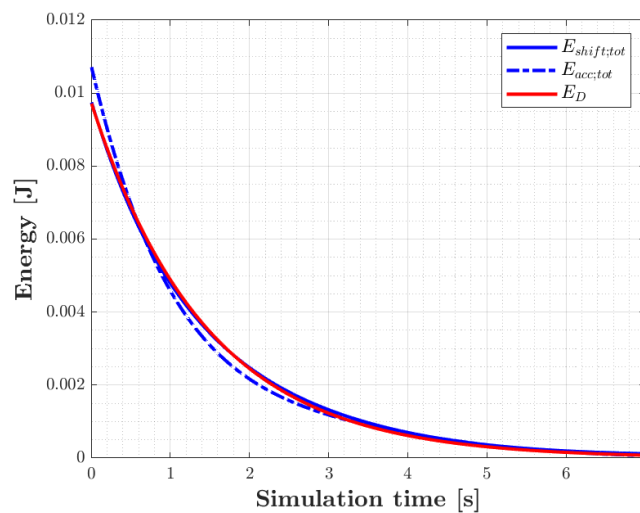


Figure 8.13: Energy with E_D fit compared to the energy from the displacement shift and acceleration fitting method.

8.4. Energy Dissipation Trends

From the data, two constants could be retrieved: the damping ratio ζ and a newly introduced energy dissipation constant E_D . As the measured data has been fitted to match the theoretical EB data, the corresponding ζ values could be extracted. A difference exists between the constants. Whereas ζ was specifically obtained for either the z - or y -direction, E_D was a constant which describes the energy dissipation in the total system, independent of the direction. For both constants, the trends observed for the different setups and displacements are discussed. It must be noted that due to the low number of tests, the accuracy of these trends is not high. To gain better insights into the trends, more research is warranted.

8.4.1. Damping ratio trends

Figure 8.14 and 8.15 depict the damping ratios for every experiment for both z - and y -direction. For almost all setups a trend could be observed for which slightly higher damping ratios were obtained for a higher initial displacement. Only ζ_z for setup 4 and ζ_y for setup 3 did not follow this trend. However, for setup 4 if one outlier at an initial displacement of 5 millimetres would be disregarded, the slightly upward trend would be noticed. A small amplitude dependency seemed to appear for the damping ratios. However, more research is necessary for concluding remarks.

The mean damping ratios per test for each setup are presented in Figure 8.16. In this figure, test 1 is the mean value of all tests with an initial displacement of 5 mm, test 2 for 10 mm and test 3 for 20 mm. For the z -direction no real trend could be determined for setups with a higher natural frequency. In the y -direction, setups with higher frequency did have lower damping ratios. Nevertheless, the trend is not strong and only limited data was available, so no clear conclusions can be drawn.

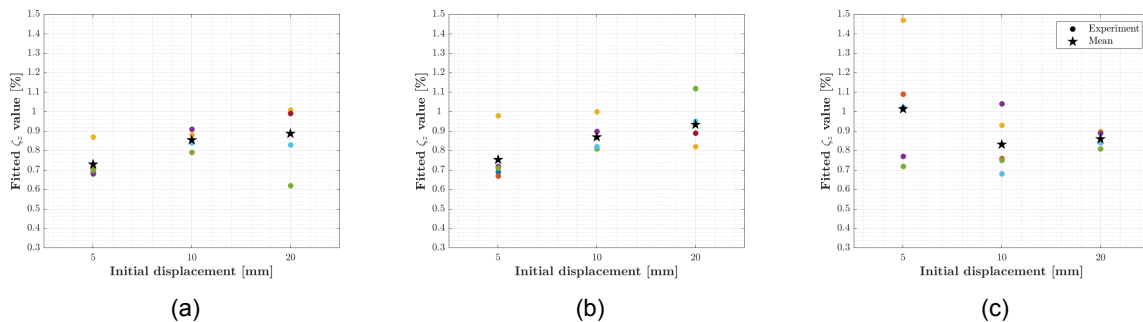


Figure 8.14: Fitted damping ratios for all tests for (a) setup 2, (b) setup 3 and (c) setup 4 and initial displacements in the z -direction.

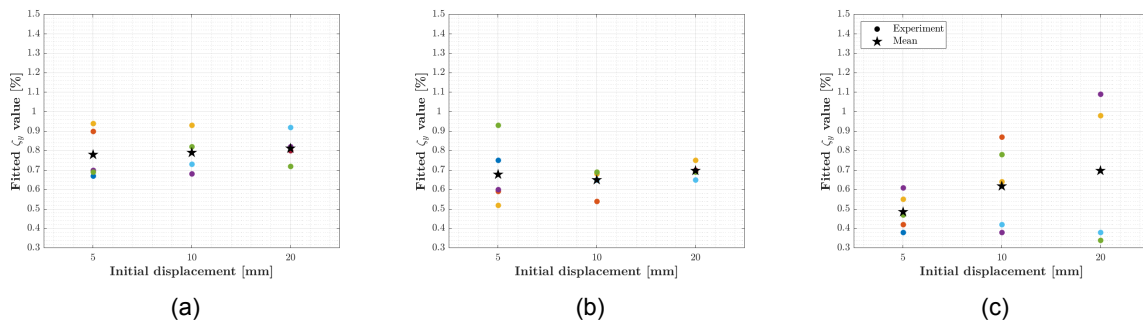


Figure 8.15: Fitted damping ratios for all tests for (a) setup 2, (b) setup 3 and (c) setup 4 and initial displacements in the y -direction.

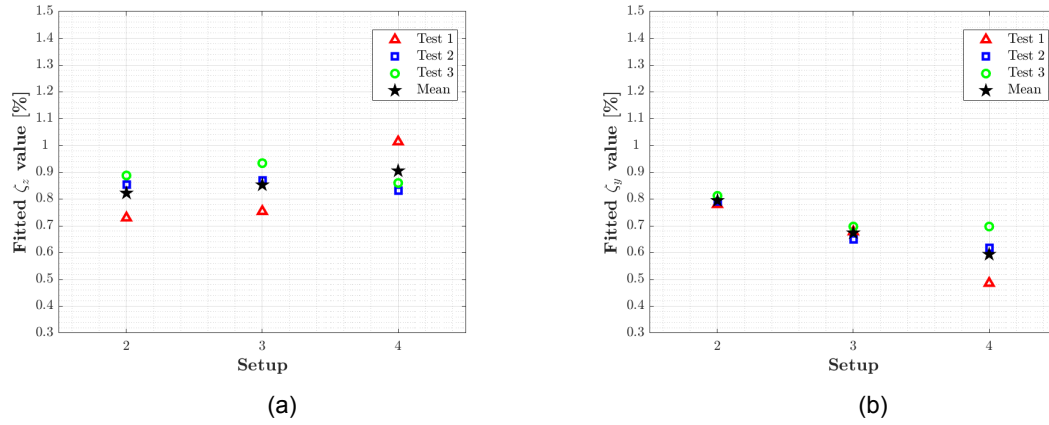


Figure 8.16: Damping ratios per setup for the (a) z- and (b) y-direction.

8.4.2. Energy dissipation constant trends

The trend in Figure 8.17 did not show a consistent pattern. For setup 2, a higher scatter appeared, which made it difficult to conclude a trend. Setup 3 seemed to have a small amplitude dependent trend. Lastly, no clear trend could be distinguished for setup 4. Figure 8.18 shows the mean values for all the tests per setup. It seemed that for the setup with higher stiffness and natural frequency, a lower E_D was obtained. This was in agreement with the ζ_y .

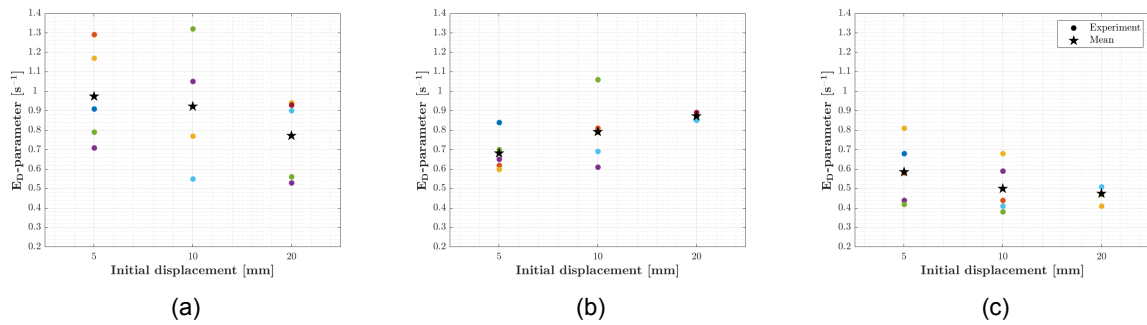


Figure 8.17: Energy dissipation constant for all tests for (a) setup 2, (b) setup 3 and (c) setup 4 and the associated initial displacements.

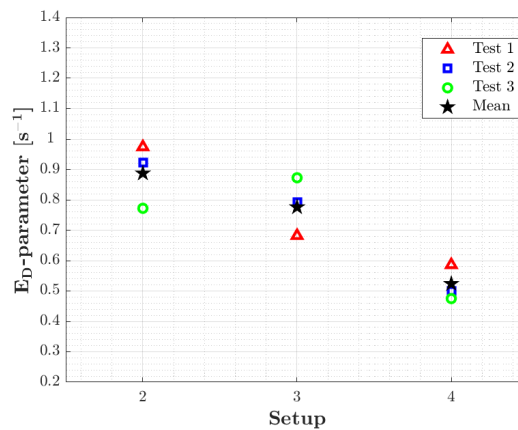


Figure 8.18: Mean energy dissipation constant for each test and setup.

8.5. Validation

The results of the energy-based approach must be validated to ensure its applicability. Although the comparison between E_D and the Kelvin-Voigt constant or a viscous constant was impossible due to the encountered beating, the damping ratios obtained from the acceleration fitting were compared to values from the literature. Furthermore, the correlation between the newly introduced E_D and the damping ratios could also be examined. The predicted natural frequency, MOE and initial energy could be compared to the actual values to determine the accuracy of the energy-based method.

8.5.1. Comparison damping ratio to the literature

From different studies Labonnote et al. [26] concluded that the material damping for timber ranged from 0.2% to 0.75%. In its own research, it was determined that for a simply supported beam of Norway spruce the mean value for the damping ratio was 0.52%. The measured damping ratios from the experiments ranged between 0.42% and 1.5%, with a mean value of around 0.8%. This is higher than would have been expected from previous experiments. This could be explained by the difference in the setups. In Labonnote's research [26] no structural damping occurred as it was a simply supported beam. Due to the imperfect clamp, it could be expected that some structural damping did occur. The difference in damping ratios could therefore be another indication that the clamped boundary condition was indeed imperfect. If the material damping of Labonnote et al. was applied to the setup in this research, it could be stated that the structural damping of the experiment setup was around 0.3%. However, no concluding remarks can be given as further research is necessary.

8.5.2. Comparison energy dissipation constant and damping ratio

For all experiments E_D is plotted against ζ in Figure 8.19. Between ζ_z and E_D no correlation was found. A moderately weak correlation was found between ζ_y and E_D . The correlation between the average of ζ_z and ζ_y for each experiment and E_D was also calculated. This also resulted in a moderately weak correlation. The not very strong correlation could be possibly explained by the low number of data points. A research with more conducted tests could give a better insight into the correlation.

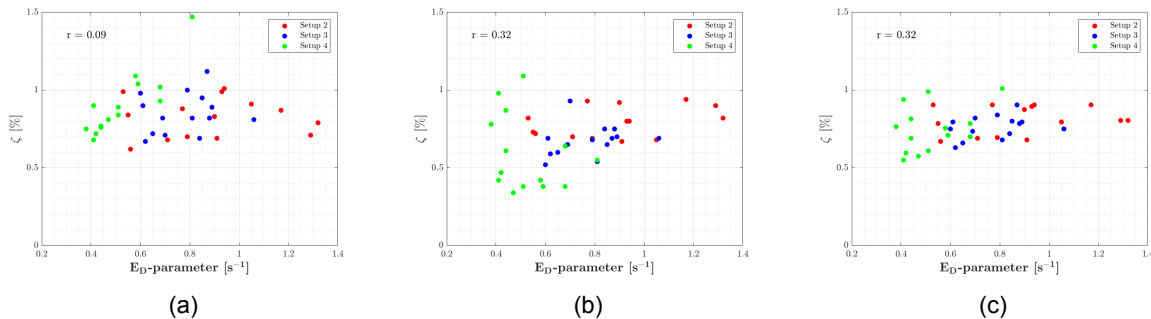


Figure 8.19: Correlation energy dissipation constant and damping ratio in (a) z-, (b) y-direction and (c) the mean value of z and y with its corresponding r value.

8.5.3. Comparison initial energy

In Section 7.5, the expected initial energy in each column for the three initial displacements was calculated. The energy graphs showed the actual initial energy in the system. The mean for every test is presented in Figure 8.1. Setup 2 only showed an accurate comparison with the expected energy for an initial displacement of 5 mm. Both the initial energy values for 5 and 10 mm displacement were consistent with the expected values for setup 3. The energy for the 20 mm displaced column was more than twice as low as expected. In the case of setup 4, the initial energy was near as expected, with only a slight difference observed for the experiments with a 5 mm displacement. This difference could be attributed to the manual imposition of displacements using a tape measure, which caused variations in the imposed displacements per experiment. This also explained the high scatter of initial energy for identical tests. A trend was observed of better agreement between the expected and initial values for the less stiff column. During the experiments, it was more challenging to hold the stiffer columns in

Table 8.1: Actual initial energy for every setup and initial displacement in Joule.

Setup	5 mm	10 mm	20 mm
2	0.008	0.019	0.072
3	0.004	0.020	0.040
4	0.004	0.008	0.034

their exact initial displacement before release, which could explain this trend. An extra factor could be the imperfect boundary condition, which would lead to a different expected value for the initial energy.

8.5.4. Validation natural frequency and modulus of elasticity

The natural frequency of a lateral vibrating EB beam in the first mode can be described as:

$$f_{n,1} = \frac{1.875^2}{2\pi} \sqrt{\frac{EI}{\rho AL^4}} \quad (8.5)$$

An initial value of 8 GPa for the MOE was assumed for all four test pieces, and with the properties as per Table 7.1 the values for the first natural frequencies were predicted beforehand as in Table 8.2. However, the tests showed that the measured natural frequencies deviated from the predicted values. Given the variation in density and the strong relationship between density and the modulus of elasticity of timber, the deviation in the predicted natural frequency is not illogical and can also be observed in the literature, as indicated by Figure 8.20. A second explanation for the difference could be found in the imperfect boundary condition. An imperfect clamped boundary condition was created, which was more flexible than assumed in the model.

Table 8.2: Predicted first natural frequency of the four setups.

Setup	$f_{n,1}$ [Hz]	E [GPa]
2	8.1	8.0
3	6.1	8.0
4	5.2	8.0

Table 8.3: Back-calculated MOE per setup based on $f_{n,1,z}$.

Setup	ρ [kg/m ³]	$f_{n,1,z}$ [Hz]	E [GPa]
2	463	8.04	7.4
3	490	6.81	10.8
4	419	4.50	8.4

The theoretical MOE of the timber columns were back-calculated, using the obtained natural frequencies which were applied to Equation 8.5. These newly calculated MOE are presented in Table 8.3. Depending on the method of testing, mean values for the MOE of 10600 (static tests) or 12000 GPa (dynamic tests) are given for Norway Spruce [29]. Although the back-calculated values for the MOE are lower than the mean values, they do fall broadly within the range for Norway spruce. Especially if the dependency of the MOE on density is taken into account. Figure 8.21 shows a positive correlation between the MOE and the density giving further credibility to the values measured and the setups created.

Additionally, the MOE for the specimens were determined in a professional lab setting, using the method described in Section 3.2. The density was recalculated using a scale in the lab. Subsequently, the MTG handheld from Brookhuis Micro Electronics was used to measure the accelerations, from which the natural frequency was obtained. The calculated values for the different MOE are presented in Table 8.4. The value for E_{10c} corresponds to the bending modulus, which is compared to the back-calculated values from Table 8.3. The final column lists ΔE , which denotes the difference between the back-calculated E in Table 8.3 and E_{10c} . The measured MOE were slightly higher than the calculated values. However, the difference for all values was similar. The imperfect clamped boundary condition could not be an explanation for these higher values, as this would have led to lower MOE. It was unclear what reason precisely lead to the higher measured MOE. Figure 8.21 presents all values compared to the density

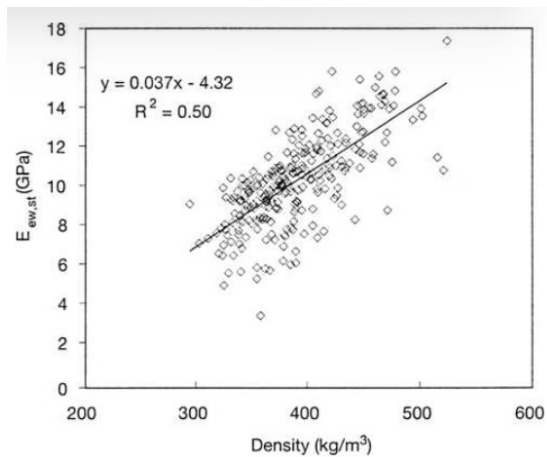


Figure 8.20: Modulus of elasticity versus density in Norway spruce [29].

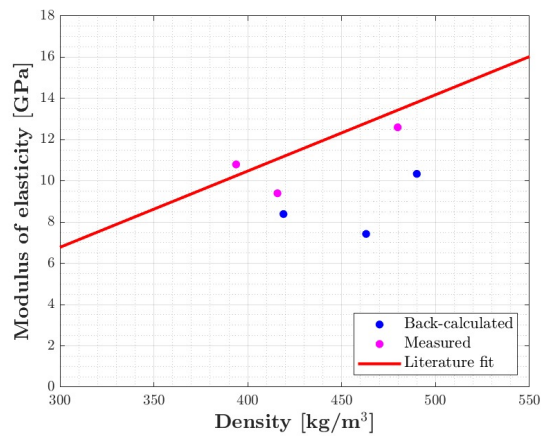


Figure 8.21: Modulus of Elasticity versus density in experiments. The red line indicates the fit from Figure 8.20.

and the regression line of Figure 8.20. The MOE all fall in the range for known values for Norway Spruce.

In conclusion, it can be stated that the energy-based approach yields adequate results for energy dissipation in a timber column. While some validation results did not align with expectations, most differences could be attributed to the limitations of the at-home experimental setup. Consequently, it is expected that conducting experiments in a professional laboratory would provide more satisfactory outcomes.

Table 8.4: Calculation of actual modulus of elasticity and comparison to theoretical modulus of elasticity

	L [m]	ρ [kg/m ³]	$f_{n,1,x}$ [Hz]	E_{dyn} [GPa]	E_{loc} [GPa]	ΔE [%]
Specimen setup 2	1.872	415.8	1269	9.4	8.9	16.9
Specimen setup 3	1.869	478.1	1410	13.3	12.6	18.2
Specimen setup 4	1.867	393.8	1405	10.8	10.3	18.4

IV

Conclusions and Recommendations

9

Conclusions

This research has confirmed with analytical models that an energy-based approach, as proposed by Sánchez Gómez [45], can describe the energy dissipation in a clamped timber column under axial, lateral and torsional loading conditions during free vibration. For lateral vibration the analytic model was further evaluated by conducting experiments. With the help of an energy balance equation, the energy flow in a timber column was formulated including any energy dissipated during vibration.

The energy balance equations for lateral, axial and torsional vibration cases have been derived. The total energy in the system during vibration consists of kinetic energy and potential energy, while the change of energy over time is equal to the dissipated energy. The analytical equation for lateral vibrations was tested in a series of simple experiments using the commonly used Norway spruce. It was found that the energy in the system can be approximated by an exponential function which introduces an energy dissipation constant E_D (s^{-1}) and the initial energy E_0 (J) as can be seen in equation 9.1. For lateral vibrating columns of Norwegian spruce, typical values of E_D were 0.4 - 0.6 s^{-1} .

$$E(t) = E_0 \exp(-E_D t) \quad (9.1)$$

The newly introduced energy dissipation constant E_D proved able to assess damping in vibrating systems with beating, which is challenging using half-power bandwidth or logarithmic decrement method. Compared to these traditional methods, the energy-based approach is a more fundamental approach. Another advantage of E_D is that it will be easier to compare the damping values for different configurations: potential influences from amplitude, modes or frequency can be avoided due to initial energy being similar and the only varying constant being E_D .

Finally, it has been established that damping has a significant influence on reducing peak accelerations and a better prediction of damping could potentially lead to lowered cost. A sensitivity analysis of a case study on the high-rise timber building HAUT showed that increasing the damping from 1.5% to 2% or 2.5% could reduce the mass by 17% or 29%, respectively, while maintaining constant peak accelerations. This largely untapped design lever warrants significant research and design improvement for these timber structures of the future.

10

Recommendations

This research serves as a starting point from which further research on energy dissipation in timber could continue. The recommendations outlined in this study provide guidance for conducting future research. The follow-up research could contribute to a more profound understanding of the energy dissipation in timber structures. Additionally, the suggestions presented here offer insights to be considered in the design of timber high-rises regarding damping.

10.1. Follow-up Research

Firstly, it is advised to conduct the experiments proposed in this thesis in a formal laboratory setting. The addition of a strain gauge would highly increase the accuracy of the experiment. Likewise, a superior accelerometer could also lead to better results. The precision of the imposed displacement could also be more accurately determined in a lab. Besides the lateral vibration tests, the experiment could be performed for torsional and axial vibration. A larger number of tests would lead to E_D values which would be statistically significant and would be able to identify any trends.

As the experiments with square cross-sections encountered beating, experiments and analyses of rectangular cross-sections would be sensible. It is expected that this would not lead to beating, making it possible to observe the energy dissipation in only the main direction. In addition, testing a glulam column rather than solid timber will be valuable, as glulam columns are used more frequently in timber design. Due to the lower scatter in natural properties in glulam, it is expected that less variance will occur in the results.

In this thesis, it was assumed that the anisotropy of the wood does not influence the vibrating behaviour and thus the damping characteristics. It seemed that the motion of a lateral vibrating timber beam was in accordance with the isotropic Euler-Bernoulli beam model. However, no extensive research was conducted on this area of topic. So to be certain the effect of the anisotropy on the vibrations and damping can be neglected in the model, further research is advised.

Subsequently, the energy dissipation in simple timber frames could be studied. It would be interesting to investigate the possibility of determining the contribution of material and structural damping to the total damping. By using the energy flow method, energy dissipation in certain areas can be observed. Therefore, it is expected that by defining the connections and members as specific regions, the energy dissipation in each can be determined.

The initial energy in a system can be determined easily if after an imposed displacement the system can vibrate freely. Therefore, a comparison between the rate of energy dissipation (E_D) can be simply made if the same initial energy is put into different systems. In this manner, various configurations of a frame could be compared for their damping properties. For example, the energy dissipation in different connection types could be compared. This might lead to engineers being able to choose which connection types they would prefer to increase the damping properties in a design.

10.2. Timber Design

At the moment it is impossible to accurately determine the damping ratio for a timber high-rise building during the design phase. It is expected that due to the complex nature of damping and the unique design of each building, this will also hold for the future. However, by gaining a better understanding of which elements or configurations increase the damping properties of a building, engineers can intentionally design for increased damping. The research suggested in the previous section could help achieve this goal. At the moment some recommendations can already be given in regard to the damping characteristics of timber high-rise buildings.

From the literature, it is clear that the damping ratio varies greatly between timber buildings. Furthermore, the existing data is limited, due to the relatively low number of timber high-rise buildings. The accuracy of predicting the damping ratio beforehand is thus low. It is therefore advised to be conservative with the assumed damping ratio. However, a lower bound of 1% seems to exist.

The damping properties of a timber structure increase if the connections are less rigid. As more movement between members is possible, more frictional forces are generated which will lead to increased damping. The connection type showing the highest added damping was found to be slotted steel plate connections. A design with relatively more non-structural elements will also increase the damping. All elements which are not rigidly connected will encounter friction and therefore will increase the total damping of the building.

In conclusion, multiple research opportunities exist for further exploring the topic of damping in timber structures which can lead to a more profound understanding of this phenomenon. This, in turn, should result in both safer and more economic designs of timber high-rise buildings.

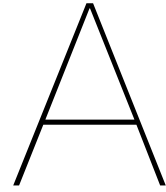
Bibliography

- [1] K LH: Stadthaus, Murray Grove. URL <http://www.klhuk.com/portfolio/residential/stadthaus,-murray-grove.aspx>.
- [2] The Stadthaus - Wood Awards, 2008. URL <http://woodawards.com/portfolio/the-stadthaus/>.
- [3] R. D. Ambrosini. Material damping vs. radiation damping in soil-structure interaction analysis. *Computers and Geotechnics*, 33(2):86–92, 2006. ISSN 0266352X. doi: 10.1016/j.compgeo.2006.03.001.
- [4] R. E. R. Aquino and Y. Tamura. Framework for structural damping predictor models based on stick-slip mechanism for use in wind-resistant design of buildings. *Journal of Wind Engineering and Industrial Aerodynamics*, 117:25–37, 2013. ISSN 01676105. doi: 10.1016/j.jweia.2013.04.001. URL <http://dx.doi.org/10.1016/j.jweia.2013.04.001>.
- [5] C. W. Bert. Material damping. An introductory review of mathematic measures and experimental technique. *Journal of Sound and Vibration*, 29(2):129–153, 1973. ISSN 10958568. doi: 10.1016/S0022-460X(73)80131-2.
- [6] H. J. Blass. *Timber Engineering STEP 1*. Centrum Hout, Almere, 1st edition, 1995. ISBN 90-5645-001-8.
- [7] S. H. Crandall. The role of damping in vibration theory. *Journal of Sound and Vibration*, 11(1): 3–18, 1970. ISSN 0022-460X.
- [8] J. Elbrecht D. Safarik and W. Miranda. State of tall timber 2022, 2022. URL <https://www.ctbuh.org/mass-timber-data>.
- [9] H. De Groot. HoHo Wien Oostenrijk, 2016. URL <http://www.houtblad.nl/Projecten/HoHo{ }Wien>.
- [10] C. W. De Silva. *Vibration: fundamentals and practice*. CRC Press, Boca Raton, 2nd edition, 2007. ISBN 9780849319877.
- [11] C. W. De Silva. *Vibration damping, control, and design*. CRC Press, Boca Raton, 2007. ISBN 9781420053210.
- [12] Z. E. Erisen and E. Cigeroglu. *Frequency Domain Optimization of Dry Friction Dampers on Buildings Under Harmonic Excitation*, pages 113–125. Springer New York, New York, NY, 2012. ISBN 978-1-4614-2413-0. doi: 10.1007/978-1-4614-2413-0_12. URL https://doi.org/10.1007/978-1-4614-2413-0_12.
- [13] European Committee for Standardization. *NEN-EN 1992-1-1:2005*. Brussel, 2005.
- [14] European Committee for Standardization. *NEN-EN 1993-1-1:2005*. Brussel, 2005.
- [15] European Committee for Standardization. *NEN-EN 1991-1-4+a1+C2*. Brussel, 2011.
- [16] European Committee for Standardization. *NEN-EN 338:2016*. Brussel, 2016.
- [17] A. Feldmann, H. Huang, W. Chang, R Harris, P Dietsch, M. Gräfe, and C. Hein. Dynamic properties of tall timber structures under wind-induced vibration. 08 2016.
- [18] W. G. Gard. Lecture 2 Timber Structures and Wood Technology, TU Delft, 2021.

- [19] G. Genta. *Vibration dynamics and control*. Mechanical engineering series; Mechanical engineering series. Springer Science+Business Media, New York ;, 2009. ISBN 978-0-387-79579-9. doi: 10.1007/978-0-387-79580-5. URL <https://link.springer.com/openurl?genre=book&isbn=978-0-387-79579-9>.
- [20] R. F. Gibson. Damping characteristics of composite materials and structures. *Journal of Materials Engineering and Performance*, 1(1):11–20, 1992. doi: 10.1007/bf02650027. URL <http://dx.doi.org/10.1007/BF02650027>.
- [21] D. Hoffmeyer. *Damping of Torsional Beam Vibrations*. PhD thesis, 8 2019.
- [22] E. Karacabeyli and D. Brad. *CLT Handbook*. 2013. ISBN 9780864885531. doi: 10.1017/CBO9781107415324.004. URL <http://www.rethinkwood.com/sites/default/files/clt/CLT{ }USA-Complete-document.pdf>.
- [23] A. Kareem and K. Gurley. *Damping in structures: its evaluation and treatment of uncertainty*, 1996. ISSN 01676105.
- [24] D. E. Kretschmann. *Wood Handbook, Chapter 05: Mechanical Properties of Wood*. 2010.
- [25] N. Labonnote. *Damping in Timber Structures*. PhD thesis, NTNU - Trondheim, 2012.
- [26] N. Labonnote, A. Rønnquist, and K. A. Malo. Modified hysteretic damping model applied to Timoshenko timber beams. *Computers and Structures*, 121:22–31, 2013. ISSN 00457949. doi: 10.1016/j.compstruc.2013.03.008. URL <http://dx.doi.org/10.1016/j.compstruc.2013.03.008>.
- [27] N. Labonnote, A. Rønnquist, and K. A. Malo. Experimental evaluations of material damping in timber beams of structural dimensions. *Wood Science and Technology*, 47(5):1033–1050, 2013. ISSN 00437719. doi: 10.1007/s00226-013-0556-5.
- [28] R. Langenbach. Building tall with timber: A paean to wood construction. *Structural Engineering International: Journal of the International Association for Bridge and Structural Engineering (IABSE)*, 18(2):130–132, 2008. ISSN 10168664. doi: 10.2749/101686608784218725.
- [29] D Larsson, S Ohlsson, M Perstorper, and J Brundin. Mechanical properties of sawn timber from norway spruce. 1998.
- [30] K. Jarnerö J. Olsson M. Johansson, A. Linderholt and T. Reynolds. Building higher with light-weight timber structures-the effect of wind induced vibrations. 2015.
- [31] R. Smith M. R Willford and R. Merello. Intrinsic and supplementary damping in tall buildings. *Proceedings of the ICE - Structures and Buildings*, 163(2):111–118, 2010. ISSN 0965-0911. doi: 10.1680/stbu.2010.163.2.111. URL <http://www.icevirtuallibrary.com/content/article/10.1680/stbu.2010.163.2.111>.
- [32] N. M. M. Maia and J. M. Montalvao e Silva. *Theoretical and experimental modal analysis*. Research Studies Press ;, Taunton, Somerset, England :. ISBN 0863802087 9780863802089 0471970670 9780471970675.
- [33] K. A. Malo, R. B. Abrahamsen, and M. A. Bjertns. Some structural design issues of the 14-storey timber framed building Treet in Norway. *European Journal of Wood and Wood Products*, 74(3): 407–424, 2016. ISSN 1436736X. doi: 10.1007/s00107-016-1022-5.
- [34] A. V. Metrikine. *Dynamics, Slender Structures and an Introduction to Continuum Mechanics CT 4145 Module Dynamics of Mechanical Systems and Slender Structures*. 2007.
- [35] A. Kjell N. Labonnote and K. Malo. Effect of annual ring patterns on norway spruce resulting material properties. *11th World Conference on Timber Engineering 2010, WCTE 2010*, 2, 01 2010.
- [36] J. A. Nairn. A numerical study of the transverse modulus of wood as a function of grain orientation and properties. 2007.

- [37] naturally:wood. Construction of a Tall Wood Building Brock Commons Tallwood House : Construction Overview. 2017.
- [38] G. A. Papagiannopoulos and G. D. Hatzigeorgiou. On the use of the half-power bandwidth method to estimate damping in building structures. *Soil Dynamics and Earthquake Engineering*, 31:1075–1079, 7 2011. ISSN 02677261. doi: 10.1016/j.soildyn.2011.02.007.
- [39] C. Petersen and H. Werkle. *Dynamik der Baukonstruktionen*. Springer Fachmedien Wiesbaden, 2017. ISBN 978-3-8348-1459-3. doi: 10.1007/978-3-8348-2109-6.
- [40] R. Rana and T. T. Soong. Parametric study and simplified design of tuned mass dampers. *Engineering structures*, 20(3):193–204, 1998.
- [41] G. Ravenshorst. Species independent strength grading of structural timber. 2015.
- [42] R. A. M. Ribeiro, M. N. M. Maia, M. J. M. Silva, L. Reis, and M. Freitas. Free Vibration Response Using the Constant Hysteretic Damping Model. *Xlth International Conference on Vibration Engineering*, (January 2005), 2014. doi: 10.13140/2.1.1970.9443.
- [43] D. Roylance. Constitutive equations. 2000.
- [44] RTS Building Information Foundation . Environmental Reporting for Building Materials. Technical report, Brussel, 1998-2001.
- [45] S. Sánchez Gómez. *Energy flux method for identification of damping in high-rise buildings subject to wind*. PhD thesis, 2019. URL <https://doi.org/10.4233/uuid:bc4fe937-2711-4ee0-95b7-baad7c5d234c>.
- [46] S. Sánchez Gómez, A. Metrikine, B. Carboni, and W. Lacarbonara. Identification of energy dissipation in structural joints by means of the energy flow analysis. *Journal of Vibration and Acoustics, Transactions of the ASME*, 140(1):1–8, 2018. ISSN 15288927. doi: 10.1115/1.4037470.
- [47] R. Smith and M. Willford. Damping in tall buildings – uncertainties and solutions. pages 66–67. International Association for Bridge and Structural Engineering (IABSE), 2008. doi: 10.2749/222137908796225618.
- [48] Wood Solutions. Forte - Building Australias First Timber Highrise. In *Atlanta Conference*, Atlanta, 2013. URL <http://www.woodworks.org/wp-content/uploads/2013-WSF-ATL-Collins.pdf>.
- [49] J. M. J. Spijkers, A. W. C. M. Vrouwenvelder, and E. C. Klaver. *Dynamics of Structures Part 1 Vibration of Structures*. Delft University of Technology, 2006.
- [50] A. Srikantha Phani and J. Woodhouse. Viscous damping identification in linear vibration. *Journal of Sound and Vibration*, 303(3-5):475–500, 2007. ISSN 10958568. doi: 10.1016/j.jsv.2006.12.031.
- [51] C. Stauder. Cross-laminated timber: An analysis of the austrian industry and ideas fostering its development in america. 2013.
- [52] S. Tesfamariam. Performance-based design of tall timber buildings under earthquake and wind multi-hazard loads: Past, present, and future. *Frontiers in Built Environment*, 8, 3 2022. ISSN 2297-3362. doi: 10.3389/fbuil.2022.848698.
- [53] W. B. Trusty and J. K. Meil. Building life cycle assessment: residential case study. Technical report, Athena Sustainable Materials Institute, Ottawa, 1999.
- [54] R. L. J. Van den Berg. Investigation to damping in high-rise buildings. Master’s thesis, Delft University of Technology, 2012.
- [55] G. P. C. Van Oosterhout. *Wind-induced Dynamic Behaviour of Tall Buildings*. PhD thesis, Delft University of Technology, 1996.

- [56] R. Verhaegh. Conversation with rob verhaegh, structural engineer for haut, 1 2023.
- [57] M. Wells. Stadthaus, london: Raising the bar for timber buildings. *Proceedings of the Institution of Civil Engineers: Civil Engineering*, 164:122–128, 11 2011. ISSN 0965089X. doi: 10.1680/cien.2011.164.3.122.
- [58] A. Wiedenhoef. *Wood Handbook, Chapter 03: Structure and Function of Wood*. 2010.
- [59] J. C. Wohlever and R. J. Bernhard. Mechanical energy flow models of rods and beams. *Journal of Sound and Vibration*, 153(1):1–19, 1992. ISSN 0022460X. doi: 10.1016/0022-460X(92)90623-6. URL <http://www.sciencedirect.com/science/article/pii/0022460X92906236>.
- [60] R. Woschitz. Hoho wien-leuchtturmprojekt für den holzhybridbau. 2019.
- [61] Haitao Yu, Yusheng Yang, and Yong Yuan. Analytical solution for a finite euler–bernoulli beam with single discontinuity in section under arbitrary dynamic loads. *Applied Mathematical Modelling*, 60: 571–580, 8 2018. ISSN 0307904X. doi: 10.1016/j.apm.2018.03.046.



Acceleration HAUT - Eurocode Calculation

The focus of this quick case study is the potential mass reduction of HAUT if the damping ratio is increased, guaranteeing the same peak acceleration. For the peak acceleration the Eurocode equation is used:

$$a_{wind} = 1.6 * \frac{\phi_2 p_{vw,1} c_{pe} b_m}{\rho_l} \quad (A.1)$$

with

ϕ_2	dynamic factor $\sqrt{\frac{0.0344(n_{1,x})^{-2/3}}{D(1+0.12n_{1,x}h)(1+0.2n_{1,x}b_m)}}$
$p_{vw,1}$	$100 \ln\left(\frac{h}{0.2}\right)$
c_{pe}	sum of the external pressure coefficient
b_m	average width of building
ρ_l	mass of building per meter
$n_{1,x}$	natural frequency
D	damping
h	height of building

In the current design, the total mass of the building is 146,800 kN. With the building being 73 meter tall, this result in a ρ_l value of 204991 kg/m. The assumed damping value is 1.5% and the natural frequency is 0.56 Hz. The calculated peak acceleration is therefore 8.1 mg. For the calculations the damping is increased to 2 and 2.5% to measure the possible mass reduction which can be achieved in order to obtain the same peak acceleration.

Firstly, the overall mass in the FEM model is reduced and the new natural frequency is calculated. It is assumed that the stiffness remains constant. With the new mass and corresponding natural frequency, Formula A.1 is filled in. The mass is reduced until the point that the peak acceleration is equal to the current situation: 8.1 mg. An overview of the different values of the mass reduction, the corresponding natural frequency and the peak acceleration for both situations can be found in Table A.1 and A.2.

This quick study shows that an increase of the damping has a significant effect on the reduction of the mass. By increasing the damping with half a percentage point the mass could potentially be decreased by 17%. An addition of one percentage point to the damping leads to a mass reduction of 29%. It must

Table A.1: Mass reduction for a damping ratio of 2%

Mass		Natural frequency [Hz]	Peak acceleration [mg]
Value [kN]	Relative [-]		
146,800	1	0.54	7.0
132,120	0.9	0.55	7.6
123,312	0.84	0.56	8.0
121,844	0.83	0.56	8.1

Table A.2: Mass reduction for a damping ratio of 2.5%

Mass		Natural frequency [Hz]	Peak acceleration [mg]
Value [kN]	Relative [-]		
146,800	1	0.54	6.3
117,440	0.8	0.57	7.4
105,696	0.72	0.58	8.0
104,228	0.71	0.58	8.1

be noted that this method is an approximation and not a full-scaled calculation. Nonetheless, it shows that damping certainly has an impact on the acceleration and the possibility to reduce mass.

B

High-Rise Timber Buildings

This appendix presents an overview of six timber high-rise buildings. Stadthaus, Forte, Treet, Tallwood and HoHo held the title of tallest timber building in the world upon completion, while Haut was the second tallest. Currently, two taller buildings have been constructed: Mjøstårnet (85m) and Ascent (87m). Both are not covered in this overview.

B.1. Stadthaus

Stadthaus was the first residential tower to be fully constructed in CLT. Not only the floors and walls are constructed in CLT, but also the core. Upon completion in 2009 it was the tallest timber building in the world. The structural system consists of a central timber core, which is surrounded by a honeycomb pattern of CLT walls and floors. This results in a cellular structure of the building. All CLT panels are part of load bearing system. As panellised buildings are prone to progressive collapse, it was made sure that the failure of one element would not lead to fatal collapse. Due to the typical layout of residential buildings, the over-structuring was utilized [57]. All the CLT panels are connected by steel angle brackets in combination with screws [2].

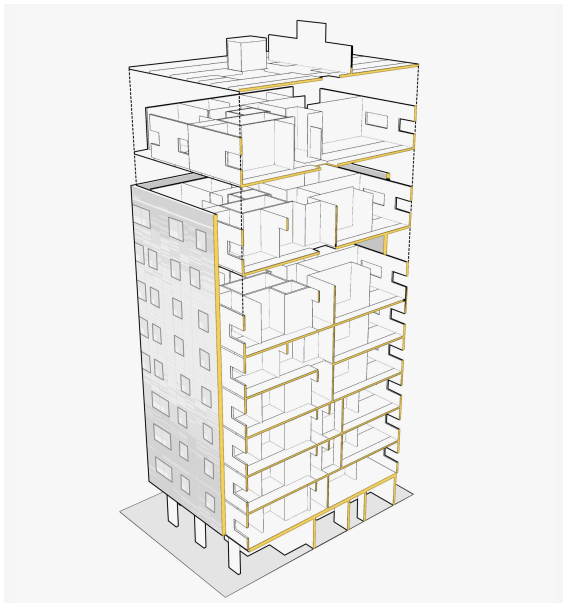


Figure B.1: CLT honeycomb structure Stadthaus [1].



Figure B.2: CLT walls and floors Stadthaus [1].



Figure B.3: Construction of Forte [48]



Figure B.4: Placement CLT with doorway already cut out [48]

B.2. Forte

In 2013, Forte surpassed Stadthaus as the highest timber building in the world. The Forte Tower is situated in Melbourne. The structural system of Forte is similar to that of Stadthaus. CLT panels are used for the core, floors and walls. From literature it was unclear if all panels are part of the load bearing system. It is however expected to be the case as the design is similar to Stadthaus. Again, steel angle brackets are used to connect the CLT. All CLT panels were prefabricated with the windows and doorways already cut out. This dramatically reduced the construction time of Forte [48].

B.3. Treet

Upon completion, Treet, located in the city of Bergen, was the highest timber building in the world. Nowadays, Treet is still the second highest building having an all timber structural system with only Mjøstårnet being higher. Treet uses a large glulam truss to provide the stability of the building. At each fifth storey a concrete slab is placed in the frame to provide extra stiffness. The structure does have a timber core, but it is not necessary for the stability. The glulam elements are connected to each other by slotted-in steel plates and dowels. Each separate house is designed as a CLT module which was lifted into the braced frame. The residential modules are not connected to the frame, but only to adjacent modules. The CLT walls are thus almost independent of the main load bearing structure [33].



Figure B.5: Glulam truss system Treet [33].

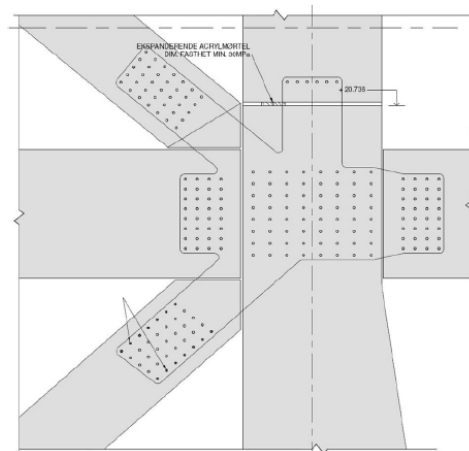


Figure B.6: Slotted-in steel connection with dowels Treet [33].

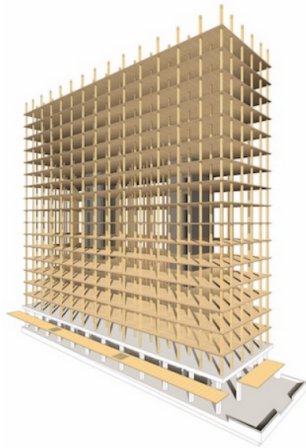


Figure B.7: Structural system Tallwood House [37].



Figure B.8: Glulam beams and CLT slabs [37].

B.4. Tallwood House at Brock Commons

Tallwood House at Brock Commons, Vancouver was completed in 2017. Standing 58 meters tall, it is not classified as an all timber building as two concrete cores provide the necessary stiffness and lateral stability. The column-floor system consists of glulam columns and CLT slabs. The columns are connected by a hollow steel connector and the slabs are linked to the columns using screws. All the connections were deliberately designed to be the same, to make the building as simple as possible. Combined with prefabricating all the structural elements, the construction time was drastically decreased. During construction they were able to erect two stories per week [37].

B.5. HAUT

The construction of HAUT in Amsterdam was finished in 2022. As in most taller timber buildings, HAUT has a concrete core providing the necessary lateral stability and stiffness. Due to the wish to have an unobstructed view from all the residential areas, the façade could not be load bearing. Therefore, interior shear walls are designed for the load bearing system in combination with the concrete core. The shear walls are made out of CLT. In contrast to the other timber buildings, HAUT utilizes different load bearing systems in one storey. A combination of glulam beams and columns, steel beams and columns, CLT walls, concrete walls and columns and composite floors are used, making it a more complex building than the relative simple Tallwood House. The high number of different structural elements also result in many different connection types.

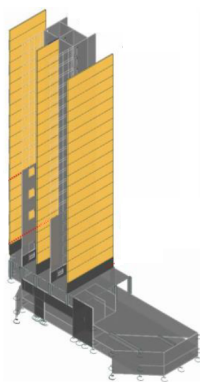


Figure B.9: Structural system HAUT.

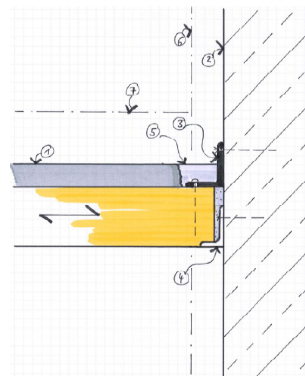


Figure B.10: Composite slab connected to concrete core.

B.6. HoHo Wien

From 2020 until 2022, HoHo Wien was the tallest tallest timber building in the world. HoHo is a combination of three towers; the tallest is 85 meter high. Concrete cores in combination with CLT shear walls provide the necessary stability of the building, but still 74% of the building will be timber. The shear walls can be found at the East and West side of the building. CLT floors are connected to the cores. At the perimeter, glulam columns are placed which in combination with concrete edge beams support the hybrid floors. The floors are made out of a combination of CLT and concrete. The outer walls will be constructed in CLT as well. These will be mounted on the glulam beams. Inner walls are also made of CLT, but do not have a structural function. To minimize the erection speed, a returning joint is designed which connects columns, beams and slabs on each storey in the same way. The glulam columns are connected to the concrete edge beams by a glued reinforcement bar. The concrete/timber floor slabs are also connected to the edge beams by reinforcement bars [60]. In contrast to the other timber buildings, the timber is mostly kept uncovered as was the wish of the architect and client [9].



Figure B.11: Structural system HoHo Wien [9].

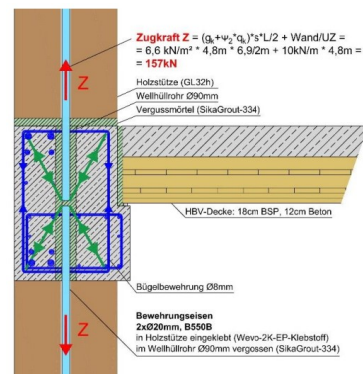
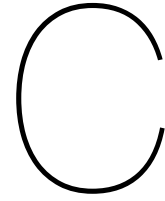


Figure B.12: Connection between glulam column and concrete beam edge [60].



Derivation Equations of Motion

C.1. Single Degree of Freedom

Single degree of freedom systems consist of a mass which can vibrate in only one direction. The system is generally represented by a mass, spring and dashpot. The equation of motion for a single degree of freedom system is described by [34]:

$$m\ddot{x} + c\dot{x} + kx = F(t) \quad (C.1)$$

In the equation, m represents the mass, c the viscous damping coefficient and k the spring stiffness. x denotes the displacement in the direction of the degree of freedom. The force on the system is given by F as a function of time t .

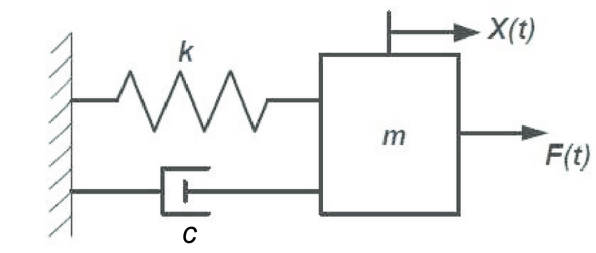


Figure C.1: Single degree of freedom.

If no external force is present and the system is excited by an initial displacement or velocity, the system is in a state of free vibration. The equation of motion simplifies to:

$$m\ddot{x} + c\dot{x} + kx = 0 \quad (C.2)$$

The equation is rewritten by dividing it by m and introducing

$$\sqrt{k/m} = \omega_n \quad \text{and} \quad c/m = 2n \quad (C.3)$$

where ω_n is the natural frequency of the undamped system and n is a measure for the damping. This results in the following equation:

$$\ddot{x} + 2n\dot{x} + \omega_n^2 x = 0 \quad (C.4)$$

By substituting the general solution into the equation of motion the characteristic equation is given.

$$s_n^2 + 2ns + \omega_n^2 = 0 \quad (C.5)$$

The general solution follows as:

$$x(t) = X_1 \exp(s_1 t) + X_2 \exp(s_2 t) \quad (\text{C.6})$$

with the characteristic exponents s_n :

$$s_1 = -n + \sqrt{n^2 - \omega_n^2} \quad \text{and} \quad s_2 = -n - \sqrt{n^2 - \omega_n^2} \quad (\text{C.7})$$

Two distinct cases exist which offer different solutions to the equation. In one case $n > \omega_n$ and in the other $n < \omega_n$. If $n > \omega_n$, s_1 and s_2 have real values and are both negative. Therefore, the mass does not vibrate, but instead slowly returns to the equilibrium. This is called aperiodic motion, which occurs if the damping coefficient is large relative to the spring stiffness. A special case of aperiodic motion exist when $n = \omega_n$, which is called critical damping.

In the case of $n < \omega_n$, the characteristic exponents are complex. In this case the damping coefficient is small relative to the spring constant. Therefore, the mass is vibrating and represents damped free vibrations. The displacement is described by:

$$x(t) = A_0 \exp(-nt) \cos(\omega_i t - \phi_0) \quad (\text{C.8})$$

with

$$\omega_i = \sqrt{\omega_n^2 - n^2}, \quad A_0 = \sqrt{x_0^2 + \left(\frac{v_0}{\omega_1} + \frac{nx_0}{\omega_1}\right)^2}, \quad \phi_0 = \arctan\left(\frac{v_0 + nx_0}{x_0 \omega_1}\right) \quad (\text{C.9})$$

From Equation C.8 it is clear that the vibration of the mass is enveloped by $A_0 \exp(-nt)$ as is shown in Figure C.2. The rate of decay depends on the value of n .

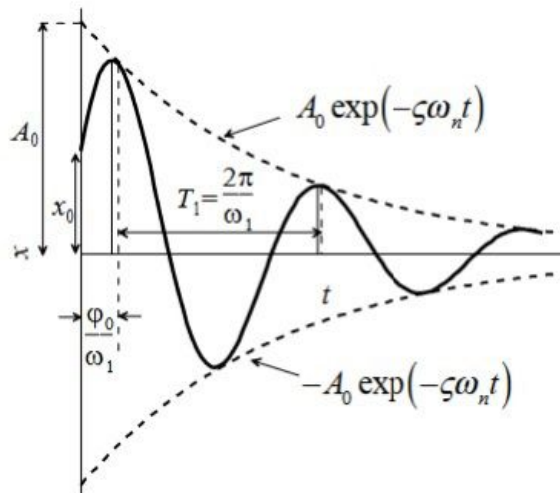


Figure C.2: Displacement-time curve of damped free vibrations.

C.2. Continuous Models

Three different models exist for describing the motion of a beam: Euler-Bernoulli, Timoshenko and Rayleigh. All are differential equations in which the manner of support are not included, because the differential equations make use of an infinitesimal part of the beam. The supports are introduced by means of imposing boundary conditions.

C.2.1. Euler-Bernoulli beam

The bending of a Euler-Bernoulli beam is described by the following fourth order partial differential equation [34]:

$$EI \frac{\partial^4 w(x, t)}{\partial x^4} + \rho A \frac{\partial^2 w(x, t)}{\partial t^2} = f(x, t) \quad (\text{C.10})$$

It is important to note that a few assumptions were made in order to simplify the model. The first assumption is that the cross-section remains perpendicular to the neutral line. Therefore, no shear deformation is taken into account. It is also assumed that plane cross-sections remain plan, meaning that the strain is linear over the height of the beam. Lastly, the rotational inertia has not been taken into account in the Euler-Bernoulli beam. By making use of these assumptions, the equation is simplified however still accurate for slender beams and low natural frequencies.

As mentioned before, the support conditions are not included in the differential equation, but will show up in the imposed boundary conditions. Two equations which are obtained during the derivation of the Euler-Bernoulli beam are very useful for setting up boundary conditions:

$$\begin{aligned} M &= -EI \frac{d^2 w}{dx^2} \\ Q &= -EI \frac{d^3 w}{dx^3} \end{aligned} \quad (\text{C.11})$$

The solution for the partial differential equation under free vibration is described by:

$$\begin{aligned} w(x) &= A \cosh \beta x + B \sinh \beta x + C \sin \beta x + D \cos \beta x \\ \text{with } \beta &= \frac{\rho A \omega^2}{EI} \end{aligned} \quad (\text{C.12})$$

The value of A, B, C, D and β depend on the boundary conditions. For a cantilevered beam, or clamped column depending on the orientation, the boundary conditions are as follows:

$$\begin{array}{ll} \text{at } x = 0 & \text{at } x = L \\ w(0) = 0 & -EI \frac{d^2 w}{dx^2} = 0 \\ \frac{dw(0)}{dx} = 0 & -EI \frac{d^3 w}{dx^3} = 0 \end{array} \quad (\text{C.13})$$

Substituting these into C.12 and evaluating it results in a relative simple equation:

$$\cos \beta L = -\frac{1}{\cosh \beta L} \quad (\text{C.14})$$

So it follows that:

$$\beta_1 L \approx 1.875, \quad \beta_2 L \approx 4.694, \quad \beta_3 L \approx 7.855... \quad (\text{C.15})$$

The natural frequencies are thus obtained as:

$$\omega_n = \beta_n^2 \sqrt{\frac{EI}{\rho A}}, \quad \omega_1 \approx \frac{3.52}{L^2} \sqrt{\frac{EI}{\rho A}} \quad (\text{C.16})$$

The eigenfunction is written as:

$$w_n(x) = A_n \left(\frac{\cosh \beta_n x - \cos \beta_n x}{\cosh \beta_n L + \cos \beta_n L} - \frac{\sinh \beta_n x - \sin \beta_n x}{\sinh \beta_n L + \sin \beta_n L} \right) = A_n \psi_n(x) \quad (n = 1, 2, \dots) \quad (\text{C.17})$$

The first three eigenmodes of a vibrating cantilever beam are depicted in Figure C.3.

As this is only the solution for the space function, it has to be combined with the harmonic time function. Thus, the complete solution for a free vibrating cantilever beam is described by:

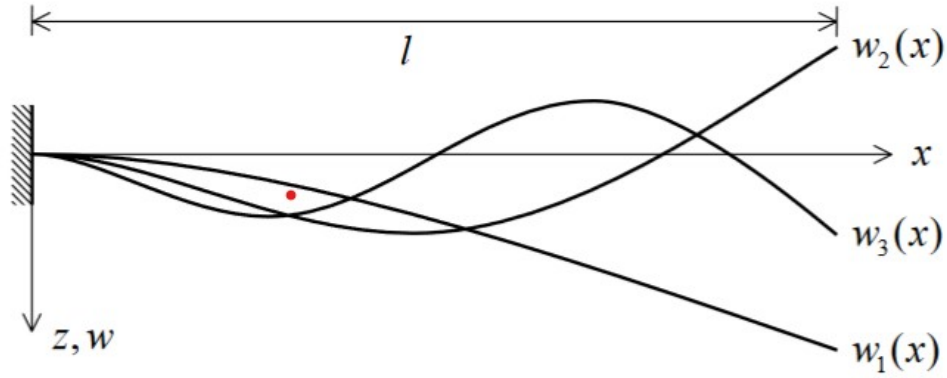


Figure C.3: First three eigenmodes of a cantilever beam [34].

$$w(x, t) = \sum_{n=1}^{\infty} A_n \psi_n(x) \sin(\omega_n t + \phi_n) \quad (\text{C.18})$$

A_n and ϕ_n are still unknowns, but can be derived by the initial conditions. For an initial displacement the boundary conditions are as follows:

$$\begin{aligned} w(L, 0) &= a \\ \frac{\partial w(L, 0)}{\partial t} &= 0 \end{aligned} \quad (\text{C.19})$$

This will lead to

$$\begin{aligned} w(x, t) &= \sum_{n=1}^{\infty} A_n \psi_n(x) \cos(\omega_n t) \\ \text{with } A_n &= \frac{a}{\psi_n(L)} \end{aligned} \quad (\text{C.20})$$

Damping

In the above equations of motion no damping was included. The described beams would thus vibrate indefinitely. Therefore, a term must be added in order to account for the damping. As discussed in Chapter 4, different terms may be added to account for energy dissipation. Two models are elaborated in this section: the Kelvin-Voigt damping and viscous damping along the beam. The resulting equation of motion of a clamped beam with Kelvin-Voigt damping is hence formulated as:

$$\left(E + E^* \frac{\partial}{\partial t} \right) I \frac{\partial^4 w(x, t)}{\partial x^4} + \rho A \frac{\partial^2 w(x, t)}{\partial t^2} = f(x, t) \quad (\text{C.21})$$

To find a solution for this equation separation of variables is applied, followed by a multiplication by the m^{th} mode and the equation being integrated over x [61].

$$\begin{aligned} \sum_{n=1}^{\infty} \ddot{\psi}_n(t) \int_0^L W_n(x) W_m(x) dx + (2\zeta \omega_n \dot{\psi}_n(t) + \omega_n^2 \psi_n(t)) \int_0^L W_n''''(x) W_m(x) dx \\ \text{with } \zeta = \frac{E^* I}{2\beta^2 \sqrt{\rho A E I}} \end{aligned} \quad (\text{C.22})$$

As the non trivial solution is of interest, only terms for which $m = n$ hold remain, due to the orthogonality of mode shapes.

$$\sum_{n=1}^{\infty} \ddot{\psi}_n(t) \int_0^L W_n(x)^2 dx + (2\zeta\omega_n \dot{\psi}_n(t) + \omega_n^2 \psi_n(t)) \int_0^L W_n''(x)^2 dx \quad (C.23)$$

This equation can be simplified to:

$$\begin{aligned} \ddot{\psi}_n(t) + 2B\zeta\omega_n \dot{\psi}_n(t) + B\omega_n^2 \psi_n(t) &= 0 \\ \text{with } B &= \frac{\int_0^L W_n''(x)^2 dx}{\int_0^L W_n(x)^2 dx} \end{aligned} \quad (C.24)$$

As only the first mode is considered this simplifies to a single degree of freedom system with a solution that reads as:

$$\begin{aligned} \psi &= A_0 e^{-B\zeta\omega t} \cos(\omega_1 t - \phi) \\ \text{with } \omega_1 &= \omega \sqrt{B - B^2\zeta^2} \end{aligned} \quad (C.25)$$

The spatial solution is equal to the one derived in equation C.17. So the total solution consists of the product of equation C.17 and C.25. To determine A_1 , A_0 and ϕ the boundary conditions are imposed.

For a beam modelled with with viscous dampers along its length the equation of motion slightly differs.

$$\begin{aligned} \omega_n^2 \frac{\partial^4 w(x,t)}{\partial x^4} + \frac{\partial^2 w(x,t)}{\partial t^2} + 2\zeta\omega_n \frac{\partial w(x,t)}{\partial t} &= 0 \\ \text{with } \zeta &= \frac{c}{2\beta^2 \sqrt{\rho A E I}} \\ \text{and } \omega_n^2 &= \beta^4 \frac{E I}{\rho A} \end{aligned} \quad (C.26)$$

The same procedure as before can be applied which results in the following equation.

$$\begin{aligned} \psi &= A_0 e^{-\zeta\omega t} \cos(\omega_1 t - \phi) \\ \text{with } \omega_1 &= \omega \sqrt{A - \zeta^2} \end{aligned} \quad (C.27)$$

C.2.2. Timoshenko beam

Lord Rayleigh introduced the effect of rotary inertia to the beam theory by Euler-Bernoulli. Subsequently, the influence of shear deformation was added by Timoshenko. The result is a coupled linear partial differential equation with the dependent variables w , the lateral displacement, and ϕ , the angle of the cross section to the neutral plane.

$$\begin{aligned} \rho A \frac{\partial^2 w}{\partial t^2} - q(x,t) &= kGA \left(\frac{\partial^2 w}{\partial x^2} - \frac{\partial \phi}{\partial x} \right) \\ \rho I \frac{\partial^2 w}{\partial t^2} &= \frac{\partial}{\partial x} \left(EI \frac{\partial \phi}{\partial x} \right) + kGA \left(\frac{\partial w}{\partial x} - \phi \right) \end{aligned} \quad (C.28)$$

In this equation k is the shear coefficient, which takes into account the variation of shear stresses across the cross section and depends on its geometry. For a rectangular cross section this is generally taken as 5/6. G is the shear modulus and I the second moment of inertia. For a linear, isotropic, homogeneous beam of constant cross section the two coupled differential equations can be combined:

$$EI \frac{\partial^4 w}{\partial x^4} + m \frac{\partial^2 w}{\partial t^2} - \left(\rho I + \frac{EI m}{kGA} \right) \frac{\partial^4 w}{\partial x^2 \partial t^2} + \frac{m \rho I}{kGA} \frac{\partial^4 w}{\partial t^4} = q(x,t) + \frac{\rho A}{kGA} \frac{\partial^2 q}{\partial t^2} - \frac{EI}{kGA} \frac{\partial^2 q}{\partial x^2} \quad (C.29)$$

For free vibrations this simplifies to:

$$EI \frac{\partial^4 w}{\partial x^4} + m \frac{\partial^2 w}{\partial t^2} - \left(\rho I + \frac{EI m}{kGA} \right) \frac{\partial^4 w}{\partial x^2 \partial t^2} + \frac{m \rho I}{kGA} \frac{\partial^4 w}{\partial t^4} = 0 \quad (C.30)$$

C.3. Torsional Vibration

If a torque is applied to a column, torsion will occur. For a circular cross-section, the cross-section will remain plane during the torsion. However, for a non circular cross-section warping will occur. Warping is the phenomenon where the cross-section distorts during torsion; the cross-section does not remain plane.

If warping is neglected and the column is homogeneous the equation of motion is [34]:

$$\rho J \frac{\partial^2 \psi}{\partial t^2} - G J_t \frac{\partial^2 \psi}{\partial x^2} = m_i \quad (\text{C.31})$$

J is equal to polar moment of inertia and J_t is the torque constant. For circular cross-section these properties are equal. However, for non circular cross-sections they are not identical. The torque constant and polar moment of inertia for a square cross-section are as follows:

$$J_t \approx 2.25 \left(\frac{1}{2} a \right)^4 \quad \text{and} \quad J = \frac{1}{6} a^4 \quad (\text{C.32})$$

With a being equal to the length of the sides of the cross-section. For free vibration equation of motion simplifies to:

$$\rho J \frac{\partial^2 \psi}{\partial t^2} - G J_t \frac{\partial^2 \psi}{\partial x^2} = 0 \quad (\text{C.33})$$

The method of separation of variables is used to solve the equation. The solution to the equation of motion can be represented by a multiplication of a time dependent part and space dependent part.

$$u(x, t) = U(x)\Psi(t) \quad (\text{C.34})$$

This solution is substituted into the equation of motion. Two solutions follow: one for the function dependent on time and the function dependent on spatial coordinates. They are given by:

$$\begin{aligned} \Psi(t) &= A \sin(\omega t) + B \cos(\omega t) \\ U(x) &= C \sin(\beta x) + D \cos(\beta x) \end{aligned} \quad (\text{C.35})$$

A boundary condition at $x = 0$ is determined and at $x = L$,

$$\phi(0) = 0 \quad \text{and} \quad G J_t \frac{\partial \psi(L)}{\partial x} = 0 \quad (\text{C.36})$$

With the use of the boundary and initial conditions, the unknown constants A, B, C and D can be determined.

C.3.1. Warping

If warping is taken into account an extra term is added to the equation [21].

$$E I_\psi \frac{\partial^4 \psi}{\partial x^4} + \rho J \frac{\partial^2 \psi}{\partial t^2} - G J_t \frac{\partial^2 \psi}{\partial x^2} = 0 \quad (\text{C.37})$$

To solve this fourth order differential equation, a harmonic solution is assumed in the form of

$$\psi(z, t) = \phi \exp(i\omega t) \quad (\text{C.38})$$

with ϕ being the amplitude of the rotation along the beam and ω the angular frequency. ϕ is defined as:

$$\phi = D_1 \cosh(\alpha z) + D_2 \sinh(\alpha z) + D_3 \cos(\beta z) + D_4 \sin(\beta z) \quad (\text{C.39})$$

The values of D_i are determined by the applied boundary conditions. α and β are given by

$$\alpha^2 = \sqrt{\frac{1}{4} k^4 + \lambda^4 + \frac{1}{2} k^2}, \quad \beta^2 = \sqrt{\frac{1}{4} k^4 + \lambda^4 - \frac{1}{2} k^2} \quad (\text{C.40})$$

with the warping length scale k , the normalized wave number λ and the wave speed v as

$$k^2 = \frac{GJ_t}{EI_\psi}, \quad \lambda^4 = \left(\frac{k\omega}{v}\right)^2, \quad v^2 = \frac{GJ_t}{\rho J} \quad (\text{C.41})$$

For a clamped beam torsion and warping is prevented at the fixed end. The boundary conditions are thus obtained as:

$$\begin{array}{ll} \text{at } x = 0 & \text{at } x = L \\ \psi(0) = 0 & k^2 \frac{\partial \psi(L)}{\partial x} - \frac{\partial^3 \psi(L)}{\partial x^3} = 0 \\ \frac{\partial \psi(0)}{\partial x} = 0 & \frac{\partial^2 \psi(L)}{\partial x^2} = 0 \end{array} \quad (\text{C.42})$$

This results in the following transcendental equation:

$$\frac{(\alpha L)^4 + (\beta L)^4}{(\alpha L)^2 (\beta L)^2} \cosh(\alpha L) \cos(\beta L) + \frac{(\alpha L)^2 - (\beta L)^2}{(\alpha L)(\beta L)} \sinh(\alpha L) \sin(\beta L) + 2 = 0 \quad (\text{C.43})$$